August 2020

Multi Sensor Multi Target Perception and Tracking for Informed Decisions in Public Road Scenarios

Andinet Negash Hunde
Clemson University, mail2andinet@gmail.com

Multi Sensor Multi Target Perception and Tracking for Informed Decisions in Public Road Scenarios

---

A Dissertation
Presented to
the Graduate School of
Clemson University

In Partial Fulfillment
of the Requirements for the Degree
Doctor of Philosophy
Automotive Engineering

---

by
Andinet Hunde
August 2020

Accepted by:
Dr. Yunyi Jia, Committee Chair
Dr. Zoran Filipi
Dr. Ioannis Karamouzas
Dr. Bing Li

Abstract

Multi-target tracking in public traffic calls for a tracking system with automated track initiation and termination facilities in a randomly evolving driving environment. Besides, the key problem of data association needs to be handled effectively considering the limitations in the computational resources on-board an autonomous car. The challenge of the tracking problem is further evident in the use of high-resolution automotive sensors which return multiple detections per object. Furthermore, it is customary to use multiple sensors that cover different and/or over-lapping Field of View and fuse sensor detections to provide robust and reliable tracking. As a consequence, in high-resolution multi-sensor settings, the data association uncertainty, and the corresponding tracking complexity increases pointing to a systematic approach to handle and process sensor detections.

In this work, we present a multi-target tracking system that addresses target birth/initiation and death/termination processes with automatic track management features. These tracking functionalities can help facilitate perception during common events in public traffic as participants (suddenly) change lanes, navigate intersections, overtake and/or brake in emergencies, etc. Various tracking approaches including the ones based on joint integrated probability data association (JIPDA) filter, Linear Multi-target Integrated Probabilistic Data Association (LMIPDA) Filter, and their multi-detection variants are adapted to specifically include algorithms that handle track initiation and termination, clutter density estimation and track management. The utility of the filtering module is further elaborated by integrating it into a trajectory tracking problem based on model predictive control.

To cope with tracking complexity in the case of multiple high-resolution sensors, we propose a hybrid scheme that combines the approaches of data clustering at the local sensor and multiple detections tracking schemes at the fusion layer. We implement a track-to-track fusion scheme that

de-correlates local (sensor) tracks to avoid double counting and apply a measurement partitioning scheme to re-purpose the LMIPDA tracking algorithm to multi-detection cases. In addition to the measurement partitioning approach, a joint extent and kinematic state estimation scheme are integrated into the LMIPDA approach to facilitate perception and tracking of an individual as well as group targets as applied to multi-lane public traffic. We formulate the tracking problem as a two hierarchical layer. This arrangement enhances the multi-target tracking performance in situations including but not limited to target initialization(birth process), target occlusion, missed detections, unresolved measurement, target maneuver, etc. Also, target groups expose complex individual target interactions to help in situation assessment which is challenging to capture otherwise.

The simulation studies are complemented by experimental studies performed on single and multiple (group) targets. Target detections are collected from a high-resolution radar at a frequency of 20Hz; whereas RTK-GPS data is made available as ground truth for one of the target vehicle's trajectory.

Dedication

To my wife, Eyerusalem, my kids and my parents, Negash and Etenesh.

Acknowledgments

I would like to express my heartfelt gratitude to my advisor, Dr. Yunyi Jia who took me in during the most difficult period of my PhD study. His guidance, support and encouragement rekindled in me the will and courage to work harder and closer to graduation. On the same tone, I would also like to thank Dr. Zoran Filipi, as part of my advising committee and as chair of the Automotive Engineering Department without whose good will, encouragement and support years of my study would have been wasted. In particular, the four plus years of my financial support comes from a competitive graduate assistantship that was generously offered by the department. My sincere gratitude also goes to my former adviser, Dr. Beshah Ayalew, who encouraged me to join one of the most exciting and reputable programs in Automotive Engineering. I would also thank Dr. Ioannis Karamouzas and Dr. Bing Li for their constructive suggestions, comments and criticisms which helped in shaping up the content of the dissertation to its present form.

The journey was long and arduous; my persistence and hard work alone meant nothing if not for the most friendly and helpful people I came to know as part of my study in Clemson. First and foremost, Dr. Jia's team, in particular Longxiang was supportive in regard to furnishing hardware and equipment for my field experiments at ICAR. Former students including Jeff Anderson, Jasprit Gill and Roberto Merco were available and informative when I needed someone to talk to. To be fair, the list should be longer; however, it cannot end without acknowledging Jeremiah for being prompt, resourceful and responsive with tones of my enquiries.

Finally, to my family and parents, for enduring with me during multiple waves of uncertainties and unforgettable ups and downs, thank you.

Table of Contents

List of Tables

List of Figures

This page is intentionally left blank.

Part I

Introduction

Introduction to Part I

Part I introduces and summarizes the background material into two chapters. Chapter 1, presents technological advances in automotive sensing and the resulting implications in perception and tracking paradigms as applied to urban traffic. The main challenges and opportunities are discussed to highlight the focus and contribution of this work. The chapter closes with a brief introduction of the material to be discussed in the rest of the dissertation.

Chapter 2 is devoted to the concise summary and introduction to Multi-Target problems including mathematical models and different tracking algorithms used in this thesis. Mainly, tracking schemes based on Joint Integrated Probability Data Association (JIPDA), Linear Multi-target Integrated Probability Data Association (LMIPDA) filter and multi-detection (MD) versions to be implemented in later chapters are highlighted. Also, the experimental setup and data collection procedures are briefly presented.

This page is intentionally left blank.

Chapter 1

Introduction

In the modern push towards increased automation of road vehicles, a proposed taxonomy by SAE (and NHTSA) outlines six discrete automation levels[1]. Central to this taxonomy is the respective roles of the (human) user and the driving automation system with each other. At the higher levels of automation (3, 4, and 5), the automated driving system executes most of the dynamic driving tasks. The most important subtask being the environmental perception, which includes real-time monitoring of the roadway environment for detection, recognition, classification of objects, and events. The objective of this study is to outline a tracking system capable of unsupervised automation of the perception process for automated driving systems in multi-target traffic. This includes the tasks of accommodating target birth (appearance or track initiation) and death events (disappearance or track termination), clutter density estimation, clustering of targets, track splitting/merging in the presence of data association uncertainty. These tracking functionalities can help facilitate perception during common events in public traffic as participants (suddenly) change lanes, navigate intersections, overtake, brake in emergencies, etc.

1.1 Challenges of Multi-Target Tracking

Multi-target tracking (MTT) systems aim to estimate both the number and the states of targets in the presence of measurement noise, false alarms, measurement origin uncertainty, missed detection, and birth/death processes [2, 3] from multiple sensor detections. Also, the control input sequences

applied to the tracked target vehicles are not generally known or given. The dynamic nature of the driving scene introduces the birth/death processes which are related to the appearance and disappearance of target vehicles within the Field of View (FoV) of the perception system. One of the key challenges mentioned above that could potentially complicate the tracking process is the data association uncertainty. Data association involves the assignment of sensor detections to the targets which generated the detections. If the measurement is not correctly assigned to the actual target, the track may end up following a different target and consequently add up to a track loss. Thus, it is apparent that a tracking algorithm capable of addressing the afore-mentioned challenges including data association uncertainty in real-time while effectively and reliably utilizing all sensor measurements is undoubtedly constrained by the available processing power of the on-board computer systems. This is further evident with the use of high-resolution automotive sensors which report multiple detections per object in what is called extended targets (objects).

In extended target tracking, in addition to estimating the motion of the (center of mass of) target detections, it is also of interest to estimate the shape, size, and orientation of the target. From the modeling point of view, the prevalent approaches are to partition the detections into mutually exclusive cells and then feed the resulting partitions into any of the conventional MTT trackers discussed above. In other approaches, extent estimation starts with an approximation of the target boundary by certain geometric shapes such as ellipses or rectangles. Then, the parameters of the assumed shape, i.e. the length of major and minor axes of an ellipse or length and width of a rectangle are estimated recursively at each scan time. However, a challenge comes when the detections originate from only one side of the target such as the rear bumper and/or when a relatively low number of detections are available from the target. Besides, the sensor-to-target distance, as well as orientation, could also affect the accuracy of the resulting estimation from noisy detections.

1.2 Opportunities of Multi-Target Tracking

The reliability and accuracy of the perception and tracking system determine the utility of higher modules that have implications in the safety of the occupant and road traffic as well. The trajectory tracking control function requires among other inputs the correct number of targets and their states in the driving scene to apply the correct control actions (steering, braking, signals, etc.) in navigating a dynamic traffic scene. Other driver assistance functions including Adaptive Cruise Control (ACC),

Automatic Parking (AP), and Blind Spot Monitoring (BSM) relay heavily on filtering and track management as well as handling of miss-detections provided by the tracking system.

The development of high-resolution automotive sensors provides a further impetus and opportunity to study the perception and tracking of target vehicles in multi-sensor multi-detection settings. Furthermore, it is customary to use multiple sensors that cover different and/or overlapping FoV and fuse sensor detections to provide robust and reliable tracking. As a consequence, in high-resolution multi-sensor settings, the data association uncertainty, and the corresponding tracking complexity increases pointing to a systematic approach to handle and process sensor detections.

Survey papers, including [2], and [4] present a detailed account of multi-target tracking (MTT) algorithms as interpreted in the context of the "point target" assumption. Here, we use a tracking algorithm based on the Linear Multi-target Integrated Probabilistic Data Association Filter (LMIPDAF) that has a linear complexity as a function of both the number of measurements and targets and adapt it to include automatic track management features. The extension of LMIPDAF to handle the possibility of multiple detections is derived via measurement partitioning approaches in [5]. The joint kinematic and extent estimation is also derived through the random matrix approach outlined in [6]. Both the measurement partitioning scheme and joint state and extent estimation through random matrix approaches are explored to address public traffic tracking and/or grouping in a manner to address measurement noise, false alarms, measurement origin uncertainty, missed detection, and birth/death processes mentioned above.

1.3 Research Gaps and Objectives

There is a need for multi-target tracking systems as applied to public traffic scenarios to process detections from multiple high-resolution automotive sensors. Higher autonomy functions that include control decisions require time-critical and reliable feedback from perception and tracking systems that operate in the presence of false alarms, sensor noise, miss-detections, and data association uncertainties. Thus, for safe and reliable operation of autonomous and/or semi-autonomous vehicles, we aim to address the following objectives to bridge the research gap and complement already existing solutions.

- Although applications of target tracking methods in the automotive realm constitute emerging

research avenues, reported studies do not specifically mention the implementation of tracking algorithms based on the Linear Multi-target Integrated Probabilistic Data Association (LMIPDA) filter implemented in this work. LMIPDA is chosen because it handles data association uncertainties that could otherwise be further complicated from the use of high-resolution multiple sensors. In this regard, we ask if this approach can address the multi-target tracking objectives when presented with both simulated and realistic experimental scenarios. We further explore if this approach could also achieve the tracking accuracy of optimal methods such as joint integrated probability data association (JIPDA) when faced with public tracking scenarios.

- Design and validate the performance of a tracking algorithm that is capable of operating on multi-sensor detections. The validation is based on a multi-target performance matrix that quantifies both the localization accuracy and cardinality error. Also, ground truth data generated from RTK GPS shall be used to validate the tracking performance.

- Incorporate the estimation of target extent with (kinematic) track estimation for high resolution (multi-detection) sensor. So far, extent estimation is not incorporated into the tracking algorithm by other authors.

1.4 Contributions

We present a multi-target tracking algorithm with a track management scheme that can track multiple targets from multiple radar reflections as used in automotive applications. For the sake of managing computational complexity, especially under multi-sensor settings, we demonstrate a hybrid structure that implements a clustering strategy at an individual sensor level and perform a multi-detection tracking on top of the clustered sensor detections. This approach is compared with alternative configurations to illustrate the performance benefits both in terms of tracking accuracy and speed of computation. The tracker is based on Multiple Detection-LMIPIDA (hereafter, abbreviated as MD-LMIPDA) and the contributions here will be its application to automotive radar tracking and a variation of the same that implements both clustering (as in conventional tracking algorithms) and multiple detection tracking. The hybrid approach combines the clustering techniques that alleviate computational complexity and multiple detection techniques that admits the

multiplicity of the target detections.

Also, a comparative performance study among different algorithms that handle the data association uncertainty differently will be presented. The joint data association that seeks an optimal measurement-to-track assignment and a linear multi-target approach will be compared for tracking accuracy and real-time suitability. Apart from an earlier work in [7] that benchmarks the performance of the GM-PHD tracker against that of the MHT, the side-by-side comparison of tracking algorithms is rare- especially as applied to automotive applications.

A third contribution aims at the inclusion of extent estimation into the LMIPDA tracker. The objective is to apply the resulting joint extent and kinematic estimation for extended and/or group target tracking as applied to public traffic scenarios. A double layer hierarchical tracking system consisting of group targets on the top layer and extended object tracking modules on the bottom layer is implemented. This arrangement enhances the multi-target tracking performance in situations including but not limited to target initialization(birth process), target occlusion, missed detections, unresolved measurement, target maneuver, etc. Besides, target groups expose complex individual target interactions and systematize the study of situation assessments which are otherwise both challenging to track and to accurately model mathematically.

1.5 Dissertation Structure

The theme of this dissertation involves the study of sensor fusion and tracking as applicable to public road traffic. To address tracking applications with autonomous track initiation, termination, and maintenance as applied to public traffic various approaches are investigated. The discussion of different tracking algorithms is introduced briefly in Chapter 2, in addition, the various mathematical models and experimental data collection procedures are also presented. Chapter 3, addresses the case of a JIPDA filter. Performance comparison to this approach is done in Chapter 4, with respect to tracking error and computational requirements. The method chosen for comparison is LMIPDA. The use of the filtering and prediction modules is also integrated into the trajectory tracking problem through model predictive control in Chapter 5. Further, to improve the reliability of the perception system and hence the tracking quality a multi-sensor configuration is studied that is applied in three different configurations:- track-to-track fusion, centralized fusion, and a proposed hybrid

fusion scheme. Chapter 6, presents literature, tracking algorithm, simulations, and key observations relevant to this case. The incorporation of extent estimation in the filtering algorithm as required in extended and group target tracking is summarized along with the intended use of a hierarchical double-layer tracking system to improve extended multi-object tracks is discussed in Chapter 7.

References

[1] S. I. J3016, "Taxonomy and definitions for terms related to driving automation systems for on-road motor vehicles," 2016.

[2] C. Qiu, Z. Zhang, H. Lu, and H. Luo, "A survey of motion-based multitarget tracking methods," *Progress In Electromagnetics Research*, vol. 62, pp. 195–223, 2015.

[3] B.-n. Vo, M. Mallick, Y. Bar-shalom, S. Coraluppi, R. Osborne, R. Mahler, and B.-t. Vo, "Multitarget tracking," *Wiley Encyclopedia of Electrical and Electronics Engineering*, 2015.

[4] B.-n. Vo, M. Mallick, Y. Bar-shalom, S. Coraluppi, R. Osborne III, R. Mahler, and B.-t. Vo, "Multitarget tracking," *Wiley Encyclopedia of Electrical and Electronics Engineering*, pp. 1–15, 1999.

[5] Y. Huang, T. L. Song, and D. S. Kim, "Linear multitarget integrated probabilistic data association for multiple detection target tracking," *IET Radar, Sonar & Navigation*, vol. 12, no. 9, pp. 945–953, 2018.

[6] M. Feldmann, D. Franken, and W. Koch, "Tracking of extended objects and group targets using random matrices," *IEEE Transactions on Signal Processing*, vol. 59, no. 4, pp. 1409–1420, 2010.

[7] K. Panta, D. E. Clark, and B. Vo, "Data association and track management for the gaussian mixture probability hypothesis density filter," *IEEE Transactions on Aerospace and Electronic Systems*, vol. 45, pp. 1003–1016, July 2009.

Chapter 2

Background

2.1 Introduction

The objective of this research focuses on the study of the multi-target state estimation problem as applied to public traffic. The estimation is based on noisy sensor detections and involves the joint estimation of [1]:

- The number of target vehicles
- The state (kinematic states as well as geometric state or extent)

In addition to measurement noises, one has to deal with complex sources of uncertainty, including measurement origin uncertainty, data association, and missed detections.

In this chapter, we briefly introduce the mathematical models that are used to simulate target trajectories, sensor measurements, or serve as motion prediction models within filtering equations. Besides, an overview of the tracking algorithms investigated in this study is presented. The differences among these algorithms are mainly concerning data association handling which is highlighted for each algorithm briefly. In the closing section, a data collection procedure including the types of sensors explored in this work is discussed. The overall experimental procedure and setup are also introduced.

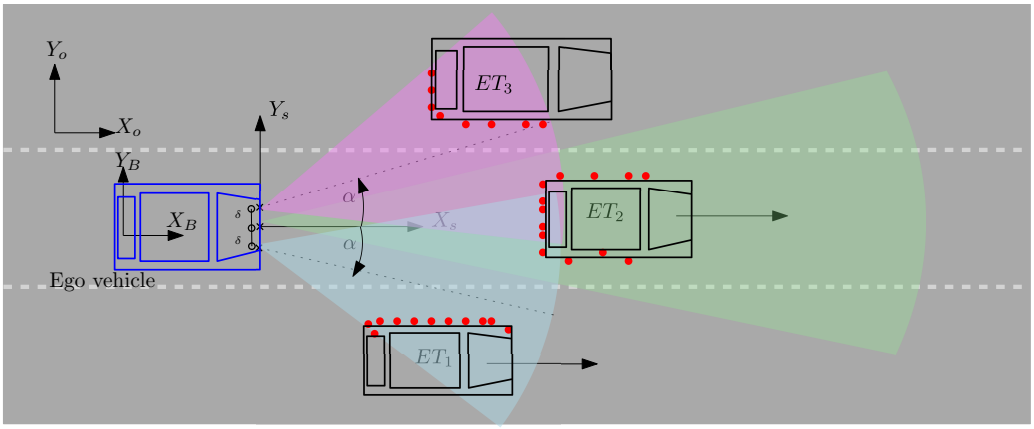

Figure 2.1: Three radar sensors with overlapping Field of View (FoV) are mounted on the ego vehicle. Such a configuration enhances the reliability of detection and tracking, minimizes chances of miss-detections but complicates the data association uncertainty especially under closely moving extended objects (ET).

2.2 Perception and Sensor Fusion

A fully autonomous vehicle is expected to perform an autonomous driving task through a sequence of events without human intervention: first, it must be able to perceive its environment and localize itself within the environment, then it must navigate to its goal position by planning and executing an obstacle-free path. To localize itself and perceive the driving environment an autonomous vehicle is fitted with a host of exteroceptive sensors (radar, lidar, and cameras), proprioceptive sensors, and other systems that enable it to communicate with the infrastructure and other vehicles.

Among the exteroceptive sensors, radar and camera are the most commonly researched. To provide a better perception, fusion offers a unique opportunity to implement both radar and camera in a manner to augment their shortcomings when used individually. A typical sensor configuration with overlapping FoV is shown in Figure 2.1. The resulting sensor detections can be treated at two layers: *centralized fusion*, where detections from both sensors are associated with tracks at the fusion center and *distributed fusion*, where each sensor generates tracks from their detections, and the data fusion center does track-to-track association [2].

2.3 Multi-Target Tracking

Multi-target tracking (MTT) systems aim to estimate both the number and the states of targets in the presence of process and measurement noise, false alarms, measurement origin uncertainty, missed detection, and birth/death processes [3, 4]. Several MTT algorithms are used at present in various tracking applications, with the most popular being the joint probabilistic data association filter (JPDAF), multiple hypothesis tracking (MHT), and random finite set (RFS) based multi-target filters [5, 6, 7]. Here, we give a brief discussion of each of these approaches.

The JPDAF uses joint association events and joint association probabilities to avoid conflicting measurement-to-track assignments [8, 9, 10, 11, 12, 13]. However, it assumes a fixed and known number of targets [4, 14]. MHT is a deferred decision approach to data association based MTT. At each observation time, the MHT algorithm attempts to propagate and maintain a set of association hypotheses with a high posterior probability or track score. In this way, the MHT approach inherently handles initiation and termination of tracks, and hence accommodates an unknown and time-varying number of targets [4, 15]. The RFS approach represents the multi-target state as a finite set of single-target states, and the MTT problem is formulated as a dynamic multi-target state estimation problem [4]. Some practical implementations of in this category include: the probability hypothesis density (PHD) filter [16, 17], the cardinalized PHD (CPHD) filter [18, 19] and the Generalized Labeled Multi-Bernoulli (GLMB) filter [20, 21, 22].

2.4 Multiple Detections, Extent and Group tracking

In extended target tracking, in addition to estimating the motion of the (center of mass of) target detections, it is also of interest to estimate the shape, size, and orientation of the target. A multi-sensor multi-detection (MD) scenario is illustrated in Figure 2.2 where the mean and co-variance of the state estimate from three sensors as well as the fused mean and co-variance state estimate is shown. From a modeling point of view, the prevalent approaches are to partition the detections into mutually exclusive cells and then feed the resulting partitions into any of the conventional MTT trackers discussed above. For the sake of extent estimation, the two well-researched methods are:- the random matrix and the star-convex shape based on the random hyper-surface model. The random matrix model, introduced by Koch [23], assumes a symmetric positive definite matrix that

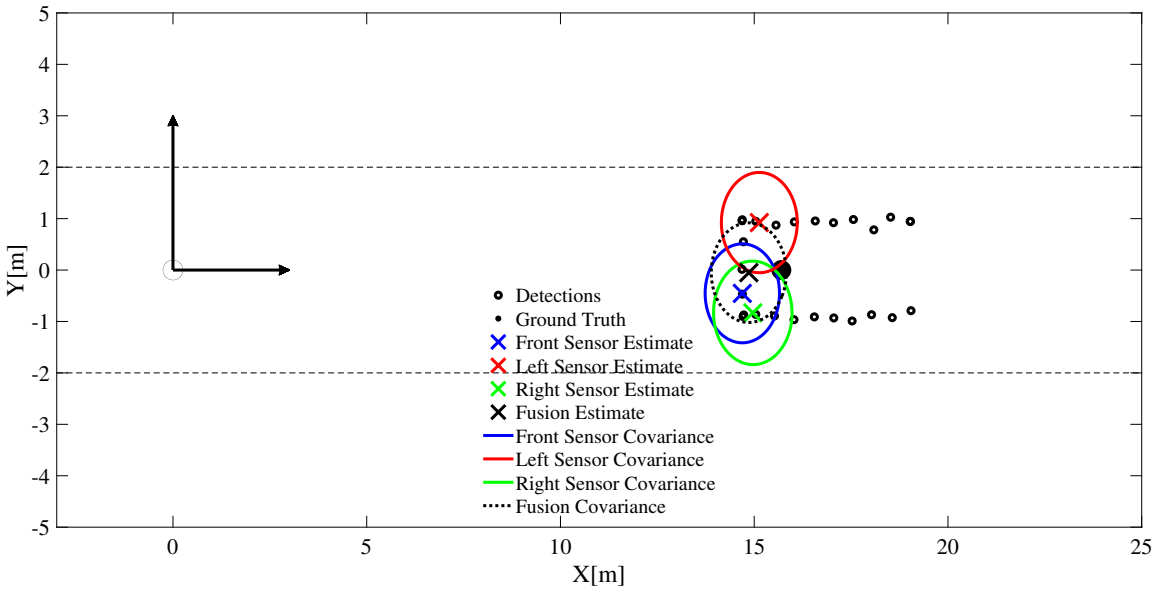

Figure 2.2: A multi-sensor multi-detection (MD) illustration. Target detections are tracked by MD-Trackers run on three sensor detections. A track-to-track detection algorithm fuses local tracks to get a point estimate at the system level.

lends itself to an approximation of the target by an elliptical shape. The overall tracking problem then becomes an estimation of the random state (composed of the target position and its derivatives) x_k that represents the motion of the object's centroid and the estimation of the object extent X_k approximated by an ellipsoid. An improvement over [23] that relaxes the process noise assumption is presented in [24, 25]. However, both the original and improved approaches are based on linear measurement models which render the straight-forward extension to radar detections that include range, azimuth, and Doppler measurements slightly complicated. Further improvements on the random matrix approach to shape modeling, shape estimation, and comparison among different implementations are discussed in the survey paper [26].

The random matrix model could be extended to the estimation of generic shapes by recasting the shape estimation into a combination of several elliptically shaped sub-objects as demonstrated in [27]. However, the second approach based on the random hypersurface model offers a flexible option, albeit at a higher computational cost, to model general star-convex shapes. In this model, measurement sources are assumed to lie on randomly scaled versions of the shape boundaries [28],[29].

In [30], a tracking technique that models the multi-target state as a generalized labeled multi-Bernoulli (GLMB) random finite set (RFS) is proposed. For extent estimation, the targets are

modeled using gamma Gaussian inverse Wishart (GGIW) distributions. The authors also provide a less accurate but faster variant of the algorithm based on the labeled multi-Bernoulli (LMB) filter. Other tracking methods based on the RFS multi-target modeling paradigm include [31],[32] that incorporate random matrices to estimate the shape of extended targets in what are termed respectively as Gaussian inverse Wishart phd (giw-phd) and gamma-Gaussian-inverse Wishart (GGIW) filters. Non-RFS filtering methods have also been reported in extending object tracking literature. The use of Gaussian processes to track boundaries of unknown shapes of extended objects is proposed in [33] and is shown to be more precise than elliptical approximations discussed above. A generalization of [23] for multiple extended targets that recursively estimates both the kinematic state and the elliptic shapes is proposed in [34]. The filter is based on probabilistic multi-hypothesis tracking (PMHT) framework that implements the expectation-maximization (EM) scheme to assign multiple detections. Generalizations of the Probabilistic Data Association (PDA) and Joint Probabilistic Data Association Filter (JPDAF) to multiple detections are presented in [35] and [36], respectively.

In general, extent estimation starts with an approximation of the target boundary by certain geometric shapes such as ellipses or rectangles. Then, the parameters of the assumed shape, i.e. the length of major and minor axes of an ellipse or length and width of a rectangle are estimated recursively at each scan time. However, a challenge comes when the detections originate from only one side of the target such as the rear of the target, and when a comparatively low number of detections are available from the target. Besides, the angles and the sensor-to-target distances might also affect the accuracy of the resulting estimation from noisy detections. Thus the joint estimation of the state and extent is a problem that we revisit in Part III of the thesis, focusing for a while on the kinematic state estimation alone. It is important to mention that some sensors such as LIDAR provide a much detailed 3-D point cloud detection (at most of the scan times) so that the target contour could be easily extracted to infer the shape, size, orientation reliably. The bounding box generated from object detection modules that operate on camera images can also provide indispensable shape information to which a 2D/3D geometry could be fitted to propagate the extent of the target at a much lower cost [37]. Nonetheless, we shall revisit the joint state estimation via both approaches and explore the problem of group target estimation to improve individual target tracks.

2.5 Mathematical Models

A range of mathematical models is investigated to simulate target-generated measurements and/or to predict target motions in the filtering equations. Next, we briefly review the mathematical models, parameters, and assumptions used.

Constant Acceleration

A general linear time-invariant model can be described with continuous-time state equations of the following form:

$$\frac{dx(t)}{dt} = Fx(t) + Lw(t) \tag{2.1}$$

where F and L are constant matrices, which characterize the behaviour of the model, $w(t)$ is a white noise process with a power spectral density Q_c.

$$F = \begin{bmatrix} 0 & 0 & 1 & 0 & 0 & 0 \\ 0 & 0 & 0 & 1 & 0 & 0 \\ 0 & 0 & 0 & 0 & 1 & 0 \\ 0 & 0 & 0 & 0 & 0 & 1 \\ 0 & 0 & 0 & 0 & 0 & 0 \\ 0 & 0 & 0 & 0 & 0 & 0 \end{bmatrix} \tag{2.2}$$

$$L = \begin{bmatrix} 0 & 0 \\ 0 & 0 \\ 0 & 0 \\ 0 & 0 \\ 1 & 0 \\ 0 & 1 \end{bmatrix} \tag{2.3}$$

where the state variable $x(t)$ is composed as $[x, y, \dot{x}, \dot{y}, \ddot{x}, \ddot{y}]$ representing the (x, y) positions, velocities and accelerations respectively. This model is also called continuous Wiener process acceleration (CWPA) model because the acceleration is modeled as a perturbing white noise. To be able to use

the model for real-time filtering applications, we need to discretize it. The discretized matrices A_k and Q_k are given next [38].

$$A_k = exp(F\Delta t_k) \tag{2.4}$$

$$Q_k = \int_0^{\Delta t_k} exp(F\Delta t_k - \tau) L Q_c L^T exp(F\Delta t_k - \tau)^T d\tau \tag{2.5}$$

If one selects $Q_c = \begin{bmatrix} 1 & 0 \\ 0 & 1 \end{bmatrix} q$, Q_k can be integrated out from Equation (2.5) to get:

$$Q_k = \begin{bmatrix} \frac{1}{20}\Delta t^5 & 0 & \frac{1}{8}\Delta t^4 & 0 & \frac{1}{6}\Delta t^3 & 0 \\ 0 & \frac{1}{20}\Delta t^5 & 0 & \frac{1}{8}\Delta t^4 & 0 & \frac{1}{6}\Delta t^3 \\ \frac{1}{8}\Delta t^4 & 0 & \frac{1}{6}\Delta t^3 & 0 & \frac{1}{2}\Delta t^2 & 0 \\ 0 & \frac{1}{8}\Delta t^4 & 0 & \frac{1}{6}\Delta t^3 & 0 & \frac{1}{2}\Delta t^2 \\ \frac{1}{6}\Delta t^3 & 0 & \frac{1}{2}\Delta t^2 & 0 & \Delta t & 0 \\ 0 & \frac{1}{6}\Delta t^3 & 0 & \frac{1}{2}\Delta t^2 & 0 & \Delta t \end{bmatrix} q \tag{2.6}$$

Constant Velocity

Likewise, a constant velocity motion model can be described by continuous-time state equations as shown in Equation (2.1). Here, the state $x(t)$ represents the (x, y) positions and corresponding velocities. The constant matrices F and L are defined as follows:

$$F = \begin{bmatrix} 0 & 0 & 1 & 0 \\ 0 & 0 & 0 & 1 \\ 0 & 0 & 0 & 0 \\ 0 & 0 & 0 & 0 \end{bmatrix} \tag{2.7}$$

$$L = \begin{bmatrix} 0 & 0 \\ 0 & 0 \\ 1 & 0 \\ 0 & 1 \end{bmatrix} \tag{2.8}$$

The discrete time equivalent can similarly be solved from Equations (2.4), (2.5) for the constant velocity model too.

Constant Turn

The constant turn kinematic model can be used to simulate the motion of target vehicles. The equation can be expressed by a nonlinear function of the states with an additive process noise component as follows:

$$x_k^\tau = \psi(x_{k-1}^\tau) + \Gamma v_k \tag{2.9}$$

where, we define the state variables as $x_k^\tau = [x, \dot{x}, y, \dot{y}, \dot{\omega}]$. $[x, y]$ and $[\dot{x}, \dot{y}]$ are, respectively the target positions and velocities, whereas $\dot{\omega}$ is the turn rate. An additive noise term v_k with $E[v_k] = 0$ and $E[v_k v_k^T] = Q_k$ models the process noise. ψ and Γ are given in (2.10) and (2.11), respectively.

$$\psi(x) = \begin{pmatrix} x + \frac{\dot{x}}{\omega}\sin(\omega\Delta t) - \frac{\dot{y}}{\omega}(1 - \cos(\omega\Delta t)) \\ \dot{x}\cos(\omega\Delta t) - \dot{y}\sin(\omega\Delta t) \\ y + \frac{\dot{x}}{\omega}(1 - \cos(\omega\Delta t)) + \frac{\dot{y}}{\omega}\sin(\omega\Delta t) \\ \dot{x}\sin(\omega\Delta t) - \dot{y}\cos(\omega\Delta t) \\ \omega \end{pmatrix} \tag{2.10}$$

$$\Gamma = \begin{pmatrix} \Delta t^2/2 & \Delta t & 0 & 0 & 0 \\ 0 & 0 & \Delta t^2/2 & \Delta t & 0 \\ 0 & 0 & 0 & 0 & 1 \end{pmatrix}^T \tag{2.11}$$

Bicycle Model

For a more realistic motion description that includes the effects of the cornering stiffnesses, as well as mass and inertia of the target/ego vehicle, we can use the bicycle model. The linearized bicycle

state space model given in Equation (2.12).

$$\begin{bmatrix} \dot{y} \\ \dot{v}_y \\ \dot{\psi} \\ \dot{r} \end{bmatrix} = \begin{bmatrix} 0 & 1 & 0 & 0 \\ 0 & -\frac{C_f+C_r}{mV_x} & 0 & -V_x - \frac{C_f l_f - C_r l_r}{mV_x} \\ 0 & 0 & 0 & 1 \\ 0 & -\frac{C_f+C_r}{mV_x} & 0 & -V_x - \frac{C_f l_f - C_r l_r}{mV_x} \end{bmatrix} \begin{bmatrix} y \\ v_y \\ \psi \\ r \end{bmatrix} + \begin{bmatrix} 0 \\ \frac{C_f}{m} \\ 0 \\ \frac{C_f l_f}{I_z} \end{bmatrix} \delta \tag{2.12}$$

y is the lateral deviation, v_y is the lateral speed and δ is the steering input. For tracking purpose, it is more convenient to describe the motion of the ego vehicle with respect to a path (road aligned coordinate frame). Thus, we introduce tracking error terms as follows:

$$\begin{aligned} \ddot{e}_1 &= \ddot{y} + V_x \left(\dot{\psi} - \dot{\psi}_{des} \right) \\ e_2 &= \psi - \psi_{des} \end{aligned} \tag{2.13}$$

where ψ and ψ_{des} are the actual orienation and the desired orientation of the ego vehicle with respect to a global frame[39]. The remaining vehicle parameters are defined and assigned values in Chapter 4, see Table 4.1.

Singer Model

The Singer model will later be used in connection with extent estimation. Thus, instead of introducing a general form here, we shall focus on the form that we intend to use for this work. The Singer model is described by a discrete-time state and measurement equations of the form:

$$x_k = \psi_k x_{k-1} + \omega_k \tag{2.14}$$

$$z_k^r = \bar{H}_k x_k + v_k^r \tag{2.15}$$

where $\psi_k = F_k \otimes I_d$ and $\bar{H}_k = H_k \otimes I_d$. As usual both noise terms are modeled as independent white Gaussian with

$$\omega_k \sim \mathcal{N}(0, D_k \otimes X_k) \tag{2.16}$$

$$v_k^r \sim \mathcal{N}(0, zX_k + R_k) \tag{2.17}$$

F_k and D_k are given as:

$$F_k = \begin{bmatrix} 1 & \Delta t & \frac{1}{2}\Delta t^2 \\ 0 & 1 & \Delta t \\ 0 & 0 & e^{\frac{-\Delta t}{\theta}} \end{bmatrix} \tag{2.18}$$

$$D_k = \begin{bmatrix} 0 & 0 & 0 \\ 0 & 0 & 0 \\ 0 & 0 & \Sigma^2(1 - e^{-2\frac{-\Delta t}{\theta}}) \end{bmatrix} \tag{2.19}$$

where, θ and Σ are respectively maneuver correlation time constant and scalar acceleration rms value.

Multi Model

To describe the motion of target vehicles in the prediction horizon, specially during maneuver executions, we use Interacting Multiple Model (IMM) for better accuracy. IMM problems involve both the estimation of continuous-valued parameters such as target positions, velocities and accelerations, and that of discrete stochastic models $M = \{M^1, M^2, \ldots, M^n\}$[38, 40, 41]. The IMM-filter used here is based on a system of equations where $j \in \{1, 2, 3, \ldots, n\}$ represents any of the kinematic/dynamic models introduced in this chapter:

$$\mathbf{x}_k = A_{k-1}^j \mathbf{x}_{k-1} + \mathbf{q}_{k-1}^j \tag{2.20a}$$

$$\mathbf{y} = H_k^j \mathbf{x}_k + \mathbf{r}_k^j \tag{2.20b}$$

Each model is defined by the prior probability $\mu_{k-1}^i = P(M_0^i)$ and a fixed transition probability $\pi_{ij} = P(M_k^j | M_{k-1}^i)$. Each recursion goes though steps of interaction, filtering and combination as briefly reviewed next.

Interaction

Each of the n filters is initialized with mixed estimates of all the filters weighted by a mixing probability:

$$\hat{\mathbf{x}}_{k-1}^{0j} = \sum_{i=1}^{n} \mu_k^{i|j} \hat{\mathbf{x}}_{k-1}^{i} \tag{2.21a}$$

$$P_{k-1}^{0j} = \sum_{i=1}^{n} \mu_k^{i|j} \left[P_{k-1}^{i} + \left(\hat{\mathbf{x}}_{k-1}^{i} - \hat{\mathbf{x}}_{k-1}^{0j} \right) \left(\hat{\mathbf{x}}_{k-1}^{i} - \hat{\mathbf{x}}_{k-1}^{0j} \right)^T \right] \tag{2.21b}$$

where $\hat{\mathbf{x}}_{k-1}^{i}$ and P_{k-1}^{i} are the updated mean and covariance at iteration $k-1$ of model i. The mixing probabilities $\mu_k^{i|j}$ are computed as:

$$\mu_k^{i|j} = \frac{\pi_{ij} \mu_{k-1}^{i}}{\sum_{i=1}^{n} \pi_{ij} \mu_{k-1}^{i}} \tag{2.22}$$

where μ_{k-1}^{i} is the probability of model i.

Filtering

Here, except for the first iteration, standard Kalman prediction steps are applied. Assuming that there are no missed detections at the current scan time, the first iteration involves both Kalman prediction and update steps from which the means and covariances $\hat{\mathbf{x}}_k^i$, P_k^i are computed and the model probabilities μ_{k-1}^{i} are updated.

$$\mu_k^{i} = \frac{\mathcal{N}(\mathbf{v}_k^i, 0, S_k^i) \mu_{k-1}^{i}}{\sum_{j=1}^{n} \mathcal{N}(\mathbf{v}_k^j, 0, S_k^i) \mu_{k-1}^{j}} \tag{2.23}$$

where $\mathbf{v}_k^i$ and S_k^j are respectively the measurement residual and covariance of model i.

Combination

Individual estimates from each model are finally combined as:

$$\hat{\mathbf{x}}_k = \sum_{i=1}^{n} \mu_k^i \hat{\mathbf{x}}_k^i \tag{2.24a}$$

$$P_k = \sum_{i=1}^{n} \mu_k^i \left[P_k^i + \left(\hat{\mathbf{x}}_k^i - \hat{\mathbf{x}}_k \right) \left(\hat{\mathbf{x}}_k^i - \hat{\mathbf{x}}_k \right)^T \right] \tag{2.24b}$$

2.6 Tracking Approaches

The key difference in the tracking approaches discussed in this work is how the data association problem is handled. Next, we summarize the tracking approaches used in this work giving a brief overview of each.

Joint Integrated Probabilistic Data Association: JIPDA

JIPDA solves the data association problem for all measurements and all targets within the cluster simultaneously. A cluster is defined as a set of tracks (and their validated measurements) that share measurements amongst themselves. For independent clusters, the data association may be computed in parallel.

Let us assume that at a particular scan time there are 3 target vehicles τ_1, τ_1 and τ_3 and the sensor returns 4 measurements m_1, m_2, m_3 and m_4 which are validated by the targets as follows:

$$\tau_1 = \{m_1, m_2\}$$
$$\tau_2 = \{m_2, m_3\}$$
$$\tau_3 = \{m_3, m_4\}$$

Since τ_1 shares m_2 with τ_2 and τ_2 shares m_3 with τ_3, the three targets are clustered together to evaluate the measurement-to-target data association optimally. The validation gates and the selected measurements are illustrated in Figure 2.3.

The above scenario can be concisely represented by a validation matrix Ω, where the rows are associated with the measurements $m_j \in \{m_1, m_2, m_3, m_4\}$ and the columns correspond to $\tau \in \{0, \tau_1, \tau_2, \tau_3\}$. The possibility that all the measurements might be originating from clutter $\tau = 0$ is denoted by the entries in the first column of Ω.

$$\Omega = \begin{pmatrix} 1 & 1 & 0 & 0 \\ 1 & 1 & 1 & 0 \\ 1 & 0 & 1 & 1 \\ 1 & 0 & 0 & 1 \end{pmatrix} \tag{2.25}$$

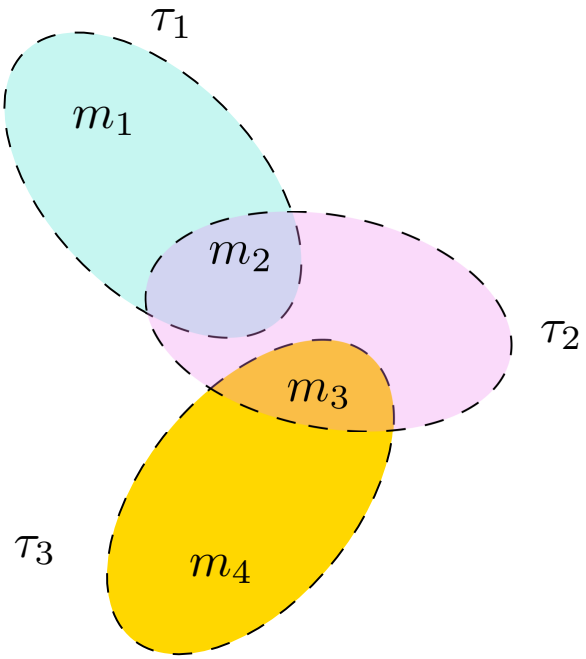

Figure 2.3: A cluster of 3 targets share 4 measurements. The feasible events are evaluated for the 3 targets and the 4 measurements jointly.

Next, we would like to enumerate all the possible joint association events so that the following two constraints are satisfied.

1. Each target τ is assigned at most one measurement. We note that this requirement effectively ignores the possibility of multiple detections from the target.

2. Each measurement is assigned to at most one target. This assumption avoids the possibility of merged measurements where a measurement could be a detection of two or more targets.

Based on the two restrictions, one can identify 21 hypotheses for the above measurement-to-target assignment example. We list these events below.

$$\omega_1 = \begin{pmatrix} 1 & 0 & 0 & 0 \\ 1 & 0 & 0 & 0 \\ 1 & 0 & 0 & 0 \\ 1 & 0 & 0 & 0 \end{pmatrix} \omega_2 = \begin{pmatrix} 0 & 1 & 0 & 0 \\ 1 & 0 & 0 & 0 \\ 1 & 0 & 0 & 0 \\ 1 & 0 & 0 & 0 \end{pmatrix} \omega_3 = \begin{pmatrix} 0 & 1 & 0 & 0 \\ 0 & 0 & 1 & 0 \\ 1 & 0 & 0 & 0 \\ 1 & 0 & 0 & 0 \end{pmatrix} \omega_4 = \begin{pmatrix} 0 & 1 & 0 & 0 \\ 0 & 0 & 1 & 0 \\ 0 & 0 & 0 & 1 \\ 1 & 0 & 0 & 0 \end{pmatrix}$$

$$\omega_5 = \begin{pmatrix} 0 & 1 & 0 & 0 \\ 0 & 0 & 1 & 0 \\ 1 & 0 & 0 & 0 \\ 0 & 0 & 0 & 1 \end{pmatrix} \omega_6 = \begin{pmatrix} 0 & 1 & 0 & 0 \\ 1 & 0 & 0 & 0 \\ 0 & 0 & 1 & 0 \\ 1 & 0 & 0 & 0 \end{pmatrix} \omega_7 = \begin{pmatrix} 0 & 1 & 0 & 0 \\ 1 & 0 & 0 & 0 \\ 0 & 0 & 1 & 0 \\ 0 & 0 & 0 & 1 \end{pmatrix} \omega_8 = \begin{pmatrix} 0 & 1 & 0 & 0 \\ 1 & 0 & 0 & 0 \\ 0 & 0 & 0 & 1 \\ 1 & 0 & 0 & 0 \end{pmatrix}$$

$$\omega_9 = \begin{pmatrix} 0 & 1 & 0 & 0 \\ 1 & 0 & 0 & 0 \\ 1 & 0 & 0 & 0 \\ 0 & 0 & 0 & 1 \end{pmatrix} \omega_{10} = \begin{pmatrix} 1 & 0 & 0 & 0 \\ 0 & 1 & 0 & 0 \\ 1 & 0 & 0 & 0 \\ 1 & 0 & 0 & 0 \end{pmatrix} \omega_{11} = \begin{pmatrix} 1 & 0 & 0 & 0 \\ 0 & 1 & 0 & 0 \\ 0 & 0 & 1 & 0 \\ 1 & 0 & 0 & 0 \end{pmatrix} \omega_{12} = \begin{pmatrix} 1 & 0 & 0 & 0 \\ 0 & 1 & 0 & 0 \\ 0 & 0 & 1 & 0 \\ 0 & 0 & 0 & 1 \end{pmatrix}$$

$$\omega_{13} = \begin{pmatrix} 1 & 0 & 0 & 0 \\ 0 & 1 & 0 & 0 \\ 0 & 0 & 0 & 1 \\ 1 & 0 & 0 & 0 \end{pmatrix} \omega_{14} = \begin{pmatrix} 1 & 0 & 0 & 0 \\ 0 & 1 & 0 & 0 \\ 1 & 0 & 0 & 0 \\ 0 & 0 & 0 & 1 \end{pmatrix} \omega_{15} = \begin{pmatrix} 1 & 0 & 0 & 0 \\ 0 & 0 & 1 & 0 \\ 1 & 0 & 0 & 0 \\ 1 & 0 & 0 & 0 \end{pmatrix} \omega_{16} = \begin{pmatrix} 1 & 0 & 0 & 0 \\ 0 & 0 & 1 & 0 \\ 0 & 0 & 0 & 1 \\ 1 & 0 & 0 & 0 \end{pmatrix}$$

$$\omega_{17} = \begin{pmatrix} 1 & 0 & 0 & 0 \\ 0 & 0 & 1 & 0 \\ 1 & 0 & 0 & 0 \\ 0 & 0 & 0 & 1 \end{pmatrix} \omega_{18} = \begin{pmatrix} 1 & 0 & 0 & 0 \\ 1 & 0 & 0 & 0 \\ 0 & 0 & 1 & 0 \\ 1 & 0 & 0 & 0 \end{pmatrix} \omega_{19} = \begin{pmatrix} 1 & 0 & 0 & 0 \\ 1 & 0 & 0 & 0 \\ 0 & 0 & 1 & 0 \\ 0 & 0 & 0 & 1 \end{pmatrix} \omega_{20} = \begin{pmatrix} 1 & 0 & 0 & 0 \\ 1 & 0 & 0 & 0 \\ 0 & 0 & 0 & 1 \\ 1 & 0 & 0 & 0 \end{pmatrix}$$

$$\omega_{21} = \begin{pmatrix} 1 & 0 & 0 & 0 \\ 1 & 0 & 0 & 0 \\ 1 & 0 & 0 & 0 \\ 0 & 0 & 0 & 1 \end{pmatrix}$$

Among the feasible events listed above, the event ω_{12} for example, assigns measurement m_1 to clutter and measurements m_2, m_3, m_4 to targets τ_1, τ_2, τ_3 respectively. This also points us to an alternative representation of the joint feasible events that would also make the computation of the posterior data association probabilities easier. For the scenario at hand, the feasible events with the target assignment hypothesis are enumerated in Table 2.1.

Feasible Joint Events	Target τ_1	Target τ_2	Target τ_3
1	0	0	0
2	1	0	0
3	1	2	0
4	1	2	3
5	1	2	4
6	1	3	0
7	1	3	4
8	1	0	3
9	1	0	4
10	2	0	0
11	2	3	0
12	2	3	4
13	2	0	3
14	2	0	4
15	0	2	0
16	0	2	3
17	0	2	4
18	0	3	0
19	0	3	4
20	0	0	3
21	0	0	4

Table 2.1: Feasible Data Association Events.

For systematic generation of feasible joint events, especially when the number of targets and measurements are large, the work in [42] identifies the data association problem as an exhaustive search problem and proposes a depth-first search (DFS) algorithm. For the 4 measurements, we have a solution of the form (X_1, X_2, X_3, X_4). Each X_i takes on the values Z_i, which is a finite and linearly ordered set of targets (or clutter) that are associated with the measurement i. i.e.,

$$Z_1 = \{0, 1\}$$

$$Z_2 = \{0, 1, 2\}$$

$$Z_3 = \{0, 2, 3\}$$

$$Z_4 = \{0, 3\}$$

Since a measurement cannot be associated with more than one (non-clutter) targets, and if $X_p = X_q$ and $p \neq q$, then $X_p = X_q = 0$. In addition, we also know in advance that $(0, 0, 0, 0)$, is a solution.

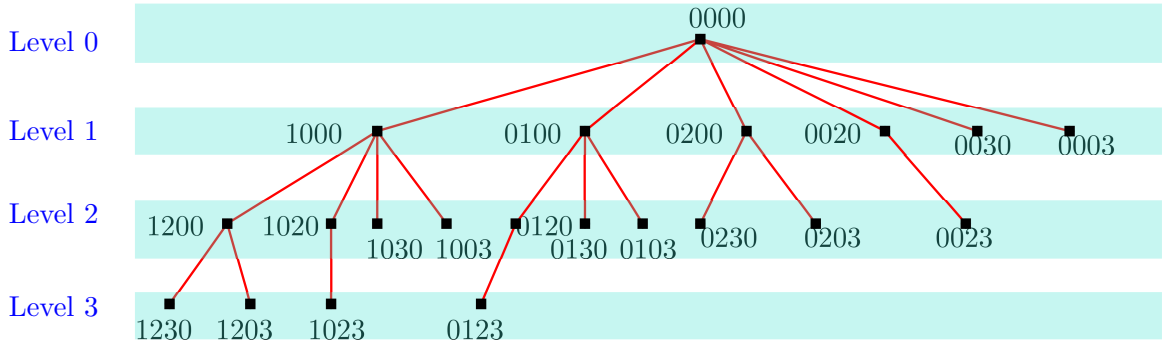

Figure 2.4: Graph Representation of Feasible Joint Events. The height of the tree is min(Number of targets, Number of measurements)

i.e. the hypothesis that all the measurements may have originated from clutter is our starting solution. Starting from the root of the tree at $(0, 0, 0, 0)$, we explore the tree with the specialized DFS algorithm as shown in the hypothesis tree of Figure 2.4.

In general, a feasible joint event ϵ_k is an allocation of measurements to all tracks in the cluster at time k. Let the cardinality of the target and measurement set are such that T_k denotes the number of tracks in the cluster and m_k denotes the number of measurements.Once, the feasible joint events are known, we sub-divide them into two coarse sets [43] $T_0(\epsilon), T_1(\epsilon)$ such that

- $T_0(\epsilon)$: Set of tracks allocated "No measurement".
- $T_1(\epsilon)$: Set of tracks allocated "One measurement".

where, $i(\tau, \epsilon)$: Index of the measurement allocated to track τ under event ϵ_k. Then, the aposteriori probability of joint events is given by:

$$p(\epsilon|Y^k) = c_k^{-1} \prod_{\tau \in T_0(\epsilon)} (1 - P_D P_G p(\chi^\tau|Y^{k-1}) \times \prod_{\tau \in T_1(\epsilon)} P_D P_G p(\chi^\tau|Y^{k-1}) \frac{p_k^\tau(i(\tau,\epsilon))}{\rho_k(i(\tau,\epsilon))} \tag{2.26}$$

where the likelihood $p_k^\tau(i(\tau, \epsilon))$ of measurement $Y_{k,i}$ with respect to track τ, given that measurement $Y_{k,i} \in Y_k^\tau$ is given by:

$$p_k^\tau(i) \equiv p^\tau(Y_{k,i}) = \mathcal{N}(Y_{k,i}; \bar{y}^\tau, S^\tau)/P_G \tag{2.27}$$

Y^k is a measurement sequence $Y_1, Y_2, ..., Y_k$, P_D is probability of detection, P_G is probability of the measurement gating, $p(\chi^\tau|Y^{k-1})$ is probability of object existence, $\rho_k(i(\tau, \epsilon))$ is clutter density at

scan time k and c_k is a normalization constant computed by noting that the feasible joint events are mutually exclusive.

Linear Multi-Target Integrated Probabilistic Data Association: LMIPDA

For LMIPDA, the number of data association operations are linear in the number of targets and measurements. Here, the measurement-to-track associations are computed for each target $\tau = \{1, 2, \ldots, T\}$ treating measurements generated by other targets (non-targets) as clutter. The LMIPDA approach modifies the clutter density to account for the presence of measurements originating from other targets [44] which are also validated by the target under consideration. Once m_k measurements are detected, the apriori data association for each measurement i is approximated as in (2.28)

$$P_{k,i}^{\tau} \approx 1 - P_D(\tau)P_G(\tau)p(\chi^{\tau}|Y^{k-1})\frac{\frac{p_k^{\tau}(i)}{\rho_i(\tau)}}{\sum_{j=1}^{m_k}\frac{p_k^{\tau}(j)}{\rho_i(\tau)}} \tag{2.28}$$

where

$$\rho_i(\tau) = \rho_{k,i}^{\tau} + \sum_{\sigma=1,\sigma\neq\tau}^{T} P_D(\tau)P_G(\tau)p(\chi^{\tau}|Y^{k-1})p_k^{\tau}(j) \tag{2.29}$$

While updating a track, the apriori "scatterer" measurement density of each measurement is obtained from (2.30)

$$\rho_i(\tau) = \rho_{k,i} + \sum_{\sigma=1,\sigma\neq\tau}^{T} p_k^{\tau}(i)\frac{P_{k,i}^{\sigma}}{1 - P_{k,i}^{\sigma}} \tag{2.30}$$

The likelihoods of the each of the selected measurements y_k is assumed to be of the form (2.31)

$$p_k^{\tau}(i) = \begin{cases} \frac{1}{P_G(\tau)}\mathcal{N}\left(y_k(i); \bar{y}_{k|k-1}; S_{\tau,k|k-1}\right) & y_k(i) \in V_k(\tau) \\ 0 & y_k(i) \notin V_k(\tau) \end{cases} \tag{2.31}$$

where $\mathcal{N}(.)$ is a normal pdf with mean $\bar{y}_{k|k-1}$ and covariance $S_{\tau,k|k-1}$.

The a posteriori state estimate pdf is assumed to be Gaussian, i.e. $p(x_k|Y^k) = \mathcal{N}(\hat{x}_{k|k}, P_{k|k})$. The mean $\hat{x}_{k|k}$ and the covariance , $P_{k|k}$ are given by (2.32) and (2.33)

$$\hat{x}_{k|k}(\tau) = \sum_{i=0}^{m_k} \beta_{k,i}(\tau)\hat{x}_{k|k,i}(\tau) \tag{2.32}$$

$$P_{k/k}(\tau) = \sum_{i=0}^{m_k} \beta_{k,i}(\tau)[P_{k|k,i}(\tau) + (x_{k|k,i}(\tau) - \hat{x}_{k|k}(\tau))(x_{k|k,i}(\tau) - \hat{x}_{k|k}(\tau))^T] \tag{2.33}$$

where the weights are computed [44] as follows:

$$\beta_{k,0}(\tau) = \frac{1 - P_D(\tau)P_G(\tau)}{1 - \delta_k^\tau} \tag{2.34}$$

$$\beta_{k,i>0}(\tau) = \frac{P_D(\tau)P_G(\tau)}{1 - \delta_k^\tau} \frac{p_k^\tau(j)}{\tilde{\rho}_i(\tau)} \tag{2.35}$$

$\delta_k(\tau)$ is defined as

$$\delta_k(\tau) = P_D(\tau)P_G(\tau)\left(1 - \sum_{j=1}^{m_k(\tau)} \frac{p_k^\tau(j)}{\tilde{\rho}_i(\tau)}\right) \tag{2.36}$$

Multi-Detection Linear Multi-Target Integrated Probabilistic Data Association: MD-LMIPDA

So far, we have assumed that at most one measurement is generated by a given target. However, high resolution automotive sensors return multiple detections. In light of this, we are entertaining the possibility of multiple detections per target. We define a partitioning scheme as discussed in [45],[46] to handle the multi-detection measurement case. As an illustration, for $\zeta_\tau = 4$, if the set of detections validated for target τ are $z_k = \left\{z_{k,1}^\tau, z_{k,2}^\tau, z_{k,3}^\tau, z_{k,4}^\tau\right\}$, the 16 measurement partitions are listed below.

- $\mathcal{P}_1$: no detections are generated from τ, $\varnothing$
- $\mathcal{P}_{2-5}$: only single detections are generated from τ, $\{z_{k,1}^\tau\}, \{z_{k,2}^\tau\}, \{z_{k,3}^\tau\}, \{z_{k,4}^\tau\}$
- $\mathcal{P}_{6-11}$: only two detections are generated from τ, $\{z_{k,1}^\tau, z_{k,2}^\tau\}, \{z_{k,1}^\tau, z_{k,3}^\tau\}, \{z_{k,1}^\tau, z_{k,4}^\tau\}$,

$\{z^{\tau}_{k,2}, z^{\tau}_{k,3}\}, \{z^{\tau}_{k,2}, z^{\tau}_{k,4}\}, \{z^{\tau}_{k,3}, z^{\tau}_{k,4}\}$

- $\mathcal{P}_{12-15}$: only three detections are generated from τ, $\{z^{\tau}_{k,1}, z^{\tau}_{k,2}, z^{\tau}_{k,3}\}, \{z^{\tau}_{k,1}, z^{\tau}_{k,2}, z^{\tau}_{k,4}\}, \{z^{\tau}_{k,1}, z^{\tau}_{k,3}, z^{\tau}_{k,4}\}, \{z^{\tau}_{k,2}, z^{\tau}_{k,3}, z^{\tau}_{k,4}\}$

- $\mathcal{P}_{16}$: all four detections are generated from τ, $\left\{z^{\tau}_{k,1}, z^{\tau}_{k,2}, z^{\tau}_{k,3}, z^{\tau}_{k,4}\right\}$

For a single target, the data associations will be computed for all the measurement cells enumerated above. Whereas, for multiple targets, the joint data association has to be computed for all targets sharing one or more measurement cells. As the number of measurements and targets increases, this will be a complex problem to solve in real-time. Thus, we maintain the simplifying assumptions of LMIPDA discussed above and feed the measurement partitions to the LMIPDA-based tracker. Similar to LMIPDA, the MD-LMIPDA the data association events are evaluated independently for each target and the contribution of other targets to the measurement cell is accounted for by modifying the clutter density for the target under consideration.

For the sake of brevity, we will denote a measurement cell as z_{ξ_τ, n_τ}, where n_τ is the index within ξ_τ detections that ranges as $1 \leq n_\tau \leq n_{\tau,max}$. For a total number of m_k gated detections, $n_{\tau,max} = \binom{m_k}{\xi_\tau}$. Next, we summarize the steps required to modify the clutter density at the measurement cell z_{ξ_τ, n_τ} [47],[48]. While updating the track for target τ, we compute the prior probability of measurement z_{ξ_τ, n_τ} that it is also a detection of target $\sigma \in T \setminus \tau$ as follows.

$$P^{\sigma}_{k, z_{\xi_\tau, n_\tau}} = P^{\sigma}_{D\xi_\tau} (P^{\sigma}_{G})^{\xi_\tau} P(\mathcal{X}^{\sigma}_{k} | Z^{k-1}) \times \left(\frac{p^{\sigma}_{k, z_{j,i}} / \rho^{\sigma}_{k, z_{j,i}}}{\sum_{j=1}^{\xi_{\tau,max}} \sum_{i=1}^{n_{\tau,max}} p^{\sigma}_{k, z_{j,i}} / \rho^{\sigma}_{k, z_{j,i}}} \right) \tag{2.37}$$

Where, T is a set of targets and $P^{\sigma}_{D\xi_\tau}, P^{\sigma}_{G}, P(\mathcal{X}^{\sigma}_{k} | Z^{k-1})$, are respectively the probability of detection, probablity of gating and probablity of target existence. Z^{k-1} represents gated measurement trajectories up to and including scan $k-1$. For a validated measurment cell z_{ξ_τ, n_τ}, the likelihood $p(z_{\xi_\tau, n_\tau} | \mathcal{X}^{\tau}_{k}, Z^{k-1})$ is computed as follows:

$$p^{\sigma}_{k, z_{\xi_\tau, n_\tau}} = \frac{1}{(P^{\tau}_{G})^{\xi_\tau}} \mathcal{N}\left(z_{\xi_\tau, n_\tau}; \eta_{\xi_\tau}(x^{\tau}_{k}), S_{\xi_\tau, n_\tau}\right) \tag{2.38}$$

Initially, we will treat the non-target measurements as single detections and the contribution to

clutter at the measurement cell z_{ξ_τ,n_τ} is simply computed as follows:

$$\rho^{\sigma}_{k,z_{\xi_\tau,n_\tau}} = \prod_{\forall z_i \in z_{\xi_\tau,n_\tau}} \rho^{\sigma}_{k,z_i} \tag{2.39}$$

The modulated clutter density that accounts for both the pure clutter and the presence of non-targets that share the measurement cell z_{ξ_τ,n_τ} is derived as [47]:

$$\rho^{\tau}_{k,z_{\xi_\tau,n_\tau}} = \sum_{\forall \sigma \in T \setminus \tau} p^{\sigma}_{k,z_{\xi_\tau,n_\tau}} \frac{P^{\sigma}_{k,z_{\xi_\tau,n_\tau}}}{\prod\limits_{\forall z_i \in z_{\xi_\tau,n_\tau}} \left(1 - P^{\sigma}_{k,z_i}\right)} + \prod_{\forall z_i \in z_{\xi_\tau,n_\tau}} \rho^{\tau}_{k,z_i} \tag{2.40}$$

where P^{σ}_{k,z_i} is evaluated by dissociating the measurement cell z_{ξ_τ,n_τ} into single detections.

2.7 Data Collection and Experimental Setup

Experimental studies that were conducted to complement the simulation part of the multi-target tracking problem will be discussed as follows. First, from the perception system perspective stereo camera and mmwave automotive radar are proposed for this work. The main reasons are due to their cost and the resulting robust detection throughput when fused. The camera is a source of the target class (car, person, traffic sign, etc.), the corresponding bounding box, and the depth point cloud relating to the 3D pose of an object. The radar, on the other hand, generates point cloud data of the position in Cartesian x, y, or polar R, θ coordinates. The camera is connected to a GPU which is required for its operation. Various platforms were tested ranging from Jetson tx1, Jetson tx2, Xavier to a PC with NVIDIA® GeForce® GTX 1660 graphics card installed. The first two were unable to match the data rate and storage capacity required in the experiment. While Xavier was able to handle the depth and RGB images at a higher resolution of 1080p (3840x1080) and even 2.2K (4416x1242) at 15Hz frame rate, the large storage capacity (close to 30Gb for 1-minute long experiment) was prohibitive for its further use. The radar detections were recorded as expected apart from the occasional data loss when the camera and radar data were recorded on the same platform. Although, the product manufacturer specified a frame rate support up to 30Hz, operating at that rate proved to be unsuccessful because of exacerbated detection loss. Thus, for the remainder of the experiment, the frame rate of the radar is limited to 20Hz.

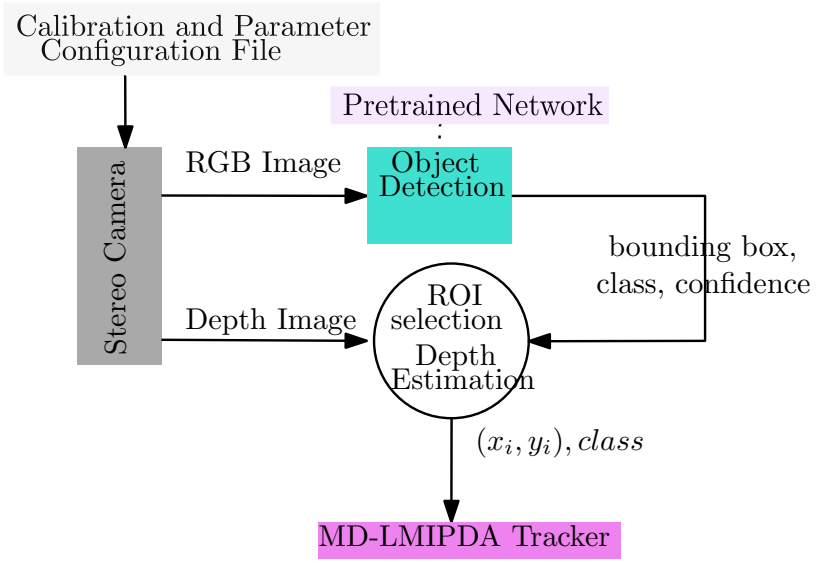

Figure 2.5: Proposed stereo camera configuration for depth estimation.

2.7.1 Target Detection and Distance Estimation from Stereo Camera

The stereo camera uses disparity images from the left and right sensors to estimate the distance from the camera out to objects of interest. It performs better under good illumination and with structured objects to a distance of 20m. The layout for the planned experiment with the stereo camera is diagrammatically depicted in Figure 2.5. It is seen that using different colored cars with varying sizes (compact car to a minivan) affected the detection performance and the distance estimation as well. In addition to RGB image resolution as mentioned above, the distance estimation relied on the quality of the depth image which is specified at different thresholds as ULTRA, QUALITY, MEDIUM, and PERFORMANCE. The quality threshold ULTRA combined with the 2.2k resolution at 15Hz performed better than the remaining combinations which were thought as optional compromises.

A sample frame with the output of the objection detection applied to the raw image is shown in Figure 2.6. The distance estimation beyond $10m$ in front of the camera remained unreliable and unsatisfactory for automotive applications. The estimation error is shown by underestimation or overestimation of depth estimation as compared to the ground truth position of the car obtained from RTK GPS. It was not in agreement with the radar detections that similarly generate measurement around the object boundary. Further, an ROI defined by a rectangular region around the centroid of the bounding box with length and width equal to $0.25, 0.3, 0.5, etc.$ of the corresponding detection box are selected to reduce the estimation uncertainty to no avail.

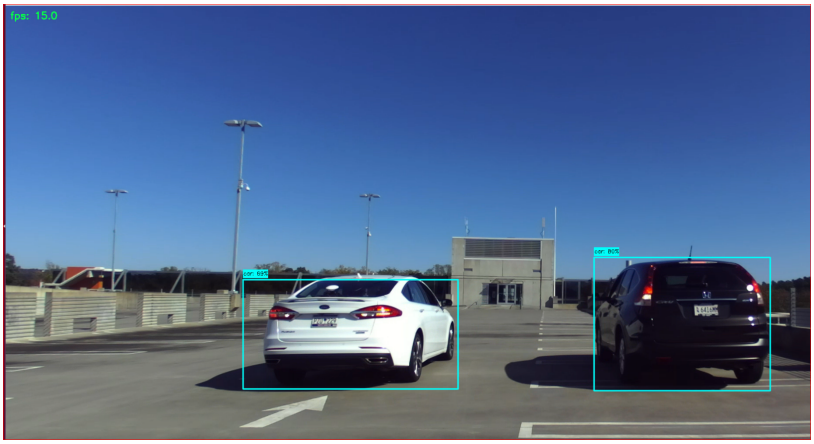

Figure 2.6: Experimental results of stereo camera in object detection and depth estimation.

2.7.2 Target Detection and Distance Estimation from Radar Sensor

The detection of single and multiple targets with the radar sensor is recorded and feed to the multi-detection LM-IPDA tracker. The tracking performance is to be compared to RTK GPS data for performance evaluation and use as a ground truth. The tracking data will be used for single and multiple target scenarios including group and extended targets in the subsequent chapters.

References

[1] B.-n. Vo, M. Mallick, Y. Bar-shalom, S. Coraluppi, R. Osborne III, R. Mahler, and B.-t. Vo, "Multitarget tracking," *Wiley Encyclopedia of Electrical and Electronics Engineering*, pp. 1–15, 1999.

[2] X. Wu, J. Ren, Y. Wu, and J. Shao, "Study on target tracking based on vision and radar sensor fusion," *SAE Technical Paper*, pp. 01–0613, 2018.

[3] C. Qiu, Z. Zhang, H. Lu, and H. Luo, "A survey of motion-based multitarget tracking methods," *Progress In Electromagnetics Research*, vol. 62, pp. 195–223, 2015.

[4] B.-n. Vo, M. Mallick, Y. Bar-shalom, S. Coraluppi, R. Osborne, R. Mahler, and B.-t. Vo, "Multitarget tracking," *Wiley Encyclopedia of Electrical and Electronics Engineering*, 2015.

[5] Y. Bar-Shalom, P. K. Willett, and X. Tian, *Tracking and data fusion*. YBS publishing Storrs, CT, USA:, 2011.

[6] S. Blackman and R. Popoli, "Design and analysis of modern tracking systems(book)," *Norwood, MA: Artech House, 1999.*, 1999.

[7] R. P. Mahler, *Statistical multisource-multitarget information fusion*, vol. 685. Artech House Norwood, MA, 2007.

[8] Y. Bar-Shalom, F. Daum, and J. Huang, "The probabilistic data association filter," *IEEE Control Systems*, vol. 29, pp. 82–100, Dec 2009.

[9] K. Na, J. Byun, M. Roh, and B. Seo, "Fusion of multiple 2d lidar and radar for object detection and tracking in all directions," in *2014 International Conference on Connected Vehicles and Expo (ICCVE)*, pp. 1058–1059, Nov 2014.

[10] M. Attari, S. Habibi, and S. A. Gadsden, "Target tracking formulation of the svsf with data association techniques," *IEEE Transactions on Aerospace and Electronic Systems*, vol. 53, pp. 12–25, Feb 2017.

[11] A. Yilmaz, O. Javed, and M. Shah, "Object tracking: A survey," *ACM Comput. Surv.*, vol. 38, Dec. 2006.

[12] T. E. Fortmann, Y. Bar-Shalom, and M. Scheffe, "Multi-target tracking using joint probabilistic data association," in *1980 19th IEEE Conference on Decision and Control including the Symposium on Adaptive Processes*, pp. 807–812, Dec 1980.

[13] J. Dezert and Y. Bar-Shalom, "Joint probabilistic data association for autonomous navigation," *IEEE Transactions on Aerospace and Electronic Systems*, vol. 29, pp. 1275–1286, Oct 1993.

[14] A. Yilmaz, O. Javed, and M. Shah, "Object tracking: A survey," *Acm computing surveys (CSUR)*, vol. 38, no. 4, p. 13, 2006.

[15] K. O. Arras, S. Grzonka, M. Luber, and W. Burgard, "Efficient people tracking in laser range data using a multi-hypothesis leg-tracker with adaptive occlusion probabilities," in *2008 IEEE International Conference on Robotics and Automation*, pp. 1710–1715, May 2008.

[16] F. Garcia, A. Prioletti, P. Cerri, A. Broggi, A. de la Escalera, and J. M. Armingol, "Visual feature tracking based on phd filter for vehicle detection," in *17th International Conference on Information Fusion (FUSION)*, pp. 1–6, July 2014.

[17] D. Meissner, S. Reuter, and K. Dietmayer, "Road user tracking at intersections using a multiple-model phd filter," in *2013 IEEE Intelligent Vehicles Symposium (IV)*, pp. 377–382, June 2013.

[18] L. Lamard, R. Chapuis, and J. P. Boyer, "Multi target tracking with cphd filter based on asynchronous sensors," in *Proceedings of the 16th International Conference on Information Fusion*, pp. 892–898, July 2013.

[19] E. Özkan, M. B. Guldogan, U. Orguner, and F. Gustafsson, "Ground multiple target tracking with a network of acoustic sensor arrays using phd and cphd filters," in *Information Fusion (FUSION), 2011 Proceedings of the 14th International Conference on*, pp. 1–8, IEEE, 2011.

[20] B.-T. Vo and B.-N. Vo, "Labeled random finite sets and multi-object conjugate priors," *IEEE Transactions on Signal Processing*, vol. 61, no. 13, pp. 3460–3475, 2013.

[21] B.-N. Vo, B.-T. Vo, and D. Phung, "Labeled random finite sets and the bayes multi-target tracking filter," *IEEE Transactions on Signal Processing*, vol. 62, no. 24, pp. 6554–6567, 2014.

[22] F. Kunz, D. Nuss, J. Wiest, H. Deusch, S. Reuter, F. Gritschneder, A. Scheel, M. Stübler, M. Bach, P. Hatzelmann, *et al.*, "Autonomous driving at ulm university: A modular, robust, and sensor-independent fusion approach," in *2015 IEEE intelligent vehicles symposium (IV)*, pp. 666–673, IEEE, 2015.

[23] J. W. Koch, "Bayesian approach to extended object and cluster tracking using random matrices," *IEEE Transactions on Aerospace and Electronic Systems*, vol. 44, no. 3, pp. 1042–1059, 2008.

[24] M. Feldmann and D. Franken, "Advances on tracking of extended objects and group targets using random matrices," in *2009 12th International Conference on Information Fusion*, pp. 1029–1036, IEEE, 2009.

[25] M. Feldmann, D. Franken, and W. Koch, "Tracking of extended objects and group targets using random matrices," *IEEE Transactions on Signal Processing*, vol. 59, no. 4, pp. 1409–1420, 2010.

[26] K. Granstrom, M. Baum, and S. Reuter, "Extended object tracking: Introduction, overview and applications," *arXiv preprint arXiv:1604.00970*, 2016.

[27] J. Lan and X. R. Li, "Tracking of maneuvering non-ellipsoidal extended object or target group using random matrix," *IEEE Transactions on Signal Processing*, vol. 62, no. 9, pp. 2450–2463, 2014.

[28] M. Baum and U. D. Hanebeck, "Random hypersurface models for extended object tracking," in *2009 IEEE International Symposium on Signal Processing and Information Technology (ISSPIT)*, pp. 178–183, IEEE, 2009.

[29] M. Baum and U. D. Hanebeck, "Extended object tracking with random hypersurface models," *IEEE Transactions on Aerospace and Electronic systems*, vol. 50, no. 1, pp. 149–159, 2014.

[30] M. Beard, S. Reuter, K. Granström, B.-T. Vo, B.-N. Vo, and A. Scheel, "Multiple extended target tracking with labeled random finite sets," *IEEE Transactions on Signal Processing*, vol. 64, no. 7, pp. 1638–1653, 2015.

[31] K. Granstrom, C. Lundquist, and O. Orguner, "Extended target tracking using a gaussian-mixture phd filter," *IEEE Transactions on Aerospace and Electronic Systems*, vol. 48, no. 4, pp. 3268–3286, 2012.

[32] K. Granström, M. Fatemi, and L. Svensson, "Gamma gaussian inverse-wishart poisson multi-bernoulli filter for extended target tracking," in *2016 19th International Conference on Information Fusion (FUSION)*, pp. 893–900, IEEE, 2016.

[33] N. Wahlström and E. Özkan, "Extended target tracking using gaussian processes," *IEEE Transactions on Signal Processing*, vol. 63, no. 16, pp. 4165–4178, 2015.

[34] M. Wieneke and W. Koch, "A pmht approach for extended objects and object groups," *IEEE Transactions on Aerospace and Electronic Systems*, vol. 48, no. 3, pp. 2349–2370, 2012.

[35] B. K. Habtemariam, R. Tharmarasa, T. Kirubarajan, D. Grimmett, and C. Wakayama, "Multiple detection probabilistic data association filter for multistatic target tracking," in *14th International Conference on Information Fusion*, pp. 1–6, July 2011.

[36] B. Habtemariam, R. Tharmarasa, T. Thayaparan, M. Mallick, and T. Kirubarajan, "A multiple-detection joint probabilistic data association filter," *IEEE Journal of Selected Topics in Signal Processing*, vol. 7, pp. 461–471, June 2013.

[37] H. Cho, Y. Seo, B. V. K. V. Kumar, and R. R. Rajkumar, "A multi-sensor fusion system for moving object detection and tracking in urban driving environments," in *2014 IEEE International Conference on Robotics and Automation (ICRA)*, pp. 1836–1843, May 2014.

[38] S. Särkkä, *Bayesian filtering and smoothing*, vol. 3. Cambridge University Press, 2013.

[39] R. Rajamani, *Vehicle dynamics and control*. Springer Science & Business Media, 2011.

[40] E. Mazor, A. Averbuch, Y. Bar-Shalom, and J. Dayan, "Interacting multiple model methods in target tracking: a survey," *IEEE Transactions on aerospace and electronic systems*, vol. 34, no. 1, pp. 103–123, 1998.

[41] X. R. Li and V. P. Jilkov, "Survey of maneuvering target tracking. part v. multiple-model methods," *IEEE Transactions on Aerospace and Electronic Systems*, vol. 41, no. 4, pp. 1255–1321, 2005.

[42] B. Zhou and N. Bose, "Multitarget tracking in clutter: Fast algorithms for data association," *IEEE Transactions on Aerospace and Electronic Systems*, vol. 29, no. 2, pp. 352–363, 1993.

[43] T. L. Song, D. MuÃ... Â¡icki, and Y. Kim, "Multi-target tracking with target state dependent detection," in *2012 15th International Conference on Information Fusion*, pp. 324–329, July 2012.

[44] D. Musicki and B. La Scala, "Multi-target tracking in clutter without measurement assignment," *IEEE Transactions on Aerospace and Electronic Systems*, vol. 44, no. 3, pp. 877–896, 2008.

[45] R. Mahler, "Phd filters for nonstandard targets, i: Extended targets," in *2009 12th International Conference on Information Fusion*, pp. 915–921, July 2009.

[46] Y. Huang, T. L. Song, and D. S. Kim, "Linear multitarget integrated probabilistic data association for multiple detection target tracking," *IET Radar, Sonar Navigation*, vol. 12, no. 9, pp. 945–953, 2018.

[47] Y. Huang, T. L. Song, and D. S. Kim, "Linear multitarget integrated probabilistic data association for multiple detection target tracking," *IET Radar, Sonar & Navigation*, vol. 12, no. 9, pp. 945–953, 2018.

[48] D. Musicki, B. F. La Scala, and R. J. Evans, "Multi-target tracking in clutter without measurement assignment," in *2004 43rd IEEE Conference on Decision and Control (CDC) (IEEE Cat. No.04CH37601)*, vol. 1, pp. 716–721 Vol.1, Dec 2004.

This page is intentionally left blank.

Part II

Single Detection Multi-Target Tracking

Introduction to Part II

Part II adapts two single-detection multi-target trackers to track targets as applied to public road traffic. The adaption includes track initiation, termination and maintenance procedures that make these algorithms applicable to a dynamic traffic. A comparison among few of the selected tracking approaches that fall under this category follows next. The comparison is drawn between the Joint Integrated Probability Data Association (JIPDA) and the Linear Multi-target Integrated Probability Data Association (LMIPDA) filters. With the tracking error and computational time demand as a performance metric, we make a decision about an algorithm that will be used for the upcoming part of this work.

For single-detection trackers, two simplifying assumptions are observed:

- The size of the object is such that, the object can be treated as a point-mass compared to the resolution of the sensor. As a consequence, at most one detection is allowed per target vehicle.
- No unresolved measurements exist. i.e. a measurement can have at most one source.

The outline for Part I of the dissertation is organized as follows. In Chapter 3, we use the joint integrated probabilistic data association filter (JIPDAF) and outline methods that relax the clutter density assumption by computing the clutter density from the measurement scan itself. We deploy track maintenance schemes to handle track splitting/merging scenarios. In addition, we include an automatic clustering algorithm for data association computations. In chapter 4, we demonstrate a tracking system based on the Linear Multi-target Integrated Probabilistic Data Association Filter (LMIPDAF), which is capable of unsupervised automation for automated driving systems in multi-target traffic. This includes specific tasks of accommodating target track initiation and track termination, clutter density estimation and handling of data association uncertainties among others. In chapter 5, as an application of the designed multi-target tracker, we use model predictive control (mpc) for the trajectory tracking task of the ego car. The motion prediction for the mpc is based on interacting multiple model.

This page is intentionally left blank.

Chapter 3

Multi Target Tracking: JIPDA Approach

3.1 Introduction

Automated driving systems of emerging and future vehicles need to resolve the behaviors of other traffic participants or targets in order to safely navigate in public traffic [1]. In this paper, a comprehensive multi-target tracking system is outlined that addresses target birth/appearance and death/disappearance processes in the presence of measurement data association uncertainties. The tracking system is based on the joint integrated probabilistic data association filter, which is adapted to specifically include algorithms that handle track initiation and termination, clutter density estimation and track maintenance. The workings of the proposed algorithms are demonstrated via multiple traffic scenario simulations that show how tracks can be initialized and terminated autonomously, and how data association uncertainties can affect tracking performance if not handled correctly.

[1] The content of this chapter is based on the conference paper *A. Hunde and B. Ayalew, "Automated multi-target tracking in public traffic in the presence of data association uncertainty," in 2018 Annual American Control Conference (ACC), pp. 300–306, June 2018.*

3.2 Related Works

In the modern push towards increased automation of road vehicles, a proposed taxonomy by SAE (and NHTSA) outlines six discrete automation levels[1] . Central to this taxonomy is the respective roles of the (human) operator and the driving automation system in relation to each other. At the higher levels of automation (3, 4 and 5), the automated driving system executes most of the dynamic driving task. The most important subtask being the environmental perception, which includes real-time monitoring of the roadway environment for detection, recognition, and classification of objects and events. The objective of this paper is to outline a tracking system capable of unsupervised automation of the perception process for automated driving systems in multi-target traffic. This includes the tasks of accommodating target birth (appearance or track initiation) and death events (disappearance or track termination), clutter density estimation, clustering of targets, track splitting/merging in the presence of data association uncertainty. These tracking functionalities can help facilitate perception during common events in public traffic as participants change lanes, navigate intersections, overtake, and/or brake in emergencies.

Multi-target tracking (MTT) systems aim to estimate both the number and the states of targets in the presence of process and measurement noise, false alarms, measurement origin uncertainty, missed detection, and birth/death processes [2, 3]. MTT methods can generally be classified into two groups: Detect-before-Track (DBT) methods and Track-before-Detect (TBD) schemes. The main idea in the later approach is to search all possible tracks and select the most possible one as the output. The advantage is that it can accumulate target information by multiple frames in low signal to noise ratio (SNR) scenarios. However, this comes at the cost of complex computation; moreover, the track output is time-delayed too[2]. With the DBT methods, on the other hand, a set of detections are first produced from raw sensor returns and then the detections are fed into the tracking algorithms. A number of MTT algorithms are used at present in various tracking applications, with the most popular being the joint probabilistic data association filter (JPDAF), multiple hypothesis tracking (MHT), and random finite set (RFS) based multi-target filters [4, 5, 6]. Here, we give a brief discussion of each of these approaches.

The JPDAF uses joint association events and joint association probabilities in order to avoid conflicting measurement to track assignments. [7, 8, 9, 10, 11, 12] However, it assumes a fixed and known number of targets[3, 13]. MHT is a deferred decision approach to data association based

MTT. At each observation time, the MHT algorithm attempts to propagate and maintain a set of association hypotheses with high posterior probability or track score. In this way, the MHT approach inherently handles initiation and termination of tracks, and hence accommodates an unknown and time-varying number of targets [3][14]. The RFS approach represents the multi-target state as a finite set of single-target states, and the MTT problem is formulated as a dynamic multi-target state estimation problem [3]. Some practical implementations of RFS include: the probability hypothesis density (PHD) filter [15, 16], the cardinalized PHD (CPHD) filter [17, 18] and the Generalized Labeled Multi-Bernoulli (GLMB) filter [19, 20, 21].

In this paper, we use the joint integrated probabilistic data association filter (JIPDAF)[22, 23, 24, 25, 26, 27] and we outline methods that relax the clutter density assumption by computing this density from the measurement scan itself. While also including provisions for target birth and death events by propagating target existence probabilities, we deploy track maintenance schemes to handle track splitting/merging scenarios [28, 29, 30, 31, 32, 33]. In addition, we include an automatic clustering algorithm for data association computations. We believe that operating in public traffic calls for the automated driving system to have practical solutions for automatic track initiation and termination, clutter density estimation, target existence based track maintenance, data association computations in order to achieve full autonomy in regard to its perception system.

The rest of the paper is organized as follows. In Section 3.3, we outline how the overall tracking system fits in the overall automated driving system architecture and its constituent parts. In Section 3.4, we discuss the details of the filtering steps. In Section 3.5, we present some illustrative results of the applications of the algorithms on typical traffic scenarios. The paper ends by summarizing the conclusions of the work in Section 3.6.

3.3 Architecture of the Tracking System

The overall tracking system architecture and its constituent parts are shown in Figure 3.1. In the measurement step, raw measurement data is extracted out of sensors such as radars, laser scanners and vision-based systems by applying relevent signal processing algorithms. In the segmentation procedure, the raw measurement data is segmented and clustered into objects. Next, an object classification step aims at sorting objects into different classes such as vehicles, bicycles and pedes-

trians. In the next step, a data association procedure seeks to include new measurements in which the target(s) that most probably produced the measurement is identified. In the filtering step, the position of the objects/vehicles needs to be estimated over time based on appropriate motion models. Facilities to handle missed measurements, accommodate automatic track initiation and termination as well as clustering are also included in this step [34]. The higher module in the hierarchy includes route and predictive motion planning and feedback control schemes which subsequently generate the steering, throttle and brake commands for the ego vehicle. The latter are studied extensively elsewhere (see, for example, [35]. In this paper, we concentrate on the modules indicated in the three shaded blocks in Figure 3.1.

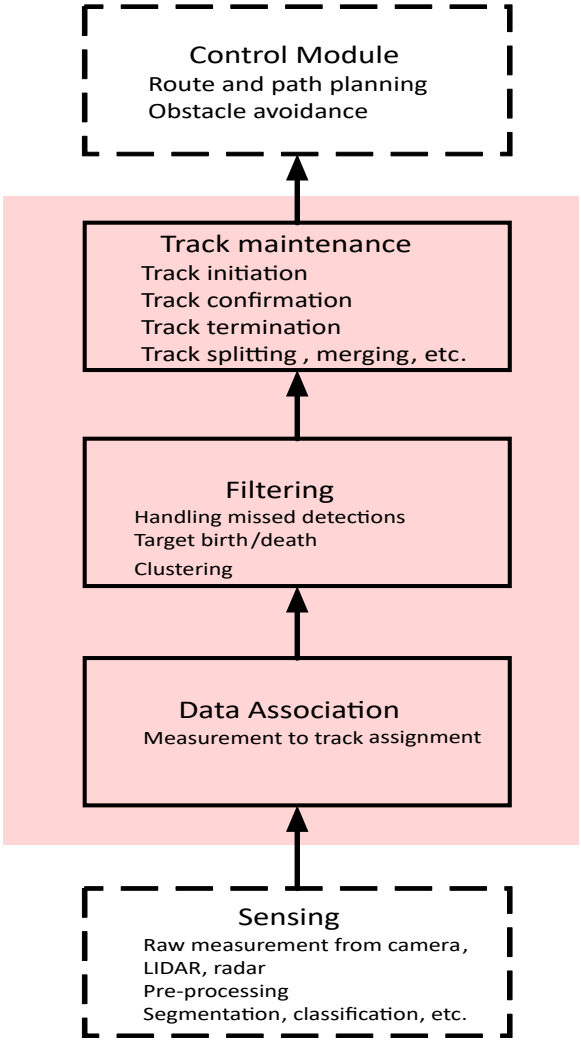

Figure 3.1: Overall tracking system architecture as part of the automated driving system

3.3.1 Measurement Data Association

As mentioned above, the data association step associates new measurements to the likely targets that generated each measurement. In this paper, we computed the data association problem via a search algorithm [36].

To illustrate the main concepts involved, we consider four targets vehicles, T_1—T_4, selecting 10 measurements, M_1—M_{10} as shown in Figure 3.2. A partial list of feasible joint events is tabulated in Table 3.1. In target tracking, one always knows a starting solution, which is the possibility of all measurements coming from clutter. The selected measurement set $Z(k)$ becomes the union of measurements validated by each target or track belonging to a cluster of objects. Hereafter, we use the terms target or track interchangeably to refer to objects being tracked. A feasible joint event

Table 3.1: Feasible Events

ϵ	T_1	T_2	T_3	T_4
1	0	0	0	0
.	.	.	.	.
.	.	.	.	.
.	.	.	.	.
217	3	0	0	4
218	3	0	0	5
219	3	0	0	10

ϵ_k is an allocation of measurements to all tracks in the cluster at time-step k, with T_k denoting the number of tracks in the cluster and m_k denoting the number of measurements. The following definitions regarding feasible joint event (FJE) ϵ_k are needed [37].

$T_0(\varepsilon_k)$: The set of tracks allocated "No measurement" under event ϵ_k.

$T_1(\varepsilon_k)$: The set of tracks allocated "One measurement" under event ϵ_k.

$i(\tau, \varepsilon_k)$: Index of the measurement allocated to track τ under event ϵ_k.

$\Xi(\tau, i)$: The set of feasible joint events which allocate measurement i to track τ. Then, the a posteriori probability of joint events is given as follows.

$$p(\epsilon|Y^k) = c_k^{-1} \prod_{\tau \in T_0(\epsilon)} (1 - P_D P_G p(\chi^\tau|Y^{k-1}) \times \prod_{\tau \in T_1(\epsilon)} P_D P_G p(\chi^\tau|Y^{k-1}) \frac{p_k^\tau(i(\tau,\epsilon))}{\rho_k} \tag{3.1}$$

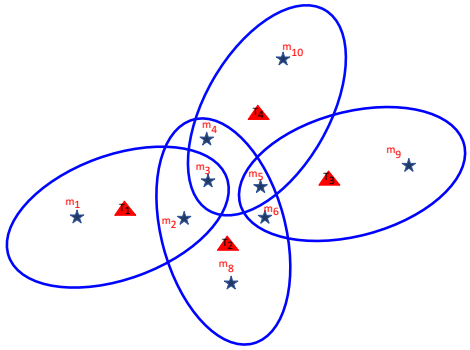

Figure 3.2: An illustration of data association: 4 targets and 10 measurement sets

where the likelihood $p_k^\tau(i(\tau,\epsilon))$ of measurement $Z_{k,i}$ with respect to track τ, given that measurement $Z_{k,i} \in z_k^\tau$ is given by:

$$p_k^\tau(i) \equiv p^\tau(Z_{k,i}) = \mathcal{N}(Z_{k,i}; \bar{y}^\tau, S^\tau)/P_G \tag{3.2}$$

where: Y^k is a measurement sequence $y_1, y_2, ..., y_k$, P_D is the probability of target detection, P_G is probability of the measurement gating, $p(\chi^\tau|Y^{k-1})$ is the probability of object existence given all the past measurements, ρ_k is a clutter density at scan time k.

3.3.2 Target Existence Estimation

In public traffic, targets may randomly enter and exit the surveillance space FOV of the sensor); thus the existence of targets is a priori unknown. The probability of target existence can be computed and used as a decision parameter to confirm or terminate tracks. The tracking system can be designed to terminate tracks with a probability of existence below a given threshold or confirm a track if it is above that threshold. The target existence propagation is modeled as a Markov process. Denote by $\chi_{k,i}$ the target existence event at time k. The probability that the target exists at measurement time k, given that it did exist at $k-1$ is [37]:

$$P\{\chi_k \,|\, \chi_{k-1}\} = 1 - \frac{\Delta T_{k-1,k}}{T_{ave}} \tag{3.3}$$

where $\Delta T_{k-1,k}$ denotes the time interval between measurement times $k-1$ and k, and T_{ave} denotes the average duration of target existence in the surveillance space. The complementary probability $P\{\chi_k \,|\, \overline{\chi}_{k-1}\}$ that the target exists at time k, given that it did not exist at $k-1$ is assumed to be zero. The targets which did not exist at $k-1$ and then appear at k are new targets and their tracks

will be separately initialized by their measurements.

In this paper, we use the Markov Chain One model in which, if the target exists, it is always detectable, i.e., the target measurement exists in each scan with a probability of detection P_D (which in this case depends on the target trajectory state). In each scan, each existing target generates zero or one measurement.

3.3.3 Target Birth and Death Process (Track Initialization and Termination)

Figure 3.3 shows two target vehicles which were not initially inside the FOV of the ego vehicle, but can suddenly appear as birth processes in the FOV during motion of the ego vehicle. Automatic target tracking systems initialize tracks using measurements. Both true tracks (which follow targets) and false tracks (which do not follow any target) may be present. In this paper we use one point initialization on each measurement not used in the update step to initialize a new track. Prior information on target velocity and acceleration vectors are, as a rule, limited to the maximum speed v_{max} and (sometimes) the maximum acceleration a_{max} of the class of targets of interest. The key to one point initialization is to assume 0 mean velocity (acceleration), and choose the covariance of each velocity component equal to, say, $v_{\max}^2/3$ (or $v_{\max}^2/4$), the components being mutually uncorrelated [38].

A death process happens when objects suddenly fall out of the FOV of the ego-vehicle. A speeding target T_1 as shown in Figure 3.3, or a target changing to a different lane or exiting through a ramp are examples of target death processes. A target may also be undetectable due to the characteristic behavior of the sensing system or owing to its geometric size or color, it may go undetected. Thus, due to one or more of these reasons, if a target goes undetected during consecutive scans, the corresponding track will be terminated. However, temporary loss of measurement is not a reason for track termination as the target may still be available in subsequent scan times. The surrounding infrastructure and the environment may temporarily cast shadows, obstruct signals, cause multi-path fading delays and thus contribute to missing measurements.

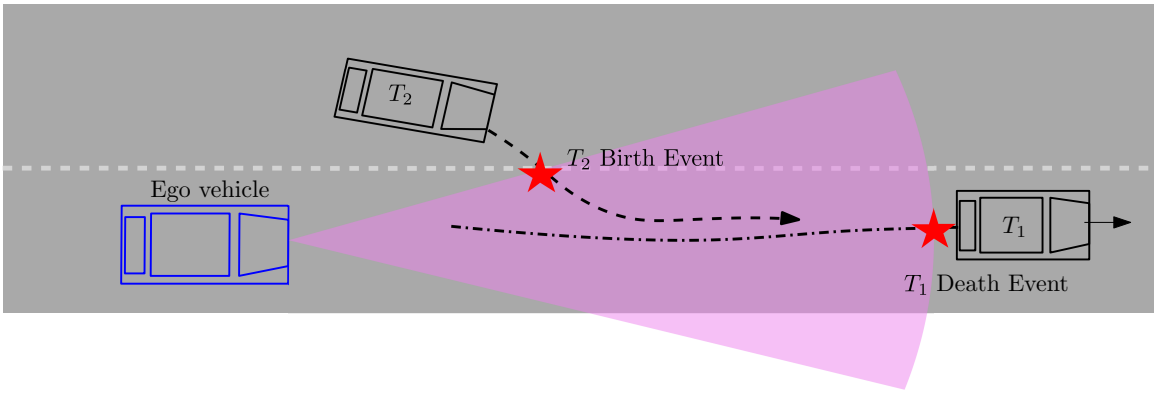

Figure 3.3: Illustration of target birth and death processes: T_1 will register as a birth process after its detection is available within the sensor's FoV. When T_2 accelerates beyond the FOV of the ego vehicle, a death event is registered.

3.4 Filtering

Let us consider a discrete time stochastic model of a target vehicle described by Markov transition density f:

$$x_k \sim f(x_k|x_{k-1}) \tag{3.4}$$

where, x_k is the motion (position, velocity and acceleration) state of the target at time k, $x_k \in \mathbb{R}^n$.

Likewise, we model the measurement or observation process as follows.

$$y_k \sim g(y_k|x_k) \tag{3.5}$$

$y_k \in \mathbb{R}^m$. In this paper, we only consider the common setting where sensor measurements at each instance have been preprocessed into a set of points or clusters. The Bayesian filtering equations for estimating the state of the targets then proceed as follows: [39]

- **Initialization**. The recursion starts from the prior distribution $p(x_0)$
- **Prediction step**. The predictive distribution of the state x_k at the time step k, given the dynamic model, can be computed by the Chapman-Kolmogorov equation

$$p(x_k|y_{1:k-1}) = \int p(x_k|x_{k-1})p(x_{k-1}|y_{1:k-1})dx_{k-1} \tag{3.6}$$

- **Update step**. Given the measurement y_k at time step k, the posterior distribution of the

state x_k can be computed by Bayes' rule

$$p(x_k|y_{1:k}) = \frac{1}{Z_k} p(y_k|x_k) p(x_k|y_{1:k-1}) \tag{3.7}$$

where the normalization constant Z_k is given as

$$Z_k = \int p(y_k|x_k) p(x_k|y_{1:k-1}) dx_k \tag{3.8}$$

Here, a number of alternative methods can be applied to recursively predict and update the estimate of the motion state of the targets; however, the computational requirements of each approach should be examined to meet the realtime requirements of target tracking in public traffic. In addition, to be practically useful the algorithm should have mechanisms in place or be flexible enough to add track initiation, track termination, clutter density estimation, target existence based track maintenance, and data association handling in order to achieve full autonomy. The tracking system outlined in this paper is based on joint integrated probabilistic data association filter (JIPDAF). The state estimation proceeds with the above Bayesian filter and the target existence is predicted as in Equation 3.3. Then, the measurement selection for each target is based on a validation gate which is defined around the prediction/estimate. Figure 3.4 illustrates the effect of variation of gate size on measurement validation. Mathematically, We define a validation gate as:

$$G = y_k \in \mathcal{R}^n : \left[y_k - H\hat{x}_{k|k-1}\right]^T S_{k|k-1}^{-1} \left[y_k - H\hat{x}_{k|k-1}\right] \leq \gamma \tag{3.9}$$

where $H\hat{x}_{k|k-1}$, is the predicted measurement, y_k is the received measurement,$S_{k|k-1}$ is the measurement covariance,$\sqrt{\gamma}$ is the gate size and the n-dimensional gate volume is given by:

$$V_k = \frac{\pi^{n/2}}{\Gamma(\frac{n}{2}+1)} \sqrt{|S(k)|} \gamma^{1/2} \tag{3.10}$$

For the sake of clutter density estimation, the track validation window is approximated by the union of the individual target validation windows [22].

$$V_k \approx \max \left(\sum_{\tau=1}^{N_\tau(k)} V_k(\tau) \frac{m_k}{\sum_\tau m_k(\tau)}, \max V_k(\tau) \right) \tag{3.11}$$

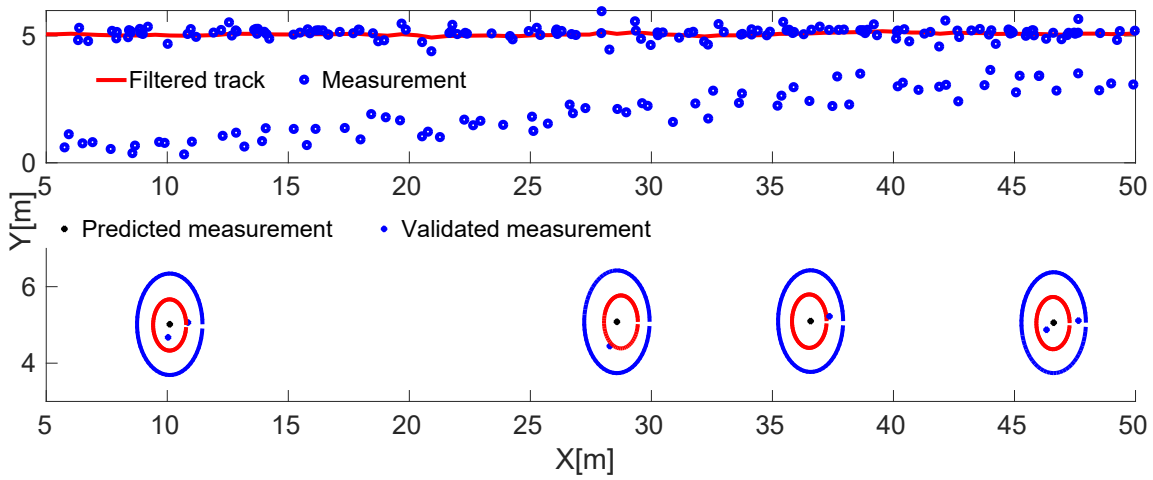

Figure 3.4: Evolution of measurement selection by a target (blue ellipses), note how a measurement from a close target is validated at some scan steps. The red ellipses are validation gates for small $\gamma = 4$ or $P_G = 0.739$ and the blue ellipses correspond to large $\gamma = 16$ or $P_G = 0.9997$.

where $N_\tau(k)$ is the number of targets and $V_k(\tau)$ is the validation gate of a target τ. The total number of expected clutter measurements equals

$$\hat{m_k} = \sum_{j=1}^{m_k} \prod_{\tau} \left(1 - P_D P_G p(\chi^\tau | Y^{k-1}) \frac{p_k^\tau(i)}{\sum_j p_k^\tau(j)} \right) \tag{3.12}$$

The clutter density is then approximated as

$$\rho = \frac{\hat{m_k}}{V_k} \tag{3.13}$$

where $p_k^\tau(i)$ is the likelihood of measurement $y_k(i)$ with respect to track τ and m_k is the number of selected measurements. In addition to treating individual targets for tracking, we also cluster them together based on the overlap observed in the validated measurements at that scan time as in Figure 3.5. The purpose of clustering is to minimize the number of operations by separating the tracks into groups or clusters. For computational reasons, at each scan k tracks are separated in clusters of tracks which share selected measurements. The tracks and their selected measurements belong to the cluster. For each measurement and target in the cluster, the data association computations are performed simultaneously and can not be parallelized. However, different clusters are treated independently, and are parallelized [40] to save computation time.

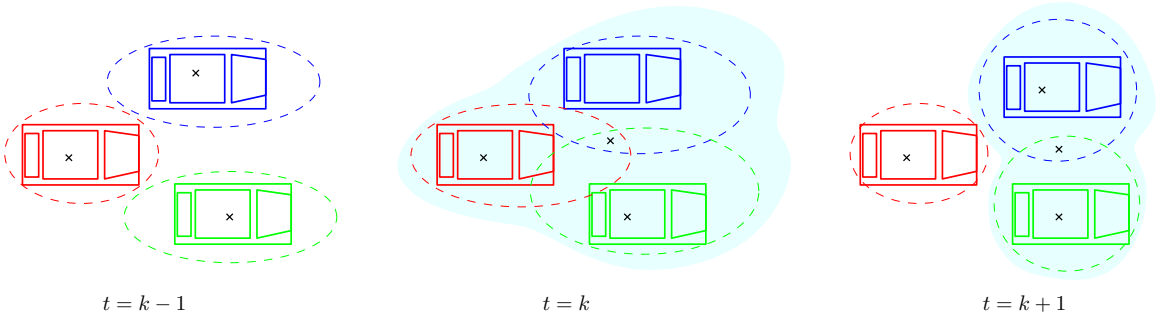

Figure 3.5: Cluster evolution: merging and splitting of targets. Ellipses represent validation gates that select measurements (shown as crosses) for each target. Clusters of targets (shown by the shaded region) are autonomously created and include all targets and corresponding validated measurements.

3.5 Results and Discussions

3.5.1 Model of Targets and Sensors

To illustrate, the workings and performance of the proposed schemes, we consider the target traffic object motion to be modeled by:

$$x_k = Fx_{k-1} + v_k \tag{3.14}$$

Assuming that the sensor measurement is a linear function of the target state, we have:

$$y_k = Hx_k + w_k \tag{3.15}$$

v_k and w_k are white, uncorrelated, Gaussian noise sequences with a zero mean and covariance Q_k and R_k, respectively; and the prior conditional pdf of target state $p(x_{k-1}|y_{k-1})$ is a Gaussian density with mean $\hat{x}_{k-1|k-1}$ and covariance $P_{k-1|k-1}$. For our simulations, we consider the mathematical model of a traffic object in motion with an uncertain acceleration input (i.e, we model it with continuous Wiener process acceleration (CWPA)), whose F, H, R_k, and Q_k matrices are easy to construct and can be found in the appendix.

3.5.2 Simulation Results

Target Birth (Track Initiation)

Figure 3.6 shows the situation in a traffic intersection where the initial states for the targets are as follows: $T_1 = [6\ 0\ 0\ 15\ 0\ 2]^T$, $T_2 = [2\ 0\ 0\ 15\ 0\ 2]^T$, $T_3 = [-2\ 50\ 0\ -15\ 0\ -2]^T$.

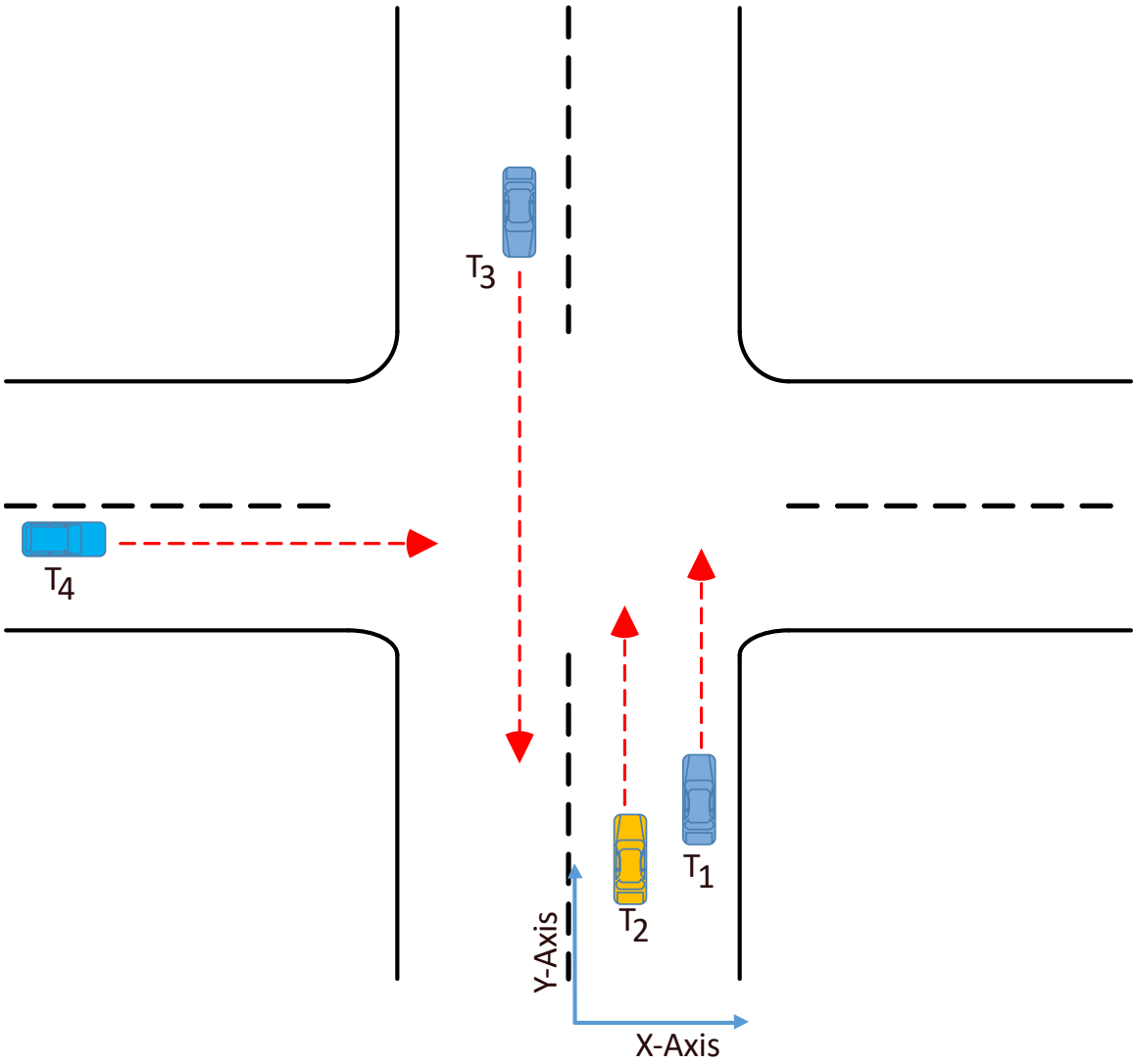

Figure 3.6: Public traffic intersection scenario: T_4 is introduced at a scan time $k = 50$; T_1, T_2, T_3 are persistent throughout the simulation

The new target T_4 is tracked starting from scan time 51. At scan time 50, this track is assigned to one of the tentative tracks initiated based on measurement sets not used in the update step. These new tracks will not be confirmed until three further consecutive measurements are validated. Figure 3.7 illustrates a birth process as a new target is correctly initiated and being tracked.

Data Association in Traffic Intersection, I

Five target vehicles with initial states as follows are simulated.

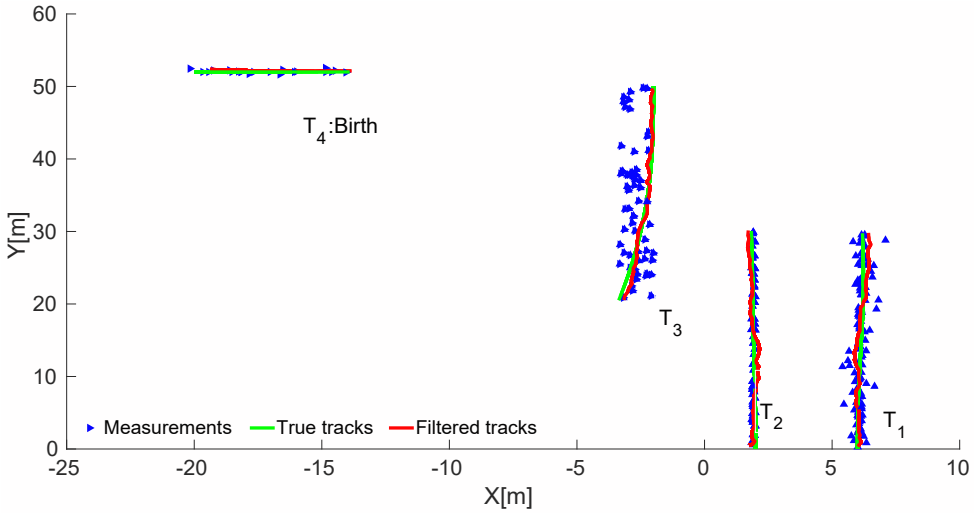

Figure 3.7: Public traffic intersection scenario: Intersection : T_4 is being tracked starting $t(k) = 51$; T_1, T_2, T_3 are all persistent throughout the simulation

$$T_1 = \begin{bmatrix} 6 & 0 & 0 & 15 & 0 & 2 \end{bmatrix}^T,$$

$$T_2 = \begin{bmatrix} 2 & 0 & 0 & 15 & 0 & 2 \end{bmatrix}^T,$$

$$T_3 = \begin{bmatrix} -60 & 52 & 20 & 0 & 2 & 0 \end{bmatrix}^T,$$

$$T_4 = \begin{bmatrix} -2 & 50 & 0 & -15 & 0 & -2 \end{bmatrix}^T,$$

$$T_5 = \begin{bmatrix} -2 & 50 & 0 & -15 & 0 & -2 \end{bmatrix}^T.$$

Figure 3.9 shows that targets 1 and 3 share measurement at $t(k) = 95$, thus they are clustered together to evaluate the posterior data association probability that will be used in the update step. The computations show that the probability of a correct measurement assignment is 0.0815. Whereas, the largest posterior data association probability is 0.7225 and it assigns measurement 1 to target 1 and target 3 is not assigned measurement according to this event. This is what is actually used in the update step. We could have updated the track with a wrong measurement and hence missed the track if we had to use the 'nearest' measurement as is the case in global nearest neighbor filter. In dense traffic, where targets are moving close to each other and data associations are more frequent, such data miss associations result in tracking loss leading to an incorrect count of number of targets and their states.

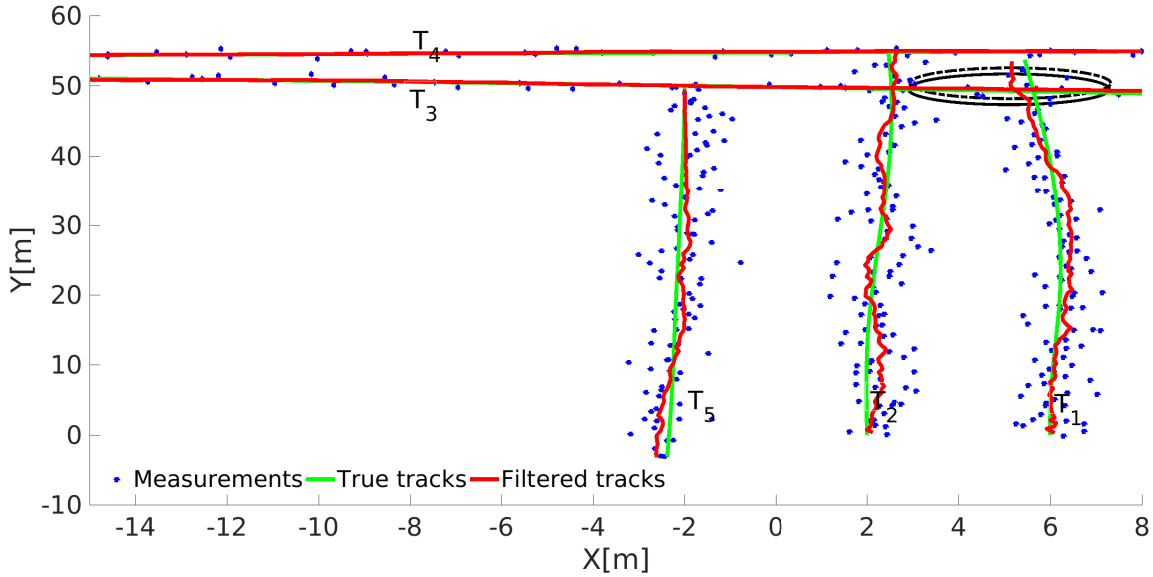

Figure 3.8: Public traffic intersection scenario: At $t(k) = 95$, T_1 and T_3 share measurements. The elliptical validation gates are also shown.

Data Association in Traffic Intersection, II

With the five targets as initialized above, targets 1, 2 and 3 share measurements at $t(k) = 93$, thus they are clustered together to evaluate the posterior data association probability that will be used in the update step of the filtering algorithm. The three validation gates corresponding to the three targets are seen to overlap as shown in Figure 3.9. For this particular scan time, the posterior data association probabilities are computed and are tabulated in Table 3.2. The results show that the probability of correct measurement assignment (Event 4) has the highest posterior data association probability of 0.9535 and hence this event has more weight in the update step than the other 15 events shown in the table. This event (Event 4) assigns measurements to each target correctly.

Table 3.2: Posterior joint probability of feasible events

Event	T_1	T_2	T_3	Data association probability
1	0	0	0	0.0000
2	1	0	0	0.0000
3	1	0	3	0.0032
4	1	2	3	0.9535
5	1	0	2	0.0002
6	1	3	2	0.0271
7	1	3	0	0.0025
8	1	2	0	0.0046
9	0	0	3	0.0000
10	0	2	3	0.0076
11	0	0	2	0.0000
12	0	3	2	0.0002
13	0	0	1	0.0000
14	0	3	1	0.0009
15	0	3	0	0.0000
16	0	2	0	0.0000

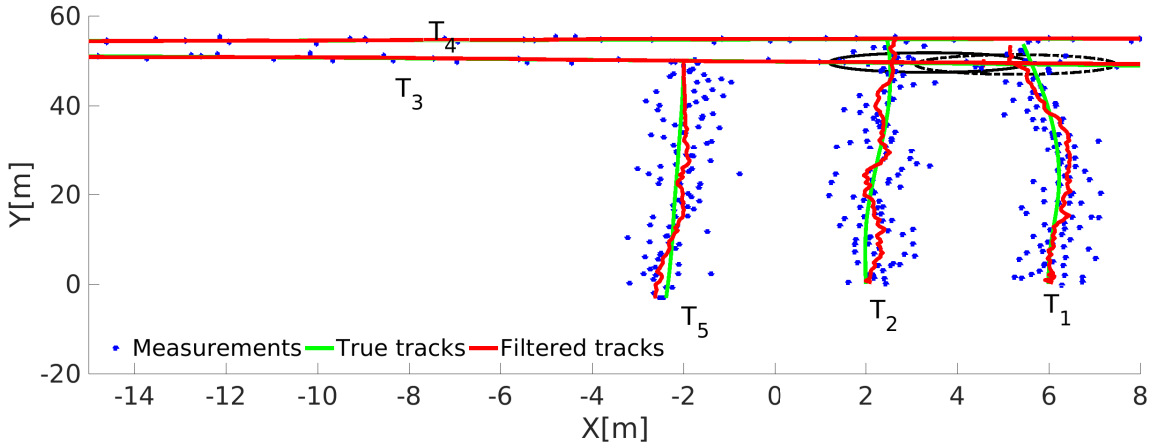

Figure 3.9: Public traffic intersection scenario: At $t(k) = 93$, T_1,T_2 and T_3 share measurements. The elliptical validation gates are also shown here.

3.6 Conclusion

In this paper, we have outlined functions that an automatic tracking system should have in order to enable a highly automated vehicle operate in public road traffic. The randomness in the number of vehicles that enter or leave a public road through ramps, vehicles that execute lane changes or split and/or merge into groups or negotiate intersections all call for such an automatic tracking system.

This paper has outlined probabilistic target existence estimation, track initiation and termination, filtering and data association algorithms that can apply for these situations. The workings and performance of the algorithm has been demonstrated with simulation of a public traffic intersection scenario. It is shown that successful track initiation and high confidence measurement data association can be achieved with the outlined functions. These above issues including clutter estimation, track maintenance, and clustering of targets are part of this work.

As a future work, higher-order motion (such as interactive multi-model) descriptions of traffic objects will be used to further demonstrate the workings of the proposed automatic tracking functions in even more complex traffic scenarios. Eventually, these functions will be tested along with control modules on prototype automated driving systems.

References

[1] S. I. J3016, "Taxonomy and definitions for terms related to driving automation systems for on-road motor vehicles," 2016.

[2] C. Qiu, Z. Zhang, H. Lu, and H. Luo, "A survey of motion-based multitarget tracking methods," *Progress In Electromagnetics Research*, vol. 62, pp. 195–223, 2015.

[3] B.-n. Vo, M. Mallick, Y. Bar-shalom, S. Coraluppi, R. Osborne, R. Mahler, and B.-t. Vo, "Multitarget tracking," *Wiley Encyclopedia of Electrical and Electronics Engineering*, 2015.

[4] Y. Bar-Shalom, P. K. Willett, and X. Tian, *Tracking and data fusion.* YBS publishing Storrs, CT, USA:, 2011.

[5] S. Blackman and R. Popoli, "Design and analysis of modern tracking systems(book)," *Norwood, MA: Artech House, 1999.*, 1999.

[6] R. P. Mahler, *Statistical multisource-multitarget information fusion*, vol. 685. Artech House Norwood, MA, 2007.

[7] Y. Bar-Shalom, F. Daum, and J. Huang, "The probabilistic data association filter," *IEEE Control Systems*, vol. 29, pp. 82–100, Dec 2009.

[8] K. Na, J. Byun, M. Roh, and B. Seo, "Fusion of multiple 2d lidar and radar for object detection and tracking in all directions," in *2014 International Conference on Connected Vehicles and Expo (ICCVE)*, pp. 1058–1059, Nov 2014.

[9] M. Attari, S. Habibi, and S. A. Gadsden, "Target tracking formulation of the svsf with data association techniques," *IEEE Transactions on Aerospace and Electronic Systems*, vol. 53, pp. 12–25, Feb 2017.

[10] A. Yilmaz, O. Javed, and M. Shah, "Object tracking: A survey," *ACM Comput. Surv.*, vol. 38, Dec. 2006.

[11] T. E. Fortmann, Y. Bar-Shalom, and M. Scheffe, "Multi-target tracking using joint probabilistic data association," in *1980 19th IEEE Conference on Decision and Control including the Symposium on Adaptive Processes*, pp. 807–812, Dec 1980.

[12] J. Dezert and Y. Bar-Shalom, "Joint probabilistic data association for autonomous navigation," *IEEE Transactions on Aerospace and Electronic Systems*, vol. 29, pp. 1275–1286, Oct 1993.

[13] A. Yilmaz, O. Javed, and M. Shah, "Object tracking: A survey," *Acm computing surveys (CSUR)*, vol. 38, no. 4, p. 13, 2006.

[14] K. O. Arras, S. Grzonka, M. Luber, and W. Burgard, "Efficient people tracking in laser range data using a multi-hypothesis leg-tracker with adaptive occlusion probabilities," in *2008 IEEE International Conference on Robotics and Automation*, pp. 1710–1715, May 2008.

[15] F. Garcia, A. Prioletti, P. Cerri, A. Broggi, A. de la Escalera, and J. M. Armingol, "Visual feature tracking based on phd filter for vehicle detection," in *17th International Conference on Information Fusion (FUSION)*, pp. 1–6, July 2014.

[16] D. Meissner, S. Reuter, and K. Dietmayer, "Road user tracking at intersections using a multiple-model phd filter," in *2013 IEEE Intelligent Vehicles Symposium (IV)*, pp. 377–382, June 2013.

[17] L. Lamard, R. Chapuis, and J. P. Boyer, "Multi target tracking with cphd filter based on asynchronous sensors," in *Proceedings of the 16th International Conference on Information Fusion*, pp. 892–898, July 2013.

[18] E. Özkan, M. B. Guldogan, U. Orguner, and F. Gustafsson, "Ground multiple target tracking with a network of acoustic sensor arrays using phd and cphd filters," in *Information Fusion (FUSION), 2011 Proceedings of the 14th International Conference on*, pp. 1–8, IEEE, 2011.

[19] B.-T. Vo and B.-N. Vo, "Labeled random finite sets and multi-object conjugate priors," *IEEE Transactions on Signal Processing*, vol. 61, no. 13, pp. 3460–3475, 2013.

[20] B.-N. Vo, B.-T. Vo, and D. Phung, "Labeled random finite sets and the bayes multi-target tracking filter," *IEEE Transactions on Signal Processing*, vol. 62, no. 24, pp. 6554–6567, 2014.

[21] F. Kunz, D. Nuss, J. Wiest, H. Deusch, S. Reuter, F. Gritschneder, A. Scheel, M. Stübler, M. Bach, P. Hatzelmann, *et al.*, "Autonomous driving at ulm university: A modular, robust, and sensor-independent fusion approach," in *2015 IEEE intelligent vehicles symposium (IV)*, pp. 666–673, IEEE, 2015.

[22] D. Musicki and R. Evans, "Joint integrated probabilistic data association: Jipda," *IEEE transactions on Aerospace and Electronic Systems*, vol. 40, no. 3, pp. 1093–1099, 2004.

[23] D. Musicki and R. J. Evans, "Multiscan multitarget tracking in clutter with integrated track splitting filter," *IEEE Transactions on Aerospace and Electronic Systems*, vol. 45, no. 4, pp. 1432–1447, 2009.

[24] Y. Xie, Y. Huang, and T. L. Song, "Iterative joint integrated probabilistic data association filter for multiple-detection multiple-target tracking," *Digital Signal Processing*, vol. 72, pp. 232–243, 2018.

[25] D. Musicki and R. J. Evans, "Target existence based mht," in *Proceedings of the 44th IEEE Conference on Decision and Control*, pp. 1228–1233, IEEE, 2005.

[26] D. Musicki, R. Evans, and S. Stankovic, "Integrated probabilistic data association," *IEEE Transactions on automatic control*, vol. 39, no. 6, pp. 1237–1241, 1994.

[27] D. Musicki, S. Challa, and S. Suvorova, "Automatic track initiation of manoeuvring target in clutter," in *2004 5th Asian Control Conference (IEEE Cat. No. 04EX904)*, vol. 2, pp. 1009–1015, IEEE, 2004.

[28] D. Musicki and S. Suvorova, "Tracking in clutter using imm-ipda-based algorithms," *IEEE Transactions on Aerospace and Electronic Systems*, vol. 44, no. 1, pp. 111–126, 2008.

[29] H. A. Blom, E. A. Bloem, and D. Musicki, "Jipda: Automatic target tracking avoiding track coalescence," *IEEE Transactions on Aerospace and Electronic Systems*, vol. 51, no. 2, pp. 962–974, 2015.

[30] D. Musicki and M. Morelande, "Non parametric target tracking in non uniform clutter," in *2005 7th International Conference on Information Fusion*, vol. 1, pp. 6–pp, IEEE, 2005.

[31] D. Musicki, X. Wang, R. Ellem, and F. Fletcher, "Efficient active sonar multitarget tracking," in *OCEANS 2006-Asia Pacific*, pp. 1–8, IEEE, 2006.

[32] D. Musicki and B. La Scala, "Multi-target tracking in clutter without measurement assignment," *IEEE Transactions on Aerospace and Electronic Systems*, vol. 44, no. 3, pp. 877–896, 2008.

[33] T. L. Song and D. Musicki, "Target existence based resource allocation," *IEEE Transactions on Signal Processing*, vol. 58, no. 9, pp. 4496–4506, 2010.

[34] F. de Ponte Müller, "Survey on ranging sensors and cooperative techniques for relative positioning of vehicles," *Sensors*, vol. 17, no. 2, p. 271, 2017.

[35] T. Weiskircher, Q. Wang, and B. Ayalew, "Predictive guidance and control framework for (semi-)autonomous vehicles in public traffic," *IEEE Transactions on Control Systems Technology*, vol. PP, no. 99, pp. 1–13, 2017.

[36] B. Zhou and N. Bose, "Multitarget tracking in clutter: Fast algorithms for data association," *IEEE Transactions on Aerospace and Electronic Systems*, vol. 29, no. 2, pp. 352–363, 1993.

[37] T. L. Song, D. MuÃ…Â¡icki, and Y. Kim, "Multi-target tracking with target state dependent detection," in *2012 15th International Conference on Information Fusion*, pp. 324–329, July 2012.

[38] D. Musicki and T. L. Song, "Track initialization: Prior target velocity and acceleration moments," *IEEE Transactions on Aerospace and Electronic Systems*, vol. 49, pp. 665–670, Jan 2013.

[39] S. Särkkä, *Bayesian filtering and smoothing*, vol. 3. Cambridge University Press, 2013.

[40] S. Challa, M. R. Morelande, D. Mušicki, and R. J. Evans, *Fundamentals of object tracking*. Cambridge University Press, 2011.

This page is intentionally left blank.

Chapter 4

Multi Target Tracking: LMIPDA Approach

4.1 Introduction

Target tracking in public traffic calls for a tracking system with automated track initiation and termination facilities in a randomly evolving driving environment [1]. In addition, the key problem of data association needs to be handled effectively considering the limitations of the computational resources on-board an autonomous car. In this paper, we discuss a multi-target tracking system that addresses target birth/initiation and death/termination processes with automatic track management features. The tracking system is based on Linear Multi-target Integrated Probabilistic Data Association Filter (LMIPDAF), which is adapted to specifically include algorithms that handle track initiation and termination, clutter density estimation and track management. The performance of the proposed tracking algorithm is compared to other single and multi-target tracking schemes and is shown to have acceptable tracking error. It is further illustrated through multiple traffic simulations that the computational requirement of the tracking algorithm is less than that of optimal multi-target tracking algorithms that explicitly address data association uncertainties. A fully au-

[1]The content of this chapter appeared in the article: *A. Hunde and B. Ayalew, "Linear Multi-Target Integrated Probabilistic Data Association Filter With Automatic Track Management for Autonomous Vehicles," vol. Volume 2: Control and Optimization of Connected and Automated Ground Vehicles of Dynamic Systems and Control Conference, 09 2018.*

tonomous vehicle is expected to perform an autonomous driving task through a sequence of events without human innervation: first, it must able to perceive its environment and localize itself within the environment, then it must navigate to its goal position by planning and executing an obstacle free path. To localize itself and perceive the driving environment an autonomous vehicle is fitted with a host of exteroceptive sensors (radar, lidar and cameras), proprioceptive sensors and other systems that enable it to communicate with the infrastructure and other vehicles.

Among the exteroceptive sensors, radar and camera are the most commonly researched. In an effort to provide better perception, fusion offers a unique opportunity to implement both radar and camera in a manner to augment their shortcomings when used individually. Data fusion can be conducted at two layers: centralized fusion, where detections from both sensors are associated with tracks at the fusion center and distributed fusion, where each sensor generates tracks from their detections and the data fusion center does track-to-track association [1]. In either case the challenges involved are the reliability and the computational complexity of the data association and track management of the tracking algorithm.

In this paper, we demonstrate a tracking system based on the Linear Multi-target Integrated Probabilistic Data Association Filter (LMIPDAF) [2, 3], which is capable of unsupervised automation for automated driving systems in multi-target traffic. This includes specific tasks of accommodating target track initiation and track termination, clutter density estimation and handling data association uncertainties among others. These tracking functionalities can help facilitate perception during common events in public traffic as participants (suddenly) change lanes, navigate intersections, overtake and/or brake in emergencies, etc [4].

Autonomous vehicles are equipped with diverse sensors in order to navigate in public traffic. Detections from heterogeneous sensors undergo sensor fusion in order to represent a consistent perception of the driving environment. In addition to process and measurement noise, false alarms, random birth/death processes and measurement origin uncertainties complicate the tracking process. The manner in which the the data association probabilities are handled makes a key distinction among various tracking approaches [2, 3]. Data association involves the assignment of sensor detections to the targets which are hypothesized to have generated the detections. If the measurement is not correctly assigned to the actual target, the track may end up following a different target and consequently add up to a track loss. Thus, it is apparent that a tracking algorithm capable of effectively

addressing the afore-mentioned challenges of data association in a real-time setting is undoubtedly constrained by the available processing power of the on-board computer systems.

Multiple target tracking (MTT) algorithms could be classified into two types based on the approach taken to handle data association uncertainties. The most basic MTT algorithms are a simple extension of Single target tracking (STT) algorithms into a bank of parallel filters that perform independent target tracking. Thus, in the data association step, the measurement is hypothesized to have originated from either the target under consideration or from a clutter. The above hypothesis might hold true if targets are well separated to eliminate any data association ambiguities. However, this method rarely proves satisfactory in practice [2]. In contrast, more rigorous MTT algorithms attempt to resolve the origin of each measurement. Optimal data association approaches iterate all possible feasible joint events and compute their a posteriori probabilities. This clearly exacerbates the computational problem as the number of possible joint measurement assignments grows combinatorially with the number of tracks and the number of measurements [2, 3].

In the literature, numerous approaches to multi-target tracking (MTT) have been proposed [5, 6]. With the most popular being the joint probabilistic data association filter (JPDAF), multiple hypothesis tracking (MHT), joint integrated probabilistic data association filter (JIPDAF)[7, 8, 9, 10, 11, 12, 13, 14]. The key in all of these methods is to compute joint association probabilities by iterating through the joint association events in order to avoid conflicting measurement to track assignments [15, 16, 17, 18, 19, 20].

An alternative approach to the data association problem called Linear Multi-Target (LM) procedure is proposed in [2]. Therein, the measurement-to-track assignment is computed on a track-by-track basis even when measurements are shared among tracks. That is, when updating a track, all measurements that are shared by other non-targets (which are followed by other tracks) are assumed as interfering measurements. For the track under consideration, the clutter spatial density is modified to account for the presence of other tracks that share the measurement instead of enumerating and evaluating a posteriori probabilities for all feasible joint events. Once this step is completed, each track can then be updated as if it were following a single target by using the modified clutter spatial density.

In this paper, we extend the Linear Multi-target Integrated Probabilistic Data Association Filter (LMIPDAF) to include automatic track management modules for fully autonomous target tracking

in public traffic. While allowing for an occasional missing of measurement updates for existing targets due to occlusions or signal losses, we terminate false tracks that are more likely to originate from a clutter source. Tentative tracks will be confirmed upon successive detections and gating of measurements for that target. The track maintenance module also makes sure that no tentative track is initiated on an existing track following a given target. In addition, we will demonstrate multiple target tracking by including the motion of the autonomous ego vehicle equipped with an on-board sensor having limited Field of View (FoV). Thus, by incorporating target birth/death handling schemes with systematic treatment of the data association uncertainty problem, we address part of the computational complexity required for an autonomous navigation in public traffic.

The rest of the paper is organized as follows. In Section 2, we outline how the overall tracking system fits into the overall automated driving system architecture and its constituent parts. In Section 3, we discuss the details of the tracking system as well as target motion control methods. In Section 4, we present some illustrative results of the applications of the algorithms on typical traffic scenarios. The paper ends by summarizing the conclusions of the work in Section 5.

4.2 Overall System Architecture

The overall tracking system architecture and its constituent parts are shown in Figure 4.1. The objective in this paper includes sensor modeling, target detection and tracking, trajectory and path planning as well as motion control of the ego vehicle to follow lane centerline. In the measurement step, raw measurement data is extracted out of sensors such as radars, laser scanners and vision-based systems by applying relevant signal processing algorithms. In the segmentation procedure, the raw measurement data is segmented and clustered into objects. Next, an object classification step aims at sorting objects into different classes such as vehicles, bicycles and pedestrians. It is possible that, sensors with poor resolution might merge detections from more than one source and hence complicate the data association step (which is performed in the following layer). A measurement selection followed by a measurement-to-track assignment procedure computes the weight of a set of measurements from the current scan that are to be included in the update of individual tracks. The filtering module handles the estimation of the states of objects/vehicles over time based on appropriate motion models. Facilities to handle missed measurements, accommodations for automatic track initiation and termination as well as target clustering are also included in this step [21]. The

higher module in the hierarchy includes route and predictive motion planning and feedback control schemes which subsequently generate the steering, throttle and brake commands for motion control of the ego vehicle. We assume that waypoints are available from the route planning block.

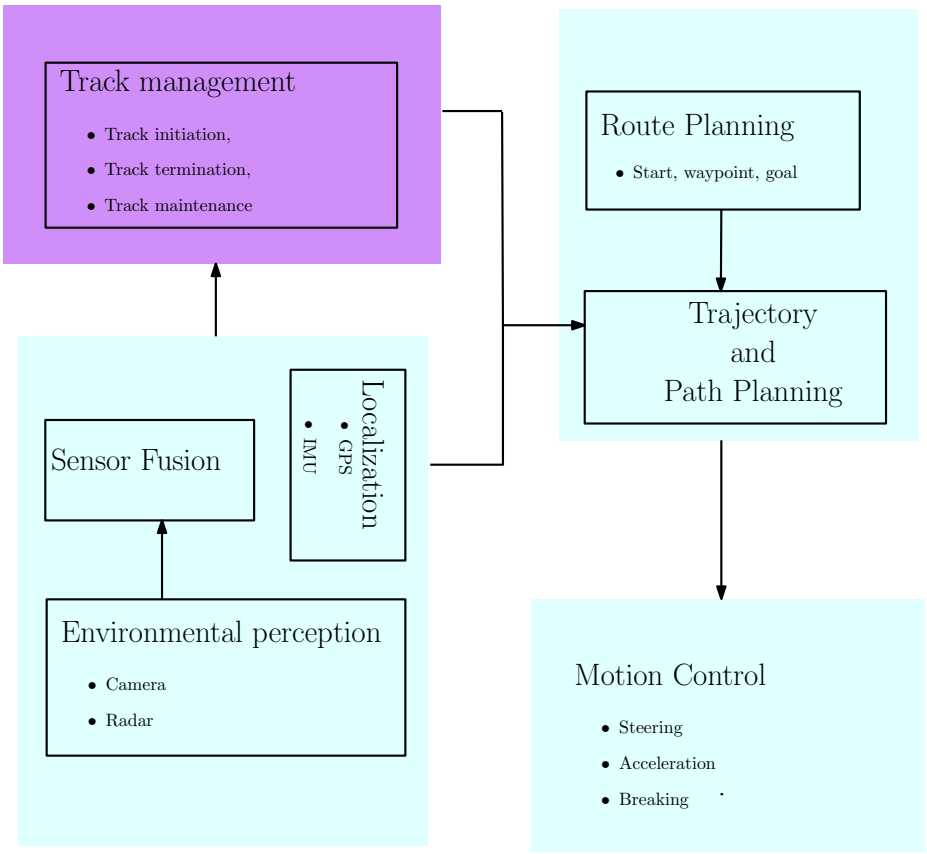

Figure 4.1: Autonomous vehicle: an outline of modules for situational awareness,target detection and tracking, motion planning and control.

4.3 A Multi-Object Tracker with LMIPDA

A number of alternative methods can be applied to estimate the number of targets and the state of individual targets; however, the computational requirements of these approaches should be examined to meet the realtime requirements of target tracking in public traffic. In addition, to be practically relevant for autonomous vehicle applications, the algorithm should have mechanisms in place or be flexible enough to add track initiation and termination, clutter density estimation, target existence based track maintenance, and data association handling. Here we discuss a multi-object tracker based on LMIPDA. For LMIPDAF, the number of computations grows linearly with the number

of targets and measurements. Here, the measurement-to-track associations are computed for each target treating measurements generated by other targets as clutter. The LMIPDA approach modifies the clutter density in an effort to account for the presence of measurements originating from other targets [2]. The measurement sets validated at scan time k satisfy Equation (4.1).

$$y_k \in \mathcal{R}^{2\times m_k} : \left[z_{k,i} - H\hat{x}_{k|k-1}\right]^T S^{-1}_{\tau,k|k-1} \left[z_{k,i} - H\hat{x}_{k|k-1}\right] \leq \gamma \tag{4.1}$$

where $\bar{y}_{k|k-1} = H\hat{x}_{k|k-1}$, is the predicted measurement for each target, $z_{k,i}$ is the detected measurement, and $S_{\tau,k|k-1}$ is the measurement covariance,$\sqrt{\gamma}$ is the gate size. The volume of the gate is

$$V_k(\tau) = \pi\sqrt{\gamma|S_{\tau,k|k-1}|} \tag{4.2}$$

Once m_k measurements are detected, the a priori data association for each measurement i is approximated as in Equation (4.3).

$$P^{\tau}_{k,i} \approx 1 - P_D(\tau)P_G(\tau)p(\chi^{\tau}|Y^{k-1})\frac{\frac{p^{\tau}_k(i)}{\rho_i(\tau)}}{\sum_{j=1}^{m_k}\frac{p^{\tau}_k(j)}{\rho_i(\tau)}} \tag{4.3}$$

where

$$\rho_i(\tau) = \rho^{\tau}_{k,i} + \sum_{\sigma=1,\sigma\neq\tau}^{T} P_D(\tau)P_G(\tau)p(\chi^{\tau}|Y^{k-1})p^{\tau}_k(j) \tag{4.4}$$

While updating a track, the a priori "scatterer" measurement density of each measurement is obtained from Equation (4.5).

$$\rho_i(\tau) = \rho_{k,i} + \sum_{\sigma=1,\sigma\neq\tau}^{T} p^{\tau}_k(i)\frac{P^{\sigma}_{k,i}}{1 - P^{\sigma}_{k,i}} \tag{4.5}$$

The measurement likelihood of each of the selected measurements y_k is assumed to be Gaussian

with the form given in Equation (4.6).

$$p_k^\tau(i) = \begin{cases} \frac{1}{P_G(\tau)} \mathcal{N}\left(y_k(i); \bar{y}_{k|k-1}; S_{\tau,k|k-1}\right) & y_k(i) \in V_k(\tau) \\ 0 & y_k(i) \notin V_k(\tau) \end{cases} \tag{4.6}$$

where, $\mathcal{N}(.)$ is a normal pdf with mean $\bar{y}_{k|k-1}$ and covariance $S_{\tau,k|k-1}$.

The a posteriori state estimate pdf is assumed to be Gaussian, i.e. $p(x_k|Y^k) = \mathcal{N}(\hat{x}_{k|k}, P_{k|k})$. The mean $\hat{x}_{k|k}$, and the covariance $P_{k|k}$ are given by (4.7) and (4.8)

$$\hat{x}_{k|k}(\tau) = \sum_{i=0}^{m_k} \beta_{k,i}(\tau) \hat{x}_{k|k,i}(\tau) \tag{4.7}$$

$$P_{k/k}(\tau) = \sum_{i=0}^{m_k} \beta_{k,i}(\tau)[P_{k|k,i}(\tau) + (x_{k|k,i}(\tau) - \hat{x}_{k|k}(\tau))(x_{k|k,i}(\tau) - \hat{x}_{k|k}(\tau))^T] \tag{4.8}$$

where the weights are computed [2] as follows:

$$\beta_{k,0}(\tau) = \frac{1 - P_D(\tau)P_G(\tau)}{1 - \delta_k^\tau} \tag{4.9}$$

$$\beta_{k,i>0}(\tau) = \frac{P_D(\tau)P_G(\tau)}{1 - \delta_k^\tau} \frac{p_k^\tau(j)}{\tilde{\rho}_i(\tau)} \tag{4.10}$$

$\delta_k(\tau)$ is defined as

$$\delta_k(\tau) = P_D(\tau)P_G(\tau)\left(1 - \sum_{j=1}^{m_k(\tau)} \frac{p_k^\tau(j)}{\tilde{\rho}_i(\tau)}\right) \tag{4.11}$$

According to the LM procedure the posteriori probability of target existence is given by

$$P(\chi_k(\tau)|Y^k) = \frac{(1 - \delta_k(\tau)) \times P(\chi_k(\tau)|Y^{k-1})}{1 - \delta_k(\tau) \times P(\chi_k(\tau)|Y^{k-1}))} \tag{4.12}$$

4.3.1 Track Initiation

We outline the track initiation procedure next. Tentative tracks are initialized on each measurement not validated by any of the targets being tracked. We assume that our knowledge of the prior information on the tentative target velocity and acceleration vectors are limited to the maximum

speed v_{max} and (sometimes) the maximum acceleration a_{max} [22],[23]. We compute the initial state estimate and its covariance matrix are shown in Equations 4.13 and 4.14.

$$x_{k|k} = \begin{bmatrix} y_k(i) \\ \mathbf{0}_2 \\ \mathbf{0}_2 \end{bmatrix} \tag{4.13}$$

$$P_{k|k} = \begin{bmatrix} \mathbf{R} & \mathbf{0}_2 & \mathbf{0}_2 \\ \mathbf{0}_2 & \frac{v_{max}^2}{3}\mathbf{I}_2 & \mathbf{0}_2 \\ \mathbf{0}_2 & \mathbf{0}_2 & \frac{a_{max}^2}{3}\mathbf{I}_2 \end{bmatrix} \tag{4.14}$$

where, $\mathbf{R}$ is the measurement covariance, $\mathbf{0}_2$ are zeros of dimension 2×2 and $\mathbf{I}_2$ is an identity matrix of dimension 2×2. To compute the initial probability of object existence, we use Equation 4.15.

$$P(\chi_k(\tau)|y_k(i)) = P_0 \times \prod_{\tau} \big(1 - P(\chi_k(\tau)|Y^k)\beta_{k,i}(\tau)\big) \tag{4.15}$$

where, P_0 is a tuning parameter for a false track discrimination step.

4.3.2 Ego vehicle model and motion control

We can derive a linearized bicycle model to capture the motion of the ego vehicle as shown in Equation 4.16.

$$\begin{bmatrix} \dot{y} \\ \dot{v}_y \\ \dot{\psi} \\ \dot{r} \end{bmatrix} = \begin{bmatrix} 0 & 1 & 0 & 0 \\ 0 & -\frac{C_f+C_r}{mV_x} & 0 & -V_x - \frac{C_f l_f - C_r l_r}{mV_x} \\ 0 & 0 & 0 & 1 \\ 0 & -\frac{C_f+C_r}{mV_x} & 0 & -V_x - \frac{C_f l_f - C_r l_r}{mV_x} \end{bmatrix} \begin{bmatrix} y \\ v_y \\ \psi \\ r \end{bmatrix} + \begin{bmatrix} 0 \\ \frac{C_f}{m} \\ 0 \\ \frac{C_f l_f}{I_z} \end{bmatrix} \delta \tag{4.16}$$

where, y is the lateral deviation, v_y is the lateral speed and δ is the steering input. For tracking purposes, it is more convenient to describe the motion of the ego vehicle with respect to a path (a

road aligned coordinate frame). Thus, we introduce tracking error terms as follows:

$$\begin{aligned} \ddot{e}_1 &= \ddot{y} + V_x \left(\dot{\psi} - \dot{\psi}_{des} \right) \\ e_2 &= \psi - \psi_{des} \end{aligned} \tag{4.17}$$

where ψ and ψ_{des} are the actual orienation and the desired orientation of the ego vehicle with respect to a global frame[24]. The rest are defined in Table 4.1.

Table 4.1: Vehicle Parameters

NO	Notation	Definition	Value	Unit
1	C_f	Front tire cornering stiffness	80000	N/rad
2	C_r	Rear tire cornering stiffness	80000	N/rad
3	L_f	Front axle to c.g. distance	1.1	m
4	L_r	Rear axle to c.g. distance	1.58	m
5	I_z	Moment of Inertia	2873	Kg m^2
6	m	Mass of the car	1573	Kg

4.3.3 Sensor Model and Measurement Generation

We assume that target measurements are obtained as pairs of (r, θ) values for range and azimuth locations respectively. The sensing system introduces uncertainty in the measurements which we describe in the form of an additive Gaussian noise. We assume that target-generated detections are based on the "small target" model assumption in that

1. A single target generates at most one detection.

2. Each target can give rise to at most one detection per scan

As a result, each measurement has one source (either the clutter or one of the targets) and consequently no unresolved measurements exist. In addition, because of the second condition, the discussion of extended objects is not treated here. In addition, we assume that environment perception sensors have a limited Field of View (FoV) in both range and azimuth resolutions. For detection, measurements generated by target vehicles must fall within the sensor's FoV defined by

its range and azimuth as given in (4.18).

$$d = \sqrt{(x_i^t - x^{ego})^2 + (y_i^t - y^{ego})^2}$$
$$\theta = \tan^{-1}\left\{\frac{|y_i^t - y^{ego}|}{|x_i^t - x^{ego}|}\right\} \tag{4.18}$$

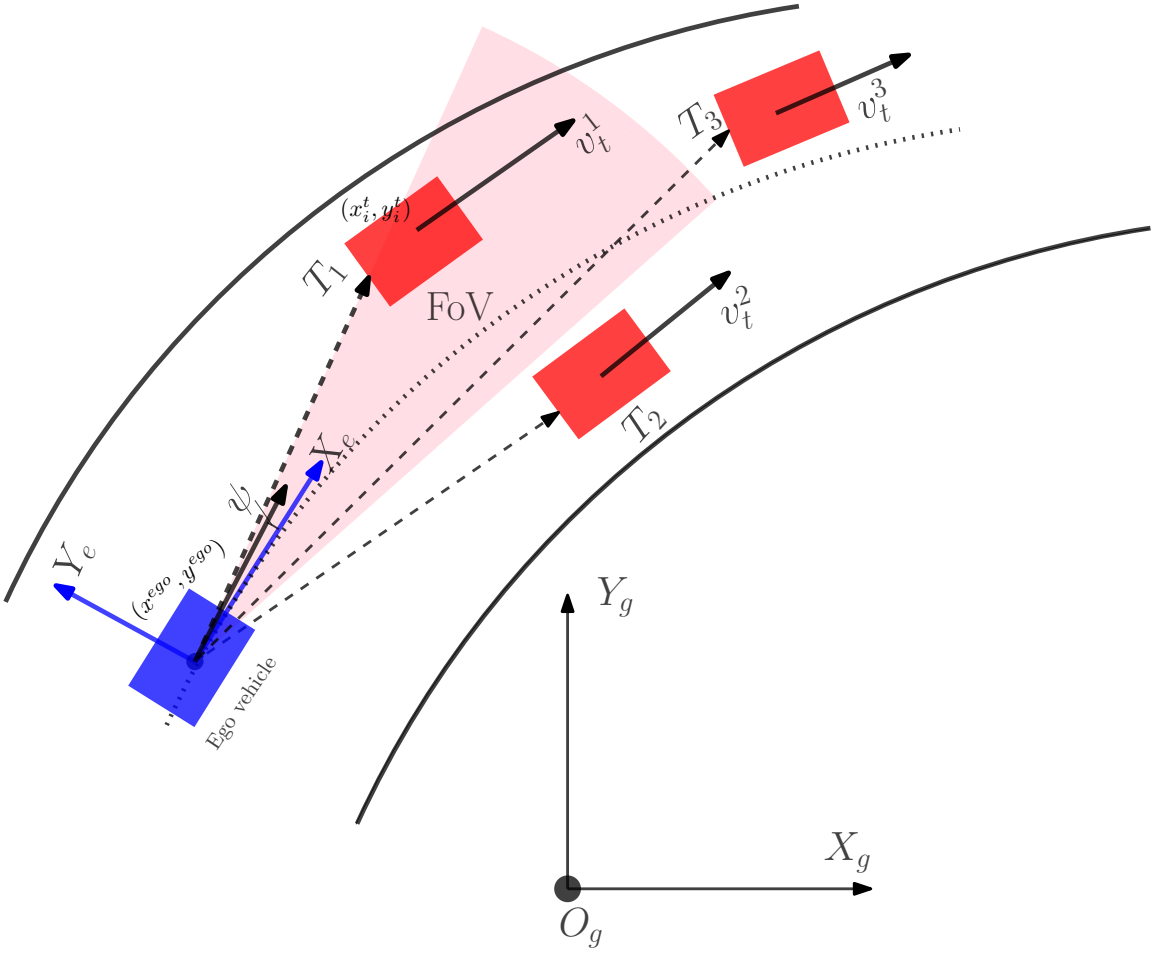

Figure 4.2: Public traffic scenario. The ego vehicle is shown shaded in blue at an instant when the sensing module is selecting a target measurement that falls within the FoV.

Target measurement is generated from a nonlinear kinematic motion model as given in Equation 4.19. We control the motion of the target vehicles along a reference trajectory by a nested form of a higher order sliding mode controller that has a relative order of 3.

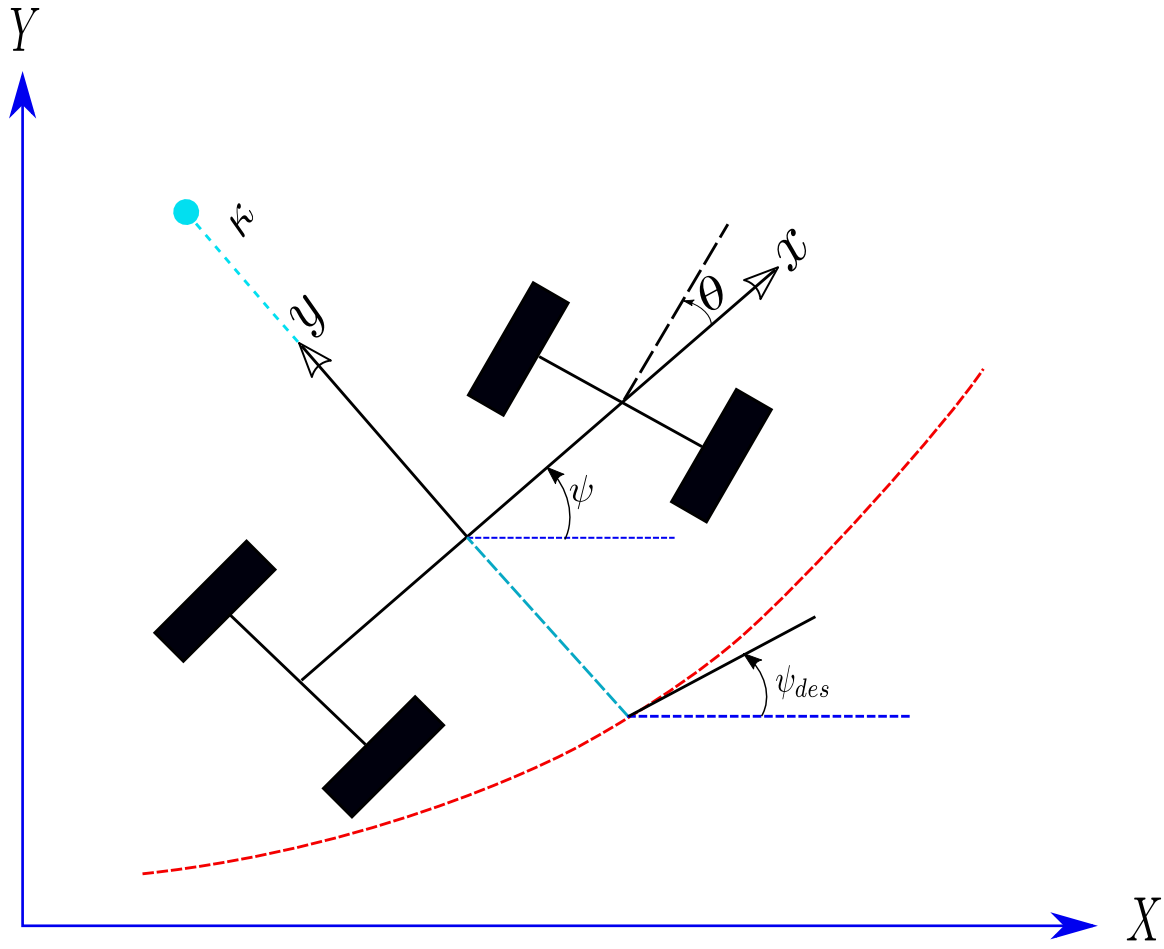

Figure 4.3: Target tracking scenario

$$\begin{aligned}
\dot{x}_i^t &= v_t^i \cos(\psi^t) \\
\dot{y}_i^t &= v_t^i \sin(\psi^t) \\
\dot{\psi}_i^t &= \frac{v_i^t}{l} \tan(\delta^t) \\
\dot{\delta}_i^t &= u_i^t \\
y_i^t &= x_i^t
\end{aligned} \tag{4.19}$$

The control input is selected to be a super twisting sliding mode controller of the form:

$$u = -\alpha sign(z_2 + 2|z_1|^3 + |z_0|^2) \times sign\left(z_1 + 2|z_0|^{\frac{2}{3}} sign(z_0)\right) \tag{4.20}$$

where we obtain the z_i terms from robust exact differentiators as outlined in [25]

While the kinematic model used to generate measurements for the simulated targets is a nonlinear constant speed model, the LMIPDA filter uses a linear constant acceleration Wiener process model.

4.4 Simulated Traffic Scenarios and Discussions

In this section, we demonstrate the performance of the tracking module in tracking target vehicles under various scenarios and we will also present the computational estimate for the same.

4.4.1 Changes in Target Detections as Seen in the Moving Sensor's FoV

Figure 4.4 shows three target vehicles and an ego vehicle equipped with a sensor of limited FoV. For this illustration, the ego vehicle travels in the middle lane at a constant speed of 20 m/s. Target vehicles are each moving at 15 m/s, one of which is initially detectable in the ego vehicle's sensor FoV. The tracking module initiates, maintains or terminates individual tracks as the target vehicles enter, remain or leave the FoV. For track confirmation, we require consecutive measurement updates for a given track. Hence, the actual track confirmation is delayed by a duration of some finite sampling scans. The radial range of the sensor is assumed to be 200m. Figure 4.5 shows the change in the target cardinality as tracks are being managed (initiated, maintained or terminated) based on target detections received within the FoV of the ego sensor.

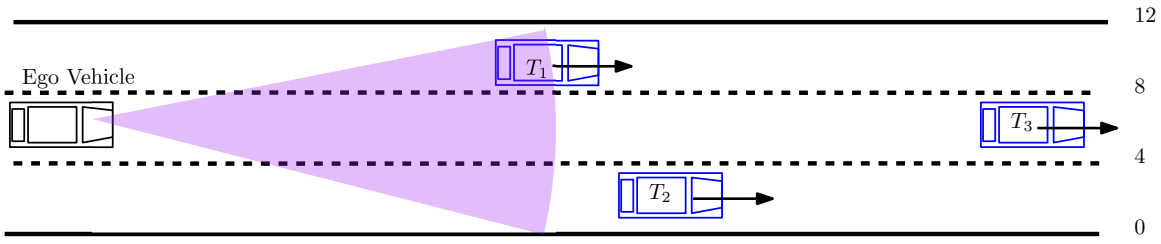

Figure 4.4: Simulation setup to demonstrate track initiation, maintenance and termination of the tracking module.

4.4.2 Performance of the Tracking Module in the Face of Missed Detections

Figure 4.6 shows a scenario where detections from the maneuvering target is missing for 10 consecutive scan times (the sampling time is 50ms) because of environmental interference. A typical

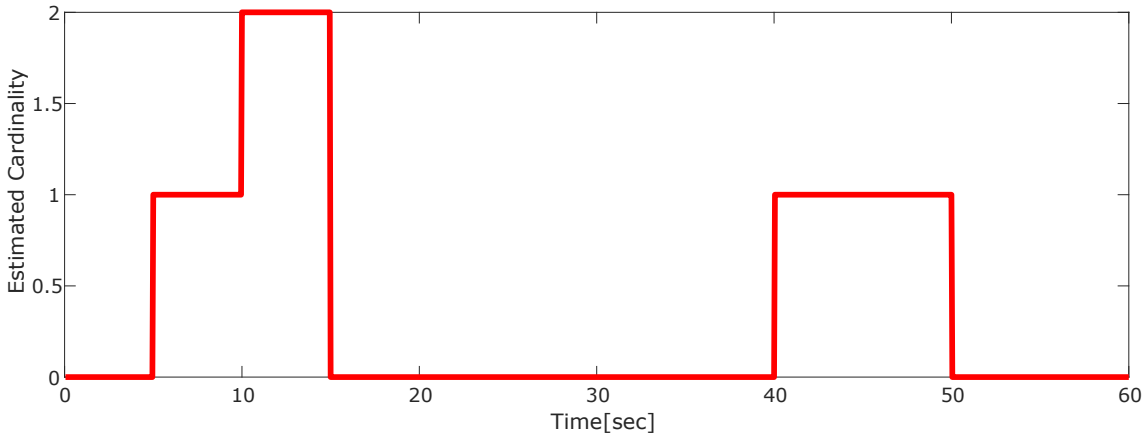

Figure 4.5: The time evolution of the estimated cardinality of target vehicles.

example of such cases arises when road-side infrastructures cast shadow on the trajectory of the tracked vehicle or parked cars give rise to interfering detections that impact the detection threshold of target vehicles. The tracking module continues to maintain tracks of target vehicles by motion prediction alone without the measurement update step involved. The reference trajectory used for the simulation of lane change maneuver of the target vehicle is based on a cubic Bezier curve [26]. The radial range of the sensor is kept at 200 m. The performance of the tracking module is shown

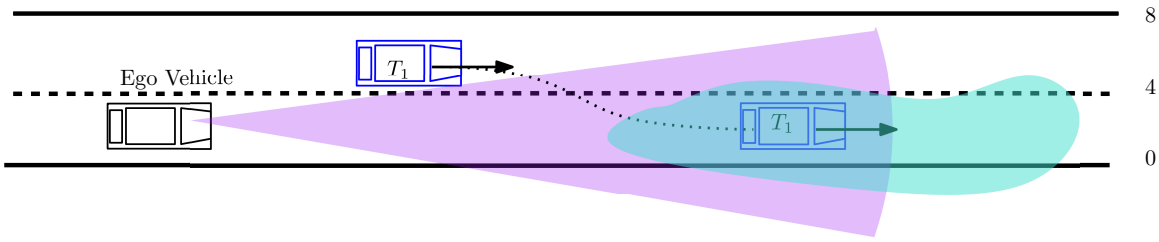

Figure 4.6: An illustration of missed target detections. The target vehicle changes a lane from the center-line of the outer lane to the inner lane where the infrastructure influences the detection threshold in the shaded region.

in Figure 4.7 demonstrating continuity of track during the scan interval where detections for the target are missing. The steady state error shown between the actual and the estimated trajectory is due to the steady state error arising from the ego vehicle's motion controller which also influences the relative motion of the vehicles. Note that the result shown is with respect to the reference frame attached to the ego vehicle.

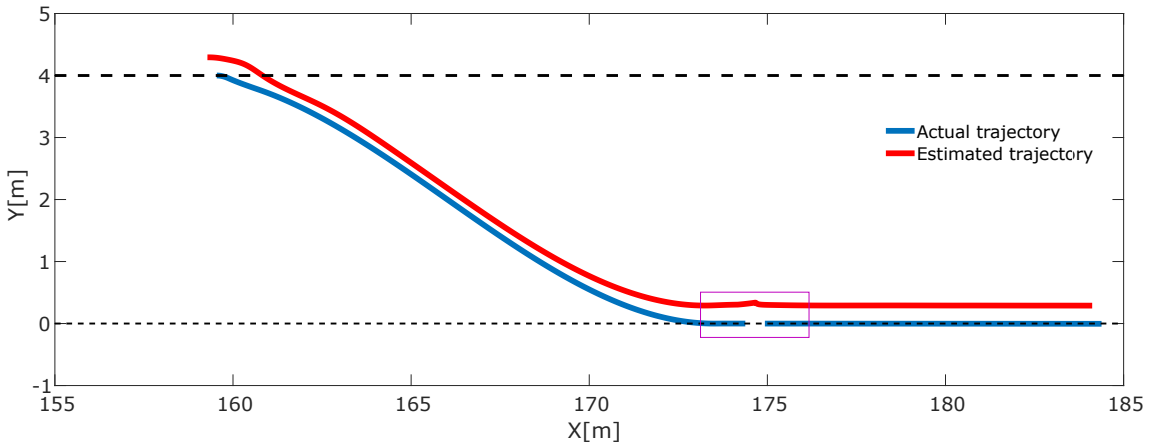

Figure 4.7: Target tracking estimation amid missing detections. The rectangular region highlights the portion of the trajectory where detections are not available.

4.4.3 Tracking Performance Comparison

In what follows, a simulation setup shown in Figure 4.8 is conducted to track trajectories of three target vehicles. To simplify the comparison, we choose two well-known tracking techniques which involve similar analysis except for the data association computation. The two tracking algorithms compared are the LMIPDAF used in this paper and JIPDAF which solves the data association explicitly. The result of the comparison shown in Figure 4.9 reveals that LMIPDAF has better approximation in terms of the mean squared error as the data association step involves an optimal measurement-to-track assignment. Three target vehicles are tracked for 100 scan times and this is iterated for 100 runs to get the average time for each tracking algorithm. The JIPDA (0.1220 sec) takes slightly more time than the LMIPDA (0.1183 sec). For more target vehicles as is the case for public traffic (specially in congested traffic situations), the computational demand of JIPDA will increase exponentially as compared to the LMIPDA which increases linearly with the number of target vehicles and measurements.

Conclusions

In this paper we have demonstrated using simulated public traffic scenarios how an LMIPDA based tracking system performs in a comparable manner to the optimal filter that explicitly computes the data association assignment. The Performance comparison shows that for the computational complexity that is linear in the number of measurements and the number of targets that LMIPDA

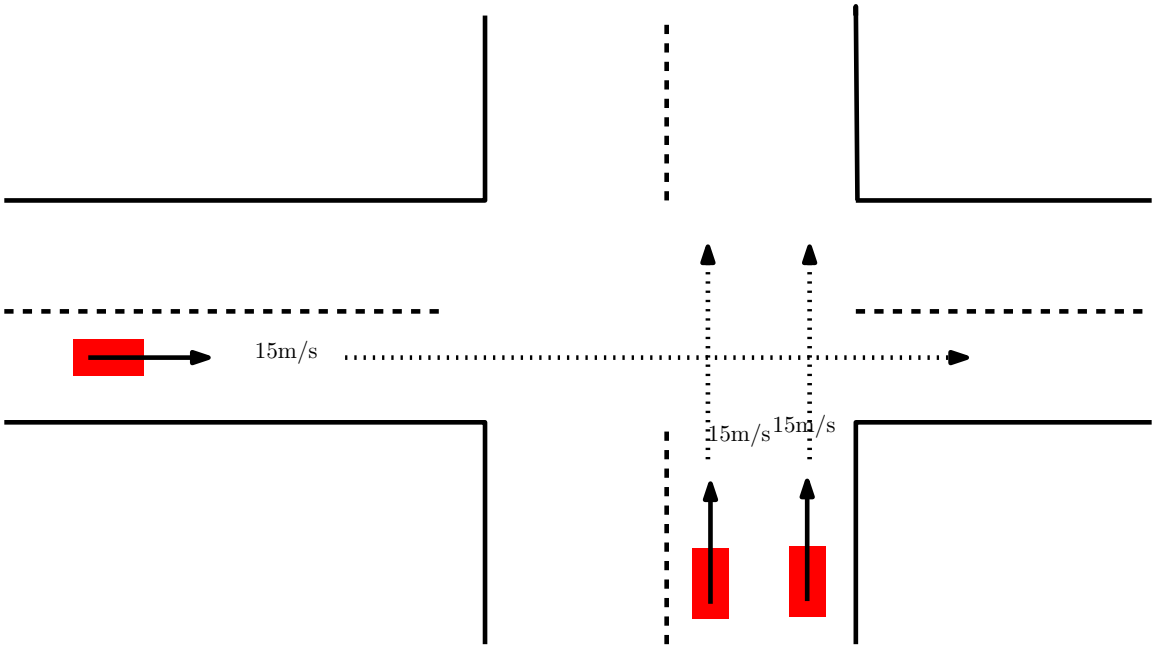

Figure 4.8: Simulation setup for three targets whose trajectories are intersecting.

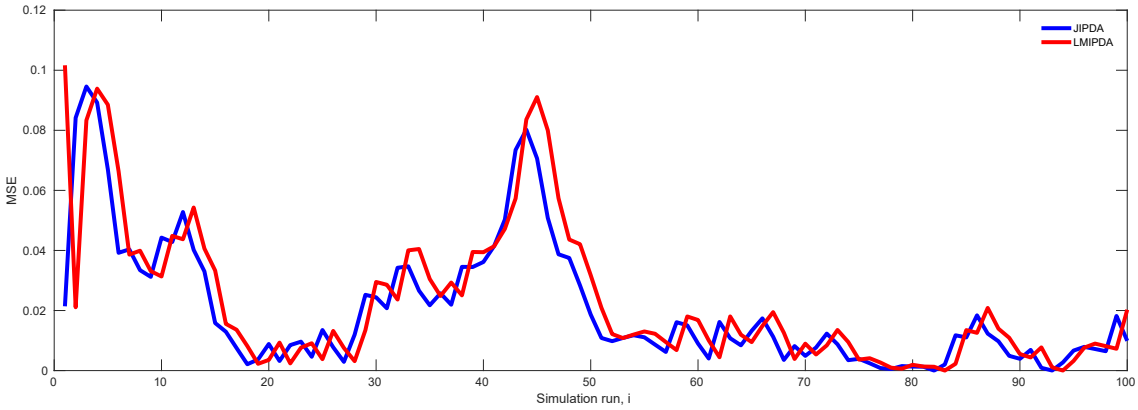

Figure 4.9: Comparison of JIPDAF and LMIPDA in terms of Mean Squared Error (MSE) estimation of target position.

offers, the observed tracking errors in position, speed and acceleration are an acceptable compromise. For this work, the LMIPDA filter has been modified to handle track initiation, maintenance and termination to adapt it for autonomous cars. In addition, under the simulated scenarios generated, the tracking module is able to perform robustly for a number of missed detections a quality required in public traffic where occlusions are anticipated. Future extensions to this work includes a discussion of multiple sensors to address the current trends in autonomous perception in an effort to improve

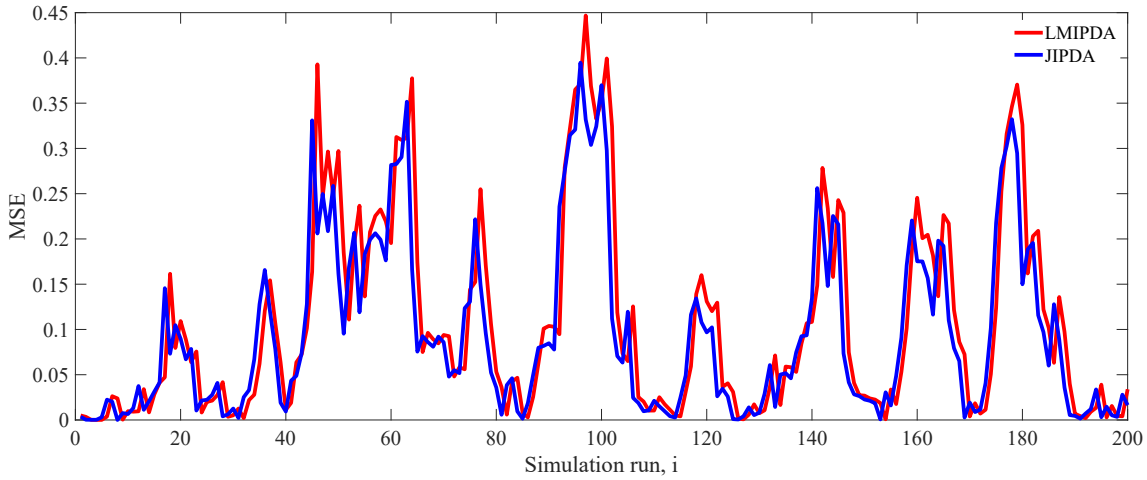

Figure 4.10: Comparison of JIPDAF and LMIPDA in terms of Mean Squared Error (MSE) estimation of target speed.

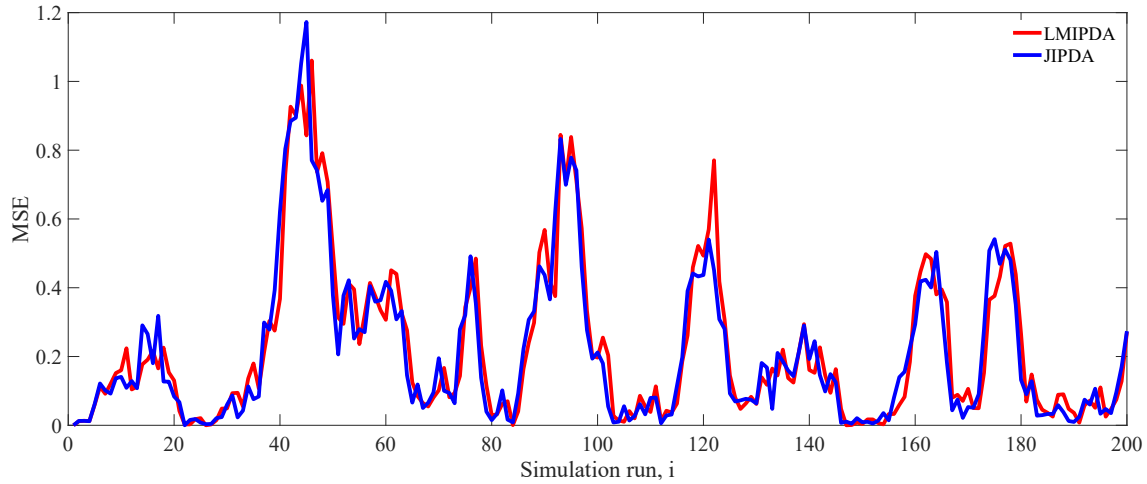

Figure 4.11: Comparison of JIPDAF and LMIPDA in terms of Mean Squared Error (MSE) estimation of the target acceleration.

the FoV of the ego vehicle. In addition, an extension of the same algorithm to the case of extended object tracking will offer a better understanding of the driving scene.

References

[1] X. Wu, J. Ren, Y. Wu, and J. Shao, "Study on target tracking based on vision and radar sensor fusion," *SAE Technical Paper*, pp. 01–0613, 2018.

[2] D. Musicki and B. La Scala, "Multi-target tracking in clutter without measurement assignment,"

IEEE Transactions on Aerospace and Electronic Systems, vol. 44, no. 3, pp. 877–896, 2008.

[3] D. Musicki, "Limits of linear multitarget tracking," in *2005 7th International Conference on Information Fusion*, vol. 1, pp. 6–pp, IEEE, 2005.

[4] A. Hunde and B. Ayalew, "Automated multi-target tracking in public traffic in the presence of data association uncertainty," in *2018 Annual American Control Conference (ACC)*, pp. 300–306, IEEE, 2018.

[5] C. Qiu, Z. Zhang, H. Lu, and H. Luo, "A survey of motion-based multitarget tracking methods," *Progress In Electromagnetics Research*, vol. 62, pp. 195–223, 2015.

[6] B.-n. Vo, M. Mallick, Y. Bar-shalom, S. Coraluppi, R. Osborne, R. Mahler, and B.-t. Vo, "Multitarget tracking," *Wiley Encyclopedia of Electrical and Electronics Engineering*, 2015.

[7] D. Musicki and R. Evans, "Joint integrated probabilistic data association: Jipda," *IEEE Transactions on Aerospace and Electronic Systems*, vol. 40, pp. 1093–1099, July 2004.

[8] D. Musicki and R. J. Evans, "Multiscan multitarget tracking in clutter with integrated track splitting filter," *IEEE Transactions on Aerospace and Electronic Systems*, vol. 45, pp. 1432–1447, Oct 2009.

[9] T. L. Song, H. W. Kim, and D. Musicki, "Iterative joint integrated probabilistic data association for multitarget tracking," *IEEE Transactions on Aerospace and Electronic Systems*, vol. 51, pp. 642–653, January 2015.

[10] D. Musicki and R. J. Evans, "Target existence based mht," in *Proceedings of the 44th IEEE Conference on Decision and Control*, pp. 1228–1233, Dec 2005.

[11] D. Musicki, R. Evans, and S. Stankovic, "Integrated probabilistic data association (ipda)," in *[1992] Proceedings of the 31st IEEE Conference on Decision and Control*, pp. 3796–3798 vol.4, 1992.

[12] D. Musicki, S. Challa, and S. Suvorova, "Automatic track initiation of manoeuvring target in clutter," in *2004 5th Asian Control Conference (IEEE Cat. No.04EX904)*, vol. 2, pp. 1009–1015 Vol.2, July 2004.

[13] Y. Bar-Shalom, P. K. Willett, and X. Tian, *Tracking and data fusion.* YBS publishing Storrs, CT, USA:, 2011.

[14] S. Blackman and R. Popoli, "Design and analysis of modern tracking systems(book)," *Norwood, MA: Artech House, 1999.*, 1999.

[15] Y. Bar-Shalom, F. Daum, and J. Huang, "The probabilistic data association filter," *IEEE Control Systems*, vol. 29, pp. 82–100, Dec 2009.

[16] K. Na, J. Byun, M. Roh, and B. Seo, "Fusion of multiple 2d lidar and radar for object detection and tracking in all directions," in *2014 International Conference on Connected Vehicles and Expo (ICCVE)*, pp. 1058–1059, Nov 2014.

[17] M. Attari, S. Habibi, and S. A. Gadsden, "Target tracking formulation of the svsf with data association techniques," *IEEE Transactions on Aerospace and Electronic Systems*, vol. 53, pp. 12–25, Feb 2017.

[18] A. Yilmaz, O. Javed, and M. Shah, "Object tracking: A survey," *ACM Comput. Surv.*, vol. 38, Dec. 2006.

[19] T. E. Fortmann, Y. Bar-Shalom, and M. Scheffe, "Multi-target tracking using joint probabilistic data association," in *1980 19th IEEE Conference on Decision and Control including the Symposium on Adaptive Processes*, pp. 807–812, Dec 1980.

[20] J. Dezert and Y. Bar-Shalom, "Joint probabilistic data association for autonomous navigation," *IEEE Transactions on Aerospace and Electronic Systems*, vol. 29, pp. 1275–1286, Oct 1993.

[21] F. de Ponte Müller, "Survey on ranging sensors and cooperative techniques for relative positioning of vehicles," *Sensors*, vol. 17, no. 2, p. 271, 2017.

[22] D. Musicki and T. L. Song, "Track initialization: Prior target velocity and acceleration moments," *IEEE Transactions on Aerospace and Electronic Systems*, vol. 49, no. 1, pp. 665–670, 2013.

[23] S. Challa, M. R. Morelande, D. Mušicki, and R. J. Evans, *Fundamentals of object tracking.* Cambridge University Press, 2011.

[24] R. Rajamani, *Vehicle dynamics and control.* Springer Science & Business Media, 2011.

[25] A. Levant, "Robust exact differentiation via sliding mode technique," *automatica*, vol. 34, no. 3, pp. 379–384, 1998.

[26] X. Qian, I. Navarro, A. de La Fortelle, and F. Moutarde, "Motion planning for urban autonomous driving using bézier curves and mpc," in *2016 IEEE 19th International Conference on Intelligent Transportation Systems (ITSC)*, pp. 826–833, Ieee, 2016.

This page is intentionally left blank.

Chapter 5

Autonomous Control Decisions with Feedback from Perception and Tracking Layer

5.1 Introduction

Public road traffic is rich in examples of dynamic objects suddenly appearing/disappearing in/from the Field of View (FoV) of an autonomous ego vehicle, such as when target vehicles zoom out by accelerating from the ego vehicle or sensor detections deteriorate temporarily due to illumination changes and other environmental effects [1]. Thus, the guidance and control system should capture the motion of moving obstacles via a perception and tracking module capable of track management features, including but not limited to track initiation and termination. This paper presents such a module that executes multi-target tracking with the linear integrated probabilistic data association (IPDA) filter in conjunction with a model predictive control (MPC) scheme for path and reference speed tracking and obstacle avoidance. From the perception module, all the confirmed tracks are made available to an Interacting Multiple Model (IMM) subsystem which predicts the motion of

[1] The content of this chapter is based on the conference paper *Andinet Hunde, Beshah Ayalew, and Qian Wang. "Automated Multi-Object Tracking for Autonomous Vehicle Control in Dynamically Changing Traffic." 2019 American Control Conference (ACC). IEEE, 2019.*

target vehicles to constrain the optimization problem in the MPC. The paper includes illustrations of the proposed scheme with practical traffic scenarios, which show that the ego vehicle is able to autonomously react to random changes in the number and/or state of target vehicles as well as to occasional miss-detections due to environmental effects. An autonomous vehicle navigates in complex traffic by relying on accurate perception of its environment to search an obstacle free path. The vehicle can then traverse the path by applying the correct control actions (steering, braking, signals, etc.). In dynamic traffic, with multiple moving objects, sensory information is further processed by tracking algorithms that estimate and even predict the state of motion of these moving targets. In this paper, we investigate the problem of tracking dynamic targets using a filtering algorithm called Linear Multi-target Integrated Probabilistic Data Association (LMIPDA) filter [1]. We adapt and apply this filter to public traffic scenarios by integrating a track management module capable of autonomous track initiation, maintenance and termination. The output of the LMIPDA filter is used in the MPC module enabling the ego vehicle to navigate autonomously, while avoiding obstacles and trading-off path/speed tracking errors against control efforts. The MPC module uses an Interacting Multiple Model (IMM) to predict the maneuver of confirmed target tracks in the finite receding horizon. The LMIPDA filter [1] is based on a single target tracking (STT) filter called Integrated Probabilistic Data Association (IPDA) [2]- [3] which incorporates an object existence into the filtering recursion. Another popular STT filter is the Probabilistic Data Association (PDA) filter [4]. In both cases, when STT algorithms are run as a bank of parallel filters for multi-target tracking (MTT) applications, there are track loss and coalescence problems especially under settings of closely spaced targets [1]. On the other hand, popular MTT algorithms such as the Joint Probabilistic Data Association (JPDA) [5], the Joint Integrated Probabilistic Data Association (JIPDA) [6] and the multi-hypothesis tracking (MHT) [7] all involve a computationally expensive data association procedure. A random finite set (RFS) based multi-target filtering formalism such as probability hypothesis density (PHD), cardinalized PHD (CPHD) [8]- [9], generalized labeled multi-Bernoulli [10] do not involve an intractable data association computation. The paper in [11] draws an equivalence between a PHD filter and a JIPDA formalism under linear Gaussian assumptions. In [12], the computational complexity of the CPHD filter is shown to be linear in the number of targets and cubic in the number of measurements. The filtering technique that we chose for discussion in this paper has a complexity that is linear in both the number of targets and measurements; furthermore, it has a tracking accuracy better than STT approaches [1], [13]. After the number of targets and

their states are known from the filtering step, the ego vehicle is required to navigate to its goal position along a desired path. For autonomous vehicle applications, several control methods have been proposed including some based on model predictive control(MPC). In [14], a hierarchical control architecture is proposed for automated driving on highways. The high level MPC module computes a collision free maneuver and reference (X,Y) trajectory and longitudinal speed sequence for the low level controller. The lower level controller, also based on MPC, executes the reference trajectory and speed profile to determine the left and right tire forces which are fed into the acceleration and braking logic. In [15], a hierarchical control framework is proposed where an MPC-based upper level module approximates the vehicle dynamics by a particle kinematic equation to generate a reference trajectory for the lower level controller which considers a high fidelity vehicle model to compute torque and steering commands. Target vehicles are modeled by a constant lateral and longitudinal acceleration defined with respect to a path intrinsic frame. In [16], this approach is extended by integrating discrete maneuvering decisions, i.e., lane and reference speed selection automata, with the MPC-based motion trajectory planning scheme. In addition, stochastic motion models were considered and Kalman filter-based trackers were adopted. In the present paper, we adopt this enhanced MPC framework for guidance and address some of the limitations on the tracking and motion prediction. In motion estimation/tracking and prediction, the commonly used constant speed/acceleration assumption (i.e. known controlled dynamics) about other objects, may deem the ego vehicle motion control less reliable. In addition, the number of target vehicles is assumed to be fixed at the start of the simulation which makes handling of appearing/disappearing targets in/from the FoV of the ego vehicle difficult. In this paper, we outline a framework that adapts a filtering algorithm based on LMIPDA and an IMM module to describe the motion of target vehicles in the prediction horizon of the MPC module. The uncertainty in the object motion model as well as the dynamism in the number of target objects is thus automatically handled- a feature that is useful in public traffic scenarios where these uncertainties are prevalent.

5.2 Control Framework

The overall control framework is shown in Figure 5.1. The route planner provides way-points from the current position to the destination over a road network. We assume that the route is available to the controller and tracker. See [17] for a detailed discussion on this topic.

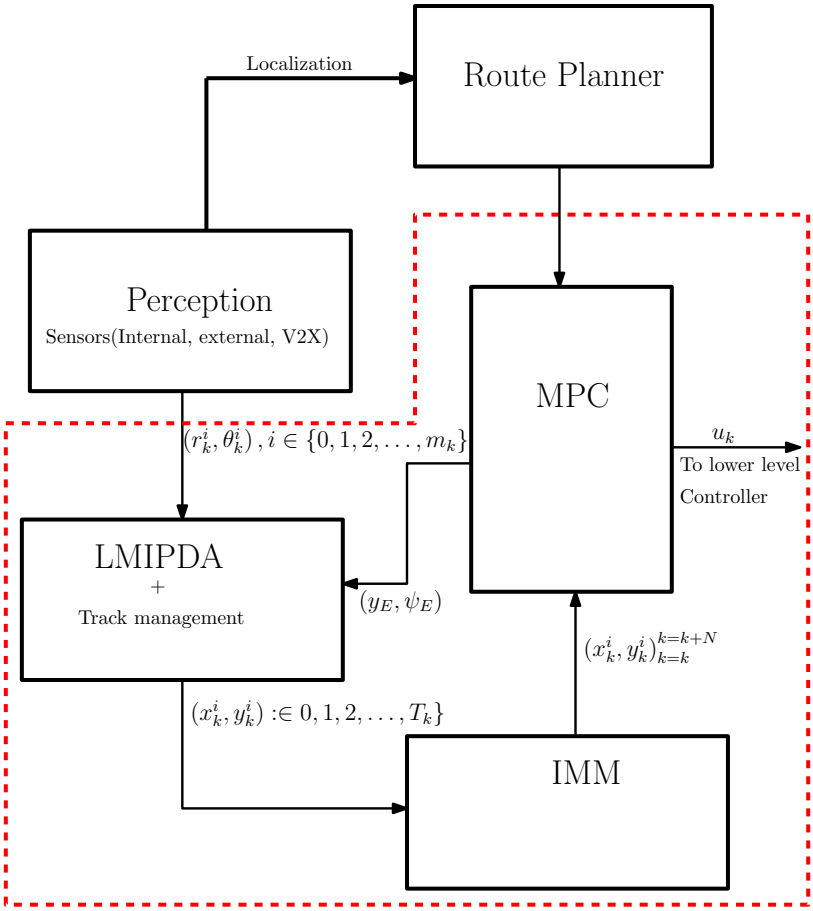

Figure 5.1: Overall Control Framework.

A set of sensors, possibly together with communicated information, generate a varying number of measurements at each scan time. Next, the LMIPDA filter associates measurements with tracks and initiates tentative tracks on new targets while also terminating tracks with no further measurement updates. The confirmed tracks, which are the result of the filtering and track management step, are propagated in the prediction horizon for evaluating the collision avoidance constraints in the MPC module.

5.3 A Multi-Object Tracker with LMIPDA

A number of alternative methods can be applied to recursively predict and update the estimate of the state of target vehicles; however, the computational demand of each approach should be examined to address the realtime requirements of target tracking in public traffic. Here, we adopt the LMIPDA

algorithm, which is shown to have linear computational complexity in the number of measurements as well the number of targets [1]. We assume the standard Wiener process acceleration model for target motions with states $\mathbf{x}_k = \begin{bmatrix} x_k & y_k & \dot{x}_k & \dot{y}_k & \ddot{x}_k & \ddot{y}_k \end{bmatrix}$ and with the state space model [18]

$$\mathbf{x}_k = A_{k-1}\mathbf{x}_{k-1} + \mathbf{q}_{k-1} \tag{5.1}$$

where x_k, y_k are the positions of the target vehicle and $\dot{x}_k, \dot{y}_k$ $\ddot{x}_k, \ddot{y}_k$ are corresponding velocity and acceleration terms. The forms of A_{k-1} and $\mathbf{q}_{k-1}$ are discussed in [18]. At each scan time detections are available as pairs of $\mathbf{z}_k = \{x_k^i, y_k^i\}$, $i = 0, 1, \ldots m_k^{'}$. Following the usual Kalman filter recursion, each target track selects a set of measurements falling within its elliptical validation gate of the form given in Equation 5.2.

$$\mathbf{y}_k \in \mathcal{R}^{2\times m_k} : \left[\mathbf{z}_{k,i} - H\hat{\mathbf{x}}_{k|k-1}\right]^T S_{\tau,k|k-1}^{-1} \left[\mathbf{z}_{k,i} - H\hat{\mathbf{x}}_{k|k-1}\right] \leq \gamma \tag{5.2}$$

where, $\bar{\mathbf{y}}_{k|k-1} = H\hat{\mathbf{x}}_{k|k-1}$, is the predicted measurement for that target track (τ), $\mathbf{z}_{k,i}$ is the i^{th} detection and $S_{\tau,k|k-1}$ is the measurement covariance,$\sqrt{\gamma}$ is the gate size. The volume of the gate is

$$V_k(\tau) = \pi\sqrt{\gamma|S_{\tau,k|k-1}|} \tag{5.3}$$

where, $|.|$ denotes the determinant. Once m_k measurements are validated, the apriori data association for each measurement i is approximated as

$$P_{k,i}^{\tau} \approx 1 - P_D(\tau)P_G(\tau)p(\chi^{\tau}|Y^{k-1})\frac{\frac{p_k^{\tau}(i)}{\rho_i(\tau)}}{\sum_{j=1}^{T}\frac{p_k^{\tau}(j)}{\rho_i(\tau)}} \tag{5.4}$$

where, $P_D(\tau), P_G(\tau), p(\chi^{\tau}|Y^{k-1})$ are respectively the probability of detection, the probability of the gating and probability of existence of a target. $p_k^{\tau}(j)$ is the likelihood of measurement $\mathbf{y}_k^i$, which is the i^{th} validated measurement and Y^{k-1} represents the measurement history upto time $k-1$. In 5.4, $\rho_i(\tau)$ is computed as:

$$\rho_i(\tau) = \rho_{k,i}^{\tau} - \sum_{\sigma=1,\sigma\neq\tau}^{T} P_D(\tau)P_G(\tau)p(\chi^{\tau}|Y^{k-1})p_k^{\tau}(j) \tag{5.5}$$

While updating a track, the apriori "scatterer" measurement density of each measurement is obtained from

$$\rho_i(\tau) = \rho_{k,i} + \sum_{\sigma=1,\sigma\neq\tau}^{T} p_k^{\tau}(i)\frac{P_{k,i}^{\sigma}}{1-P_{k,i}^{\sigma}} \tag{5.6}$$

The likelihood of the selected measurements $\mathbf{y}_k(i)$ is assumed Gaussian distributed and is computed as follows.

$$p_k^{\tau}(i) = \begin{cases} \frac{1}{P_G(\tau)}\mathcal{N}\left(y_k(i), \bar{y}_{k|k-1}, S_{\tau,k|k-1}\right) & \mathbf{y}_k(i) \in V_k(\tau) \\ 0 & \mathbf{y}_k(i) \notin V_k(\tau) \end{cases} \tag{5.7}$$

where $\mathcal{N}(.)$ is a normal pdf with mean $\bar{y}_{k|k-1}$ and variance $S_{\tau,k|k-1}$.

The a posteriori state estimate pdf is assumed to be Gaussian:- $p(\mathbf{x}_k|Y^k) = \mathcal{N}(\mathbf{x}_k, \hat{\mathbf{x}}_{k|k}, P_{k|k})$. The mean $\hat{\mathbf{x}}_{k|k}$ and the covariance, $P_{k|k}$ are computed from Equations (5.8) and (5.9)

$$\hat{\mathbf{x}}_{k|k}(\tau) = \sum_{i=0}^{m_k} \beta_{k,i}(\tau)\hat{\mathbf{x}}_{k|k,i}(\tau) \tag{5.8}$$

$$P_{k/k}(\tau) = \sum_{i=0}^{m_k} \beta_{k,i}(\tau)[P_{k|k,i}(\tau) + (\mathbf{x}_{k|k,i}(\tau) - \hat{\mathbf{x}}_{k|k}(\tau))(\mathbf{x}_{k|k,i}(\tau) - \hat{\mathbf{x}}_{k|k}(\tau))^T] \tag{5.9}$$

where, the weights are computed for LMIPDA [1] as follows:

$$\beta_{k,0}(\tau) = \frac{1 - P_D(\tau)P_G(\tau)}{1-\delta_k^{\tau}} \tag{5.10}$$

$$\beta_{k,i>0}(\tau) = \frac{P_D(\tau)P_G(\tau)}{1-\delta_k^{\tau}}\frac{p_k^{\tau}(j)}{\tilde{\rho}_i(\tau)} \tag{5.11}$$

where $\delta_k(\tau)$ is defined as

$$\delta_k(\tau) = P_D(\tau)P_G(\tau)\left(1 - \sum_{j=1}^{m_k(\tau)}\frac{p_k^{\tau}(j)}{\tilde{\rho}_i(\tau)}\right) \tag{5.12}$$

According to the linear multitarget (LM) procedure, the a posteriori probability of target existence

is composed as:

$$P(\chi_k(\tau)|Y^k) = \frac{(1 - \delta_k(\tau) \times P(\chi_k(\tau)|Y^{k-1}))}{1 - \delta_k(\tau) \times P(\chi_k(\tau)|Y^{k-1}))} \tag{5.13}$$

Track Initiation

Tentative tracks are initialized on each measurement not validated by any of the targets being tracked. We assume that our knowledge about the prior information on the tentative target velocity and acceleration vectors are limited to the maximum speed v_{max} and the maximum acceleration a_{max} [19, 20]. If we assume a constant acceleration model for the target motions(only for the purpose of track initiation), the initial state estimate and covariance matrix are:

$$x_{k|k} = \begin{bmatrix} y_k(i) \\ \mathbf{0}_{2\times 1} \\ \mathbf{0}_{2\times 1} \end{bmatrix} \tag{5.14}$$

$$P_{k|k} = \begin{bmatrix} \mathbf{R} & \mathbf{0}_2 & \mathbf{0}_2 \\ \mathbf{0}_2 & \frac{v_{max}^2}{3}\mathbf{I}_2 & \mathbf{0}_2 \\ \mathbf{0}_2 & \mathbf{0}_2 & \frac{a_{max}^2}{3}\mathbf{I}_2 \end{bmatrix} \tag{5.15}$$

where $\mathbf{R}$ is the measurement covariance, $\mathbf{0}_2$ are zeros of dimension 2×2 and $\mathbf{I}_2$ is an identity matrix of dimension 2×2. The initial probability of object existence is given by:

$$P(\chi_k(\tau)|\mathbf{y}_k(i)) = P_0 \times \prod_{\tau} \big(1 - P(\chi_k(\tau)|Y^k)\beta_{k,i}(\tau)\big) \tag{5.16}$$

where P_0 is a tuning parameter for false track discrimination step.

5.4 MPC formulation

The motion of the ego vehicle is described in the path coordinate shown in Fig. 5.2. Coordinate frame (n^s, t^s) describes the parameters such as road curvature κ, and vehicle orientation ψ_s with respect to the global frame (X_g, Y_g). Another coordinate frame (n, t) describes motion with respect to the road-aligned frame (n^s, t^s) of the the ego-vehicle which is modeled as a particle [15]. The equation of motion for the ego vehicle can be written as follows:

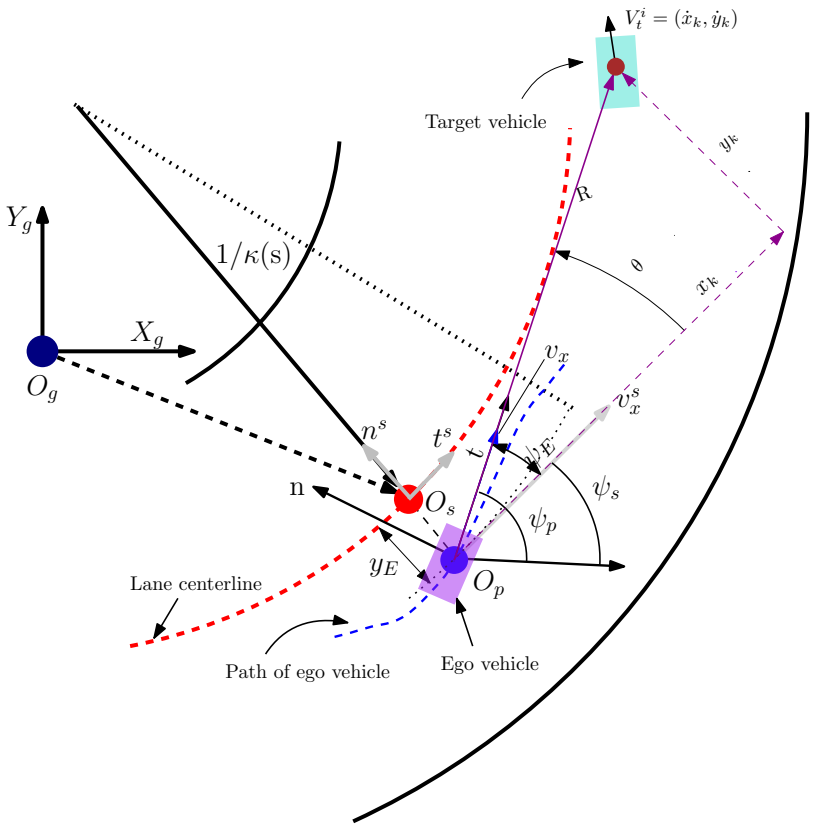

Figure 5.2: Ego vehicle motion description in the Frenet frame [15].

$$\dot{v}_x = a_x \tag{5.17a}$$

$$\dot{y}_E = v_x \sin(\psi_E) \tag{5.17b}$$

$$\dot{\psi}_E = \dot{\psi}_p - v_x \cos(\psi_E) \times \frac{\kappa(s)}{1 - y_E \kappa(s)} \tag{5.17c}$$

$$\dot{s} = v_x \cos(\psi_E) \times \frac{1}{1 - y_E \kappa(s)} \tag{5.17d}$$

$$\dot{a}_x = \tau_X (a_{Xd} - a_x) \tag{5.17e}$$

$$\ddot{\psi}_P = \tau_Y (\psi_{p_{FF}} v_x \kappa(s) + \Delta\dot{\psi}_d - \psi_p) \tag{5.17f}$$

In (5.17), the desired acceleration a_{Xd} and the deviation in the desired yaw rate $\Delta\dot{\psi}_d$ are used as inputs to guide the particle along a known reference path $\kappa(s)$. v_x and a_x are the particle speed and acceleration, y_E is the lateral deviation error from the reference path, and τ_X, τ_Y are the time constants of the first-order approximation of the longitudinal and lateral dynamics for the ego vehicle.

The upper and lower limits of speed and lane boundary are constrained as follows:

$$\Delta\overline{v}_x(s) = \overline{v}_x(s) - v_x \geq 0 \tag{5.18a}$$

$$\Delta\overline{y}_E(s) = \overline{y}_E(s) - y_E \geq 0 \tag{5.18b}$$

$$\Delta\underline{y}_E(s) = y_E - \underline{y}_E(s) \geq 0 \tag{5.18c}$$

The longitudinal and lateral accelerations are constrained according to the friction ellipse of the vehicle's tire/road contact:

$$\left(\frac{v_x \left(\kappa(s) v_x + \Delta\dot{\psi}_d \right)}{a_{n,gg}} \right)^2 + (a_{Xd})^2 \leq (\mu_H g - \zeta_{gg})^2 \tag{5.19}$$

$$0 \leq a_{n,gg} \leq 1 \tag{5.20}$$

$$0 \leq \zeta_{gg} \leq \overline{\zeta}_{gg} \tag{5.21}$$

μ_H is the tire-road friction coefficient, g is the gravitational constant, and ζ_{gg} is a slack variable. To

avoid collision with target vehicles $(s_{0_i}, y_{e,0_i})$, we introduce an elliptical constraint of the form:

$$1 \leq \left(\frac{y_E - y_{e,0_i}}{\Delta y_{e,0_i}}\right)^2 + \left(\frac{s - s_{0_i}}{\Delta s_{0_i}}\right)^2 \tag{5.22}$$

The objective function of the MPC weighs the tracking error and control efforts and the optimization problem is solved over the prediction horizon $[0, H_p]$ as follows[16]:

$$\min_{x_k, u_k, Z_{\omega,k}} \sum_{k=1}^{N_p} \sum_{\omega \in \Omega} ||Z_{\omega,k}(y_{1,k} - r_{1,\omega,k})||^2_{P_1} + \sum_{k=1}^{N_p} ||y_{2,k} - r_{2,k}||^2_{P_2} + \sum_{k=0}^{N_p - 1} ||u_k||^2_R \tag{5.23}$$

where ω is a lane index and Z_ω is an associated weight variable which facilitates the optimal switching of reference lane/speed. $r_{1,\omega}$ is the reference lane/speed. We use a relaxed constraint on the lane/speed selection variable Z_ω [16]. The optimization problem in Equation (5.23) is solved subject to

$$\dot{x} = f(x, u, Z_\omega), \quad u \in U, x \in X \tag{5.24a}$$

$$x(0) = x_0 \tag{5.24b}$$

$$0 \leq c(x, u) \tag{5.24c}$$

where (5.24a) is a compact presentation of 5.17. Similarly, (5.24c) represents all contraints.

Interacting Multiple Model

To describe the motion of target vehicles in the prediction horizon, specially when they are maneuvering, we use Interacting Multiple Model (IMM). IMM problems involve both the estimation of continuous-valued parameters such as target positions, velocities and accelerations, and that of discrete stochastic models $M = \{M^1, M^2, \ldots, M^n\}$[18, 21, 22]. The IMM-filter used here is based on a system of equations where $j \in \{1, 2\}$ represents the standard Wiener process velocity model

and acceleration model, respectively:

$$\mathbf{x}_k = A^j_{k-1}\mathbf{x}_{k-1} + \mathbf{q}^j_{k-1} \tag{5.25a}$$

$$\mathbf{y} = H^j_k\mathbf{x}_k + \mathbf{r}^j_k \tag{5.25b}$$

Again, the form of A_{k-1}, $\mathbf{q}_{k-1}$, H_k and $\mathbf{r}_k$ for the respective Weiner process velocity and acceleration models can be found in [18]. Each model is defined by the prior probability $\mu^i_{k-1} = P(M^i_0)$ and a fixed transition probability $\pi_{ij} = P(M^j_k|M^i_{k-1})$. Each recursion goes though steps of interaction, filtering and combination as briefly reviewed next.

Interaction

Each of the n filters is initialized with mixed estimates of all the filters weighted by a mixing probability:

$$\hat{\mathbf{x}}^{0j}_{k-1} = \sum_{i=1}^{n} \mu^{i|j}_k \hat{\mathbf{x}}^i_{k-1} \tag{5.26a}$$

$$P^{0j}_{k-1} = \sum_{i=1}^{n} \mu^{i|j}_k \left[P^i_{k-1} + \left(\hat{\mathbf{x}}^i_{k-1} - \hat{\mathbf{x}}^{0j}_{k-1}\right)\left(\hat{\mathbf{x}}^i_{k-1} - \hat{\mathbf{x}}^{0j}_{k-1}\right)^T \right] \tag{5.26b}$$

where $\hat{\mathbf{x}}^i_{k-1}$ and P^i_{k-1} are the updated mean and covariance at iteration $k-1$ of model i. The mixing probabilities $\mu^{i|j}_k$ are computed as:

$$\mu^{i|j}_k = \frac{\pi_{ij}\mu^i_{k-1}}{\sum_{i=1}^{n} \pi_{ij}\mu^i_{k-1}} \tag{5.27}$$

where μ^i_{k-1} is the probability of model i.

Filtering

Here, except for the first iteration, standard Kalman prediction steps are applied. Assuming that there are no missed detections at the current scan time, the first iteration involves both the Kalman prediction and update steps from which the means and covariances $\hat{\mathbf{x}}^i_k$, P^i_k are computed and the model probabilities μ^i_{k-1} are updated.

$$\mu^i_k = \frac{\mathcal{N}(\mathbf{v}^i_k, 0, S^i_k)\mu^i_{k-1}}{\sum_{j=1}^{n} \mathcal{N}(\mathbf{v}^j_k, 0, S^i_k)\mu^j_{k-1}} \tag{5.28}$$

where, $\mathbf{v}_k^i$ and S_k^j are respectively the measurement residual and covariance of model i.

Combination

Individual estimates from each model are finally combined as shown in Equation 5.29.

$$\hat{\mathbf{x}}_k = \sum_{i=1}^{n} \mu_k^i \hat{\mathbf{x}}_k^i \tag{5.29a}$$

$$P_k = \sum_{i=1}^{n} \mu_k^i \left[P_k^i + \left(\hat{\mathbf{x}}_k^i - \hat{\mathbf{x}}_k \right) \left(\hat{\mathbf{x}}_k^i - \hat{\mathbf{x}}_k \right)^T \right] \tag{5.29b}$$

5.5 Illustrative Results and Discussions

In this section, we demonstrate the tracking and control performance of the ego vehicle through simulated practical traffic scenarios. In the first scenario, observations from the target vehicle are temporarily missing because of low probability of detection (P_D). In the second scenario, we consider the case of target objects entering or leaving the sensing FoV of the ego vehicle.

Scenario I

Target vehicle T_1 is shown in Figure 5.3 entering a region of low P_D where sensor measurements are missing for consecutive scans. Figure 5.4 shows the case without track management schemes. As shown in Figure 5.4, the track of Target 1 is seen to terminate at $t = 5.28$ sec (250m) because of missed detections. Hence, the ego vehicle which was slowing down to 15 m/s to adapt to the speed of target T_1, gradually accelerates to the desired reference speed of 25.5 m/s to take advantage of the apparently obstacle-free space. By the time Target T_1 reemerges at $t = 8.97$ sec (305m) due to improved detections, the ego vehicle is in a potential collision with the target vehicle. In an effort to escape collision with target T_1, the ego vehicle decides to accelerate and steer sharply to the other lane which also violates constraints setup to keep a safe distance between the ego vehicle and target T_2. In the simulation setup, the MPC solver fails to reach a solution and terminates. Figure 5.5 shows a similar situation but with the track management scheme of the filtering module included. As seen from the figure, the ego vehicle steers safely into the other lane to follow target T_2 which is traveling at a faster speed of 20m/s. Later on, the tracking module declares the termination of the track of T_1. Then, the ego vehicle decides to switch back to its previous lane to keep its desired

reference speed and lane. We, observe from this figure that the tracking filter maintains the track of target vehicle T_1 in the time frame when detections were absent from this target. Afterwards, when detections from the missing target are available, its track is resumed with measurement updates and the ego vehicle is able to successfully avoid collision.

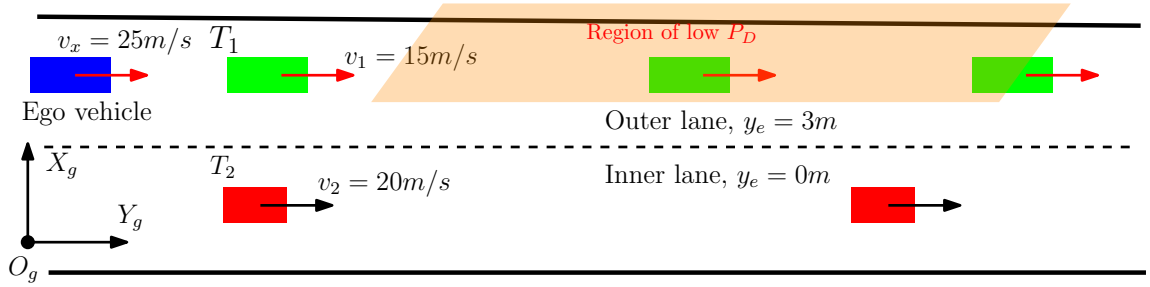

Figure 5.3: Simulation scenario to demonstrate handling of missed detections. Target vehicle T_1 passes through a region (shown shaded with dark orange) where detections are not available for some scan times.

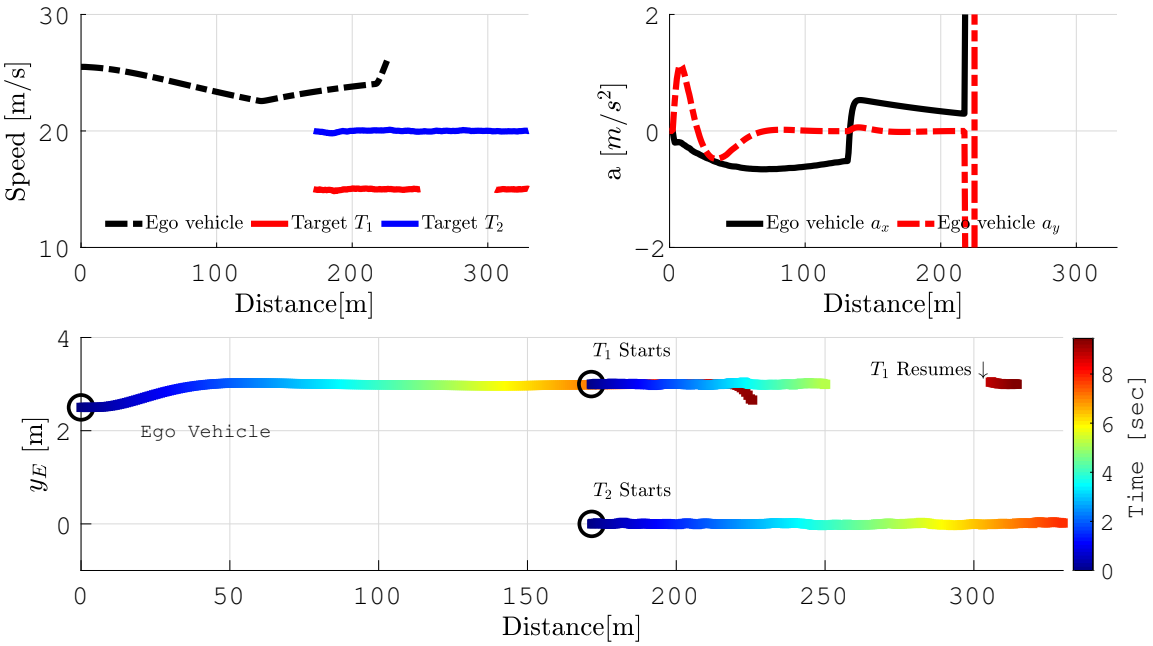

Figure 5.4: The track of Target 1 terminates at $t = 5.28$ sec due to a low probability of detection (P_D). By the time Target 1 emerges at the scene at $t = 8.97$ sec, the ego vehicle is incapable of pulling out of a potential collision with the target. By the time the motion constraints are violated, the ego vehicle has traveled a distance of 225.7 m.

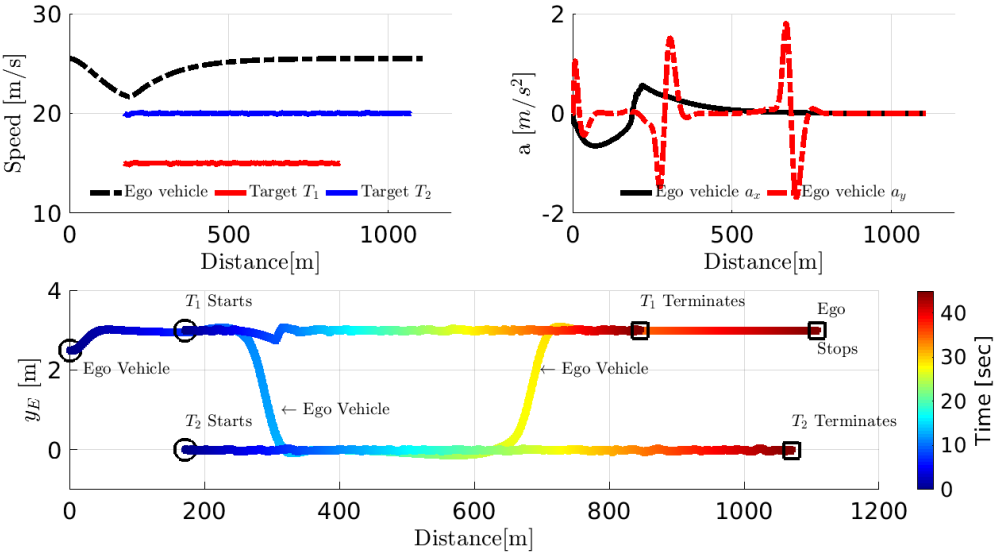

Figure 5.5: The tracking module maintains the track of target T_1 for the duration of the missed detections and resumes track when measurement updates are available from the target. For this scenario, the ego vehicle is seen to successfully avoid collision while also switching to a faster lane. When Target T_1 exits the scene, the ego vehicle initiates a lane change to track the desired reference speed and lane at 25.5 m/s and $y_E = 3$m respectively.

Scenario II

Two target vehicles are 170 m ahead of the ego vehicle. Target 1 starts in the outer lane ($y_E = 3$m) at a speed of 20 m/s and maintains that speed throughout the simulation. Target 2 likewise starts with an initial speed of 20 m/s in the inner lane ($y_E = 0$m) and its track terminates as the target exits the highway through an off-ramp. As shown in Figure 5.7, initially, the ego vehicle maintains a desired speed of 25.5 m/s and later slows down to 20 m/s to avoid collision with Target 1. After lane 1 is available due to termination of the track of Target 2, the ego vehicle switches to the inner lane. After about $t = 35$ seconds into the start of simulation, a third target (T_3) joins the traffic at roughly $s = 1051$ m; the ego vehicle has already traveled (longitudinally) a distance of 870 m by this time. T_3 is considered a birth process and the ego vehicle adjusts to the speed of T_3 in order to avoid collision.

In summary, as seen from these simulation results, data about both the track termination, track initiation as well as track maintenance information available from the track management module enables the ego vehicle to make informed decisions.

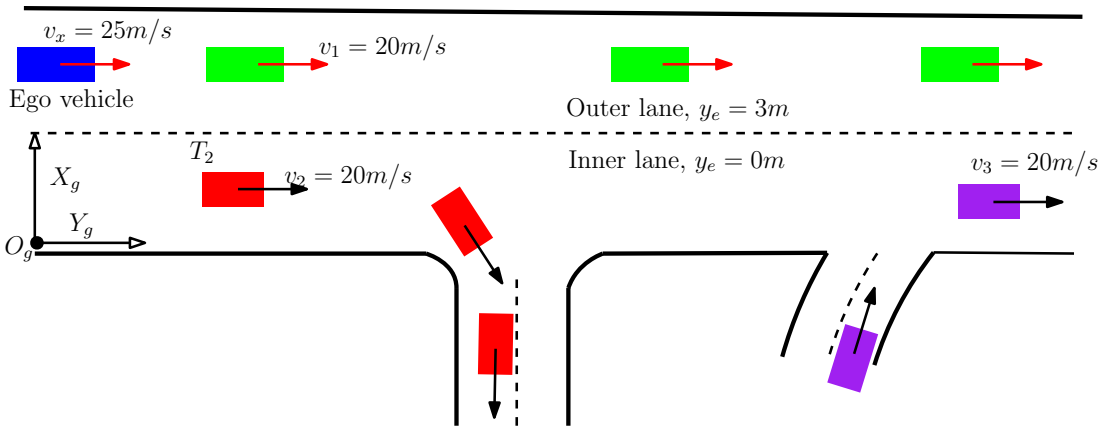

Figure 5.6: Simulation setup showing target vehicle T_2 leaving the FoV of the Ego vehicle and another target car T_3 entering the FoV later in the simulation. T_1 is persistent throughout the simulation.

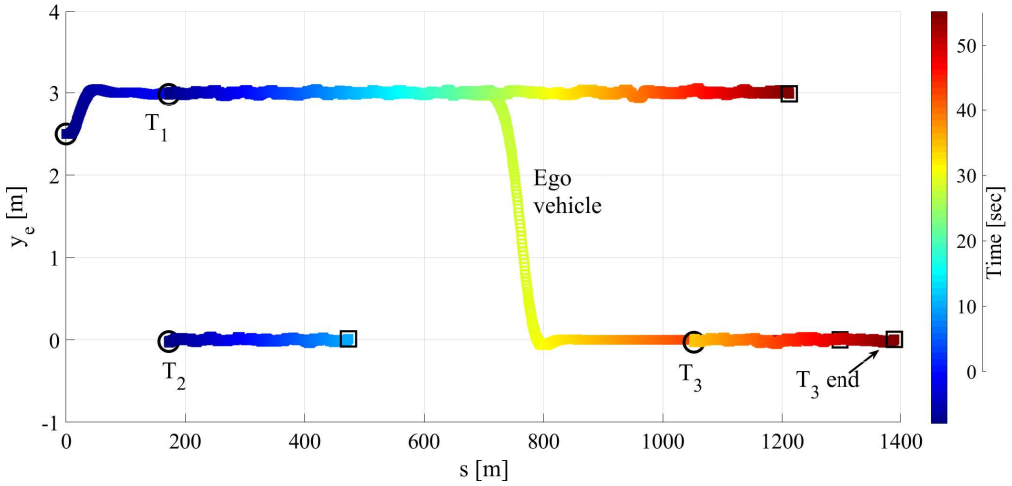

Figure 5.7: Trajectories of the two target vehicles as the ego vehicle switches lane to take advantage of the available lane due to track of target T_2 terminating.

5.6 Conclusion

In this paper, we described an automatic multi-object tracking algorithm capable of handling missed detections and target appearance and disappearance and integrated it with an MPC-based guidance algorithm for an autonomous vehicle application. Through simulated practical traffic scenarios, we illustrated how an LMIPDA-based tracking management module autonomously initiates/terminates tracks and provide track continuity under temporary miss-detections. Furthermore, we have demon-

strated how tracking data from the tracking subsystem is used in the MPC module to solve for safer informed decisions. In addition, autonomous navigation in the public traffic requires a motion prediction scheme to capture future intentions of target vehicles. In this paper, the IMM subsystem predicts the N-step ahead maneuver of target vehicles that constrains the optimization problem in the MPC module.

References

[1] D. Musicki and B. La Scala, "Multi-target tracking in clutter without measurement assignment," *IEEE Transactions on Aerospace and Electronic Systems*, vol. 44, no. 3, pp. 877–896, 2008.

[2] D. Musicki, R. Evans, and S. Stankovic, "Integrated probabilistic data association," *IEEE Transactions on Automatic Control*, vol. 39, pp. 1237–1241, June 1994.

[3] D. Musicki and S. Suvorova, "Tracking in clutter using imm-ipda-based algorithms," *IEEE Transactions on Aerospace and Electronic Systems*, vol. 44, no. 1, pp. 111–126, 2008.

[4] Y. Bar-Shalom, F. Daum, and J. Huang, "The probabilistic data association filter," *IEEE Control Systems*, vol. 29, pp. 82–100, Dec 2009.

[5] Y. Bar-Shalom, "Tracking methods in a multitarget environment," *IEEE Transactions on automatic control*, vol. 23, no. 4, pp. 618–626, 1978.

[6] D. Musicki and R. Evans, "Joint integrated probabilistic data association: Jipda," *IEEE transactions on Aerospace and Electronic Systems*, vol. 40, no. 3, pp. 1093–1099, 2004.

[7] D. Reid, "An algorithm for tracking multiple targets," *IEEE transactions on Automatic Control*, vol. 24, no. 6, pp. 843–854, 1979.

[8] R. P. Mahler, "Multitarget bayes filtering via first-order multitarget moments," *IEEE Transactions on Aerospace and Electronic systems*, vol. 39, no. 4, pp. 1152–1178, 2003.

[9] R. P. Mahler, *Statistical multisource-multitarget information fusion*, vol. 685. Artech House Norwood, MA, 2007.

[10] B.-T. Vo, B.-N. Vo, and A. Cantoni, "The cardinality balanced multi-target multi-bernoulli filter and its implementations," *IEEE Transactions on Signal Processing*, vol. 57, no. 2, pp. 409–423, 2008.

[11] R. Chakravorty and S. Challa, "Multitarget tracking algorithm-joint ipda and gaussian mixture phd filter," in *2009 12th International Conference on Information Fusion*, pp. 316–323, IEEE, 2009.

[12] B.-T. Vo, B.-N. Vo, and A. Cantoni, "Analytic implementations of the cardinalized probability hypothesis density filter," *IEEE transactions on signal processing*, vol. 55, no. 7, pp. 3553–3567, 2007.

[13] Y. Korkmaz and B. Baykal, "Track loss versus computation time dilemma in multitarget ground target tracking performance," in *Proceedings of the 16th International Conference on Information Fusion*, pp. 2168–2176, IEEE, 2013.

[14] J. Nilsson, Y. Gao, A. Carvalho, and F. Borrelli, "Manoeuvre generation and control for automated highway driving," *IFAC Proceedings Volumes*, vol. 47, no. 3, pp. 6301–6306, 2014.

[15] T. Weiskircher, Q. Wang, and B. Ayalew, "Predictive guidance and control framework for (semi-) autonomous vehicles in public traffic," *IEEE Transactions on control systems technology*, vol. 25, no. 6, pp. 2034–2046, 2017.

[16] Q. Wang, B. Ayalew, and T. Weiskircher, "Predictive maneuver planning for an autonomous vehicle in public highway traffic," *IEEE Transactions on Intelligent Transportation Systems*, vol. 20, no. 4, pp. 1303–1315, 2018.

[17] B. Paden, M. Čáp, S. Z. Yong, D. Yershov, and E. Frazzoli, "A survey of motion planning and control techniques for self-driving urban vehicles," *IEEE Transactions on Intelligent Vehicles*, vol. 1, no. 1, pp. 33–55, 2016.

[18] S. Särkkä, *Bayesian filtering and smoothing*, vol. 3. Cambridge University Press, 2013.

[19] D. Musicki and T. L. Song, "Track initialization: Prior target velocity and acceleration moments," *IEEE Transactions on Aerospace and Electronic Systems*, vol. 49, no. 1, pp. 665–670, 2013.

[20] S. Challa, M. R. Morelande, D. Mušicki, and R. J. Evans, *Fundamentals of object tracking*. Cambridge University Press, 2011.

[21] E. Mazor, A. Averbuch, Y. Bar-Shalom, and J. Dayan, "Interacting multiple model methods in target tracking: a survey," *IEEE Transactions on aerospace and electronic systems*, vol. 34, no. 1, pp. 103–123, 1998.

[22] X. R. Li and V. P. Jilkov, "Survey of maneuvering target tracking. part v. multiple-model methods," *IEEE Transactions on Aerospace and Electronic Systems*, vol. 41, no. 4, pp. 1255–1321, 2005.

Part III

Multi-Detection Multi-Target Tracking

Introduction to Part III

High resolution sensors return multiple detections per target, as such the target (called extended object) extends over multiple sensor resolution cells. In general, there is a growing trend that points towards target detection and tracking based on multiple detections. Furthermore, it is customary to use multiple sensors that cover different and/or overlapping fields of view (FOV) and fuse sensor detections in an effort to provide robust and reliable tracking. As a consequence, in high resolution multi-sensor settings, the data association uncertainty and the corresponding tracking complexity increases.

In chapter 6, to cope with tracking complexity in multiple high resolution sensors, we propose a hybrid scheme that combines the approaches of data clustering at the local sensor and multiple detection tracking scheme at the fusion layer. We implement a track-to-track fusion scheme that de-correlates local (sensor) tracks to avoid double counting and applies a measurement partitioning scheme to re-purpose the LMIPDA tracking algorithm to multi-detection cases.

In chapter 7, we discuss perception and tracking of individual as well as group targets as applied to multi-lane public traffic. We formulate the tracking problem as a two hierarchical layer: - at level 1, we distinguish multi-target tracking based on multiple detections represented in the measurement space and at level 2, dealts with group target tracking with birth and death as well as merging and splitting of group target tracks as they evolve in a dynamic scene. This arrangement enhances the multi-target tracking performance in situations including but not limited to target initialization(birth), target occlusion, missed detections, unresolved measurement, target maneuver etc. In addition, target groups expose complex individual target interactions to help in situation assessment which are challenging to capture otherwise.

This page is intentionally left blank.

Chapter 6

Tracking and Fusion of Multiple Detections for Multi-Target Multi-Sensor Tracking in Urban Traffic

6.1 Introduction

Advances in computing power and sensor technologies are enhancing resolution of automotive sensors such as radars and laser range scanners. The positive impact of which is reflected in the prevalence of advanced driver assistance system (ADAS) functionalities that enhance safety and comfort of the passenger and/or driver. However, the data association uncertainties and thus the corresponding complexity of the tracking algorithm increases, especially under stringent real-time requirements of operating in dense urban type traffic.

Traditionally, it sufficed to use what is referred in literature as a "point target" model or "small target approximation" to track multiple targets from sensor returns. No spatial extent is assumed and each object can only give rise to at most one detection per sensor scan [1],[2]. However, high

resolution sensors return multiple detections per target, as such the target (called extended object) extends over multiple sensor resolution cells. In general, there is a growing trend that points towards target detection and tracking based on multiple detections [3], [4]. For an excellent literature survey on extended object tracking including overview and applications refer to [2], [5], [1].

Several multi-target tracking (MTT) algorithms are applied in the context of the "point target" assumption to jointly estimate the unknown number of targets and their states. Recent survey papers, including [6] and [7] present a detailed account of MTT algorithms. In this paper, we use a tracking system based on the Linear Multi-target Integrated Probabilistic Data Association Filter (LMIPDAF) and adapt it to address target initiation and termination processes, clutter density estimation, and automatic track management features. The extension of LMIPDAF to handle the possibility of multiple detections is derived via measurement partitioning approaches in [8].

Furthermore, it is customary to use multiple sensors that cover different and/or overlapping fields of view (FOV) and fuse sensor detections in an effort to provide robust and reliable tracking. As a consequence, in high resolution multi-sensor settings, the data association uncertainty and the corresponding tracking complexity increases. Popular fusion architectures [9], [10] include: centralized fusion, where detections from multiple sensors are combined at the fusion center and distributed fusion, where independent trackers on each sensors' detections generate tracks that are combined at the data fusion center. The latter configuration offers a computationally attractive option by saving the communication load between local sensors and the fusion node[11],[12],[13]. Here, we implement a track-to-track fusion scheme that de-correlates local (sensor) tracks to avoid double counting. To cope with tracking complexity in multiple high resolution sensors, we propose a hybrid scheme that combines the approaches of data clustering at the local sensor and multiple detection tracking scheme at the fusion layer.

The paper is organized as follows. In Section 6.2, we briefly review related work done in multi-target and extended target tracking including experimental implementations. In Section 6.3, we discuss the multi-detection multi-target tracking algorithm based on LMIPDA approach. The results and discussions section, Section 6.4, presents evaluation of the performance of the tracking algorithm on simulated and experimental data. In the last section, Section 6.5, conclusions and future extensions of the current work are summarized.

6.2 Related Work

Multi Target Tracking

A range of Multiple target tracking (MTT) algorithms are reported in various tracking applications, with the most popular being the joint probabilistic data association filter (JPDAF) [14], multiple hypothesis tracking (MHT) [15], and random finite set (RFS) based multi-target filters [16]. MTT algorithms can be classified into two categories based on the approach taken to handle data association uncertainties. Tracking methods based on finite set statistics (FISST), avoid explicit data association and constitute the first category. Mahler introduced this approach in which target states and measurements are modeled as random finite sets (RFS). It allows multiple target tracking in the presence of clutter and with uncertain associations to be cast in a Bayesian framework [16], thereby allowing formulation of the optimal multi-target Bayes filter. An important contribution of FISST is that the statistical moments of the RFS enable practical, although approximate, implementation of the optimal implementation of the optimal multi-target Bayes filter. For example, the first order moment of an RFS is called the probability hypothesis density (PHD), and is an intensity function defined over the target state space. The PHD filter propagates the target state's PHD in time and represents an approximation to the optimal multi-target Bayes filter [6], [16]. However, the PHD and the related Cadinality PHD or CPHD filters do not formally estimate target trajectories in their basic forms. A post processing step is required to achieve this. To alleviate this problem, the generalised labelled multi-Bernoulli (GLMB) filter [17] and it computationally efficient version the labelled multi-Bernoulli (LMB) filter [18] were proposed recently.

Methods that explicitly handle data association constitute the second category. The most basic MTT algorithms use a simple extension of single target tracking (STT) algorithms into a bank of parallel filters that perform independent target tracking. Thus, in the data association step, the possibility that a measurement may have originated from a target not being followed by the current track is ignored. This method rarely proves satisfactory in practice [19]. In contrast, more rigorous MTT algorithms attempt to resolve origin of each measurement. Optimal multitarget trackers iterate all possible joint measurement-to-track assignment hypotheses and recursively calculate their posteriori probabilities. This clearly worsens the computational problem as the number of possible joint measurement assignments grows combinatorially with the number of tracks and the number of validated

measurements [20], [19]. The key in all of these methods is to compute joint association probabilities by iterating through joint association events in order to avoid conflicting measurement to track assignments. To avoid the complex hypothesis generation required by the data association in the above methods, a Linear Multi-Target (LM) procedure is proposed in [21]. Therein, measurement-to-track assignment is done on a track-by-track basis, where the clutter density from the perspective of the track under consideration is modified with the non-target detections. Each track can then be updated as in a single target tracker by utilizing the modified clutter density. This provides coupling between individual tracks without requiring an explicit combinatorial measurement-to- track enumeration step. In this paper, we adapt this approach and apply it with provisions to handle multiple detections from individual sensors.

Extended Target Tracking

In extended target tracking, in addition to estimating the motion of the (center of mass of) target detections, it is also of interest to estimate the shape, size and orientation of the target. From modeling point of view, the prevalent approaches is partitioning of the detections into mutually exclusive cells and then feed the resulting partitions into any of the conventional MTT trackers discussed above. For the sake of extent estimation the two well researched methods are:- the random matrix and the random hyper-surface model. The random matrix model, introduced by Koch [22], assumes a symmetric positive definite matrix that lends itself to a recursive approximation of the target shape by an ellipsoid. The overall tracking problem then becomes an estimation of the random state x_k (composed of target position and its derivatives) and the estimation of the object extent X_k approximated by an ellipsoid. An improvement over [22] that relaxes the sensor noise assumption is presented in [23, 24]. However, both the original and improved approaches are based on linear measurement models which render the straight-forward extension to radar detections that include range, azimuth and Doppler measurements slightly complicated. Comparison among different implementations and further improvements on the random matrix approach are discussed in [1], [25] and [26].

The random matrix model could be extended to the estimation of generic shapes by recasting the shape estimation into a combination of several elliptically shaped sub-objects as demonstrated in [27]. However, the second approach based on the random hypersurface model offers a flexible

option, albeit at a higher computational cost, to model general star-convex shapes. In this model measurement sources are assumed to lie on a randomly scaled versions of shape boundaries [28],[29].

In [30], a tracking technique that models the multi-target state as a generalized labeled multi-Bernoulli (GLMB) random finite set (RFS) is proposed. For extent estimation, the targets are modeled using gamma Gaussian inverse Wishart (GGIW) distributions. The authors also provide a less accurate but faster variant of the algorithm based on the labelled multi-Bernoulli (LMB) filter. Other tracking methods based on the RFS multi-target modeling paradigm include the results in [31] and [32] that incorporate random matrices to estimate the shape of extended targets in what are termed respectively as Gaussian inverse Wishart PHD (giw-phd) and gamma-Gaussian-inverse Wishart (GGIW) filters. Non-RFS filtering methods have also been reported in extended object tracking literature. The use of Gaussian processes to track boundaries of unknown shapes of extended objects is proposed in [33] and are shown to be more precise than the elliptical approximations above. A generalization of [22] for multiple extended targets that recursively estimates both the kinematic state and the elliptic shapes is proposed in [34]. The filter is based on probabilistic multi-hypothesis tracking (PMHT) framework that implements the expectation-maximization (EM) scheme to assign multiple detections. Generalizations of the Probabilistic Data Association (PDA) and Joint Probabilistic Data Association Filter (JPDAF) to multiple detection are presented in [35] and [36], respectively.

In general, extent estimation starts with an approximation of the target boundary by certain geometric shapes such as ellipses or rectangles. Then, the parameters of the assumed shape, i.e. the length of major and minor axes of an ellipse or length and width of a rectangle are estimated recursively at each scan time. However, a challenge comes when the detections originate from only one side of the target such as the rear of the target and when comparatively low number of detections are available from the target. In addition, the angles and the sensor-to-target distances might also affect the accuracy of the resulting estimation from distorted detections. Thus the joint estimation of the state and extent is a problem that we will postpone for now and we will primarily focus on state estimation part of it. It is important to mention that some sensors such as LIDAR provide a much detailed 3-D point cloud detection (at most of the scan times) so that the target contour could reliably be extracted to infer the shape, size, orientation reliably. The bounding box generated from object detection modules that operate on camera images can also provide an indispensable shape

information to which a 2D/3D geometry could be fitted to propagate the extent of the target at a much lower cost [37].

Practical Implementations

A multi-target tracking filter for millimeter-wave frequency-modulated continuous wave (FMCW) radar is presented in [38]. Using the "point target" assumption, the nearest neighbor data association method is used to resolve measurement-to-track assignment in a multi detection situation. The radar detections include range, radial velocity, azimuth and elevation measurements. In [3], the use of labeled multi-Bernoulli filter for tracking multiple vehicles using multiple high-resolution radars is demonstrated. For the extended object model, a direct scattering approach that computes expected measurements for given object states and then compares them to the actual measurements was proposed. Experiments conducted on single and multiple vehicles tracked by two radar sensors show the feasibility of the tracking algorithm. Performance evaluation among different waveform configurations (continuous and stepped frequency) of single automotive radar as well as fusion among multiple radars is studied in [39] for blind spot monitoring application. Detection-to-track association is based on the largest likelihood match that selects a single detection to update existing tracks. [40] presents data association methods based on PDA for single target case and JPDA for multi-target as applied to water vessel tracking using automotive radar. However, the combinatorial problem of data association due to high resolution radar and handling of unknown number of targets is not addressed. A handful of papers ([41], [42]) studied the joint object detection and tracking schemes at the sensor level to enhance the signal processing algorithm and/or add new features such as object classification that are normally unavailable otherwise. The track management module often includes false target discrimination and compensation for missing target detections and usually builds on top of detection clustering and data association steps. In this paper, we process raw detections that underwent signal processing stages. The signal processing stages include range processing through windowing and 1D fast Fourier transform (FFT), 2D windowing and FFT for Doppler processing, application of Constant False-Alarm Rate (CFAR) in the range-Doppler domain and angle estimation.

Contributions

We present a multi target tracking algorithm with track management scheme that can track multiple targets from multiple radar reflections as used in automotive applications. For the sake of managing computational complexity, especially under multi-sensor settings, we demonstrate a hybrid structure that implements a clustering strategy at individual sensor level and perform a multi-detection tracking on top of the clustered sensor detections. This approach is compared with alternative configurations to illustrate the performance benefits both in terms of tracking accuracy and speed of computation. The tracker is based on Multiple Detection-LMIPIDA (hereafter, abbreviated as MD-LMIPDA) and we focus on its application to automotive radar tracking and a variation of the same that implements both clustering (as in conventional tracking algorithms) and multiple detection tracking. The hybrid approach combines the clustering techniques that alleviate computational complexity and the multiple detection technique that admits multiplicity of the target detections. In addition, we have conducted a practical multi-target tracking experiment using an automotive radar and evaluated the performance of the MD-LMIPDA algorithm based on RTK-GPS data.

6.3 Problem Formulation

6.3.1 State Model

The motion model for a single target is described by a general nonlinear function of the states with an additive process noise:

$$x_k^\tau = \psi(x_{k-1}^\tau) + \Gamma v_k \tag{6.1}$$

We assume a constant turn kinematic equation for the motion of target τ, with state variables $x_k^\tau = [x, \dot{x}, y, \dot{y}, \dot{\omega}]$. $[x, y]$ and $[\dot{x}, \dot{y}]$ are, respectively the target positions and velocities, whereas $\dot{\omega}$ is the turn rate. An additive noise term v_k is assumed with $E[v_k] = 0$ and $E[v_k v_k^T] = Q_k$. ψ and Γ

are given in (6.2) and (6.3), respectively.

$$\psi(x) = \begin{pmatrix} x + \frac{\dot{x}}{\omega}\sin(\omega\Delta t) - \frac{\dot{y}}{\omega}(1 - \cos(\omega\Delta t)) \\ \dot{x}\cos(\omega\Delta t) - \dot{y}\sin(\omega\Delta t) \\ y + \frac{\dot{x}}{\omega}(1 - \cos(\omega\Delta t)) + \frac{\dot{y}}{\omega}\sin(\omega\Delta t) \\ \dot{x}\sin(\omega\Delta t) - \dot{y}\cos(\omega\Delta t) \\ \omega \end{pmatrix} \tag{6.2}$$

$$\Gamma = \begin{pmatrix} \Delta t^2/2 & \Delta t & 0 & 0 & 0 \\ 0 & 0 & \Delta t^2/2 & \Delta t & 0 \\ 0 & 0 & 0 & 0 & 1 \end{pmatrix}^T \tag{6.3}$$

6.3.2 Measurement Model

As shown in Figure 6.1, radar detections are given with respect to the moving sensor frame by the tuple (R_i, θ_i) for range and azimuth measurements. For a reflection point at (x_i, y_i) and a sensor located at $(x_{s,0}, y_{s,0})$, the single measurement model η is composed as:

$$R_i = \sqrt{(x_i - x_{s,0})^2 + (y_i - y_{s,0})^2} \tag{6.4a}$$

$$\theta_i = \tan^{-1}\left(\frac{y_i - y_{s,0}}{x_i - x_{s,0}}\right) \tag{6.4b}$$

A sensor collects a set of detections without apriori information about the source of origin. Let ζ_τ be the assumed maximum number of detections that a target generates at each scan time k. $\xi_\tau \leq \zeta_\tau$ multiple detections that are generated at scan time k are related to the state variables as follows:

$$z_k^\tau = \eta_{\xi_\tau}(x_k^\tau) + w_{\xi_\tau,k} \tag{6.5}$$

where η_{ξ_τ} and $w_{\xi_\tau,k}$ are composed by a vertical vectorial concatenation ($\oplus$) from a single detection measurement function η and single detection measurement noise w_k as given in (6.6) and (6.7) respectively.

$$\eta_{\xi_\tau} = \bigoplus_{\xi_\tau} \eta \tag{6.6}$$

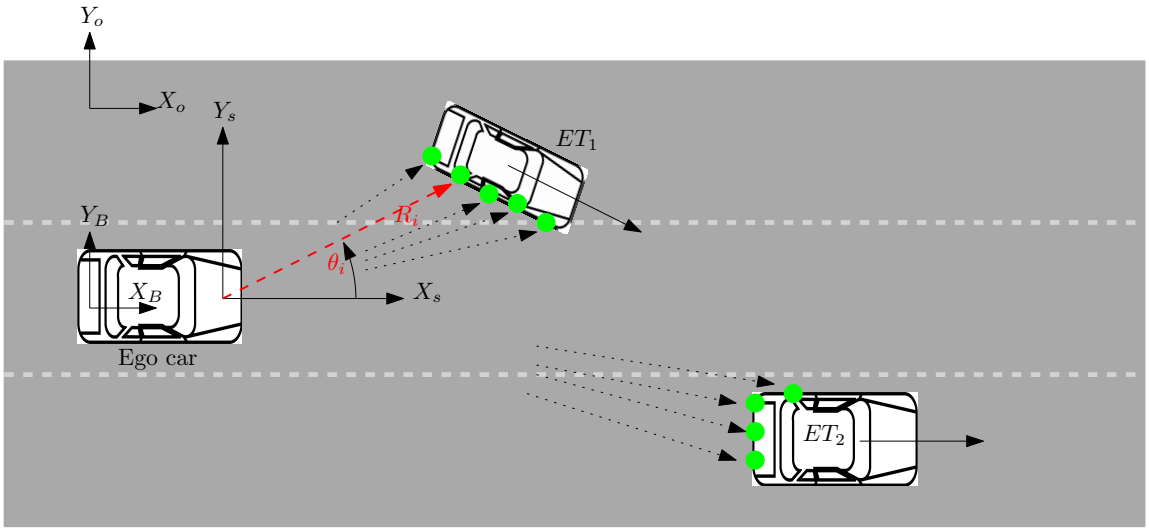

Figure 6.1: Multiple radar returns (green circles) reflected off extended targets (ET_1, ET_2) are registered as pairs of range and azimuth angle (R_i, θ_i). All measurements are reported with respect to a moving sensor frame (X_s, Y_s). The motion of the ego vehicle (X_B, Y_B) can be described with respect to a fixed frame (X_0, Y_0).

$$w_{\xi_\tau,k} = \bigoplus_{\xi_\tau} w_k \tag{6.7}$$

We assume that each of the target originated measurements $z^\tau_{k,i}$ follows a Gaussian distribution with covariance R, represented as $\mathcal{N}(z^\tau_{k,i}; \eta(x^\tau_k), R)$. The clutter is assumed to have a Poisson distribution with a uniform spacial distribution in the surveillance region.

To reduce the computation involved in the data association step, it is customary to consider only a subset of measurements that are (possibly) generated by all targets and clutter set as well. This is done by a validation gate defined around the predicted measurement of each target $\eta(x^\tau_k)$.

$$\left(z_{k,i} - \eta(x^\tau_k)\right)^T S^{-1}_\tau \left(z_{k,i} - \eta(x^\tau_k)\right) \leq \gamma \tag{6.8}$$

S_τ is the measurement innovation covariance and γ is the threshold based on the required gating probability P^τ_G of target τ. Since we are permitting multiple detections per target, we define a partitioning scheme as discussed in [43],[44]. As an illustration, for $\zeta_\tau = 4$, if the set of detections validated for target τ are $z_k = \left\{z^\tau_{k,1}, z^\tau_{k,2}, z^\tau_{k,3}, z^\tau_{k,4}\right\}$, the 16 measurement partitions are shown in Figure 6.2.

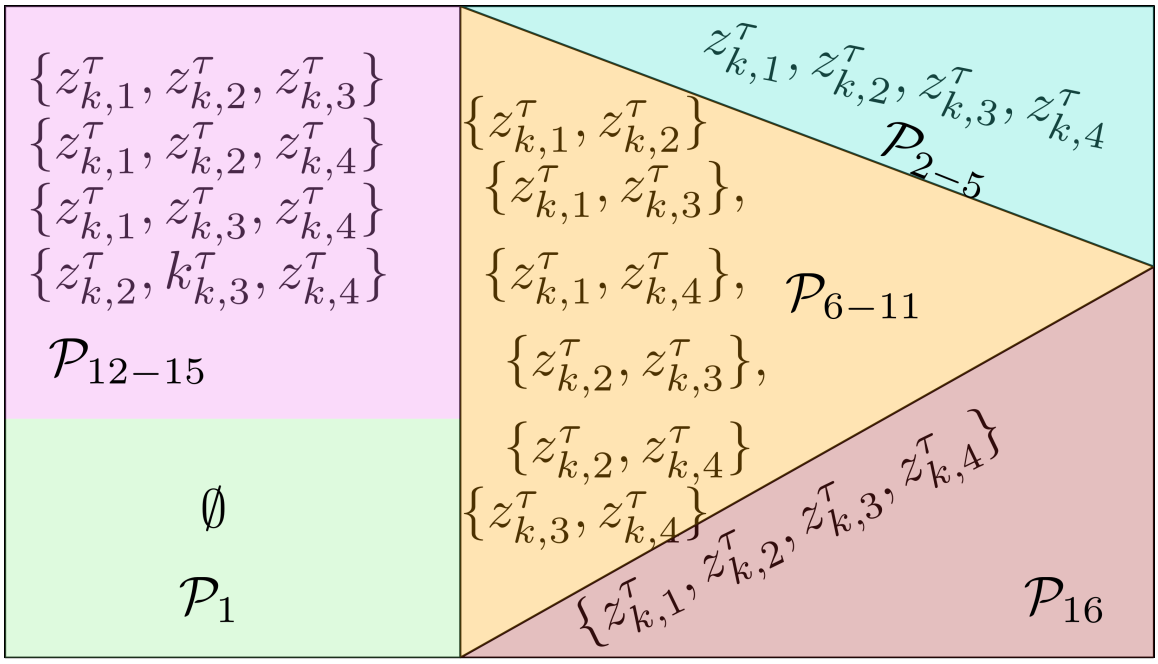

Figure 6.2: Illustration of measurement partitions for 4 target detections. The only possibilities considered in classical tracking algorithms are $\mathcal{P}_1$ and $\mathcal{P}_{2-5}$.

For a single target, the data associations will be computed for all the measurement cells enumerated above. Whereas, for multiple targets, the joint data association has to be computed for all targets sharing one or more measurement cells. As the number of measurements and targets increases, this will be an intractable problem to solve. The core of the linear multi-target method lies in its approach to data association computations, where data association events are evaluated independently for each target and the contribution of other targets to the measurement cell is accounted by modifying the clutter density for the target under consideration.

For the sake of brevity, we will denote a measurement cell as z_{ξ_τ,n_τ}, where n_τ is the index within ξ_τ detections that ranges as $1 \leq n_\tau \leq n_{\tau,max}$. For a total number of m_k gated detections, $n_{\tau,max} = \binom{m_k}{\xi_\tau}$. Next, we summarize the steps required to modify the clutter density at the measurement cell z_{ξ_τ,n_τ} [8],[45]. While updating the track for target τ, we compute the prior probability of

measurement z_{ξ_τ,n_τ} that it is also a detection of target $\sigma \in T \setminus \tau$ as follows.

$$P^{\sigma}_{k,z_{\xi_\tau,n_\tau}} = P^{\sigma}_{D\xi_\tau}(P^{\sigma}_{G})^{\xi_\tau} P(\mathcal{X}^{\sigma}_{k}|Z^{k-1})\times \left(\frac{p^{\sigma}_{k,z_{j,i}}/\rho^{\sigma}_{k,z_{j,i}}}{\sum_{j=1}^{\xi_{\tau,max}} \sum_{i=1}^{n_{\tau,max}} p^{\sigma}_{k,z_{j,i}}/\rho^{\sigma}_{k,z_{j,i}}} \right) \tag{6.9}$$

Where, T is a set of targets and $P^{\sigma}_{D\xi_\tau}, P^{\sigma}_{G}, P(\mathcal{X}^{\sigma}_{k}|Z^{k-1})$, are respectively the probability of detection, probablity of gating and probablity of target existence. Z^{k-1} represents gated measurement trajectories up to and including scan $k-1$. For a validated measurment cell z_{ξ_τ,n_τ}, the likelihood $p(z_{\xi_\tau,n_\tau}|\mathcal{X}^{\tau}_{k}, Z^{k-1})$ is computed as follows:

$$p^{\sigma}_{k,z_{\xi_\tau,n_\tau}} = \frac{1}{(P^{\tau}_{G})^{\xi_\tau}} \mathcal{N}\left(z_{\xi_\tau,n_\tau}; \eta_{\xi_\tau}(x^{\tau}_{k}), S_{\xi_\tau,n_\tau}\right) \tag{6.10}$$

Initially, we will treat the non-target measurements as single detections and the contribution to clutter at the measurement cell z_{ξ_τ,n_τ} is simply computed as follows:

$$\rho^{\sigma}_{k,z_{\xi_\tau,n_\tau}} = \prod_{\forall z_i \in z_{\xi_\tau,n_\tau}} \rho^{\sigma}_{k,z_i} \tag{6.11}$$

The modulated clutter density that accounts for both the pure clutter and the presence of non-targets that share the measurement cell z_{ξ_τ,n_τ} is derived as [8]:

$$\rho^{\tau}_{k,z_{\xi_\tau,n_\tau}} = \sum_{\forall \sigma \in T\setminus\tau} p^{\sigma}_{k,z_{\xi_\tau,n_\tau}} \frac{P^{\sigma}_{k,z_{\xi_\tau,n_\tau}}}{\prod_{\forall z_i \in z_{\xi_\tau,n_\tau}} \left(1 - P^{\sigma}_{k,z_i}\right)} + \prod_{\forall z_i \in z_{\xi_\tau,n_\tau}} \rho^{\tau}_{k,z_i} \tag{6.12}$$

where P^{σ}_{k,z_i} is evaluated by dissociating the measurement cell z_{ξ_τ,n_τ} into single detections.

6.3.3 Multi-Target Tracking Procedure

The multi-target tracking algorithm goes through a prediction and update step in a recursive manner. The prediction and update both use Unscented Kalman Filter (UKF) and are tabulated respectively under Algorithms 1 and 2.

Prediction

For each track $\tau \in T$, the time update of the state and its covariance are obtained from UKF prediction equations. For the UKF implementation, the transformation parameters $\alpha = 0.5$, $\beta = 2$ and $\kappa = 0$ are chosen. Also, $\lambda = \alpha^2(n + \kappa) - n$, where n is the dimension of the state variable. $W_i^{(m)}, W_i^{(c)}$ are respectively the mean and covariance weights [46],[47].

Algorithm 1: Unscented Kalman Filter Prediction Equation (Modified)

Input : $x_{k-1|k-1}, P_{k-1|k-1}, \psi, Q_{k-1}, W_i^{(m)}, W_i^{(c)}$
Output: $x_{k|k-1}, P_{k|k-1}$

1. Form sigma points: $i = 1, \ldots, n$
   - $\mathcal{X}_{k-1}^{(0)} = x_{k-1|k-1}$
   - $\mathcal{X}_{k-1}^{(i)} = x_{k-1|k-1} + \sqrt{n+\lambda}[\sqrt{P_{k-1|k-1}}]_i$
   - $\mathcal{X}_{k-1}^{(i+n)} = x_{k-1|k-1} - \sqrt{n+\lambda}[\sqrt{P_{k-1|k-1}}]_i$
2. Propagate the sigma points: $i = 0, \ldots, 2n$
   - $\hat{\mathcal{X}}_k^{(i)} = \psi\left(\mathcal{X}^{(i)}\right)$
3. Compute the predicted mean and Covariance
   - $x_{k|k-1} = \sum_{i=0}^{2n} W_i^{(m)} \hat{\mathcal{X}}_k^{(i)}$
   - $P_{k|k-1} = Q_{k-1} + \sum_{i=0}^{2n} W_i^{(c)} \left(\hat{\mathcal{X}}_k^{(i)} - x_{k|k-1}\right)\left(\hat{\mathcal{X}}_k^{(i)} - x_{k|k-1}\right)^T$
4. Form sigma points: $i = 1, \ldots, n$
   - $\mathcal{X}_k^{-(0)} = x_{k|k-1}$
   - $\mathcal{X}_k^{-(i)} = x_{k|k-1} + \sqrt{n+\lambda}[\sqrt{P_{k|k-1}}]_i$
   - $\mathcal{X}_k^{-(i+n)} = x_{k|k-1} - \sqrt{n+\lambda}[\sqrt{P_{k|k-1}}]_i$
5. Propagate the sigma points: $i = 0, \ldots, 2n$
   - $\hat{\mathcal{Y}}_k^{(i)} = \eta\left(\mathcal{X}^{-(i)}\right)$
6. Compute the predicted mean and Covariances
   - $\mu_k = \sum_{i=0}^{2n} W_i^{(m)} \hat{\mathcal{Y}}_k^{(i)}$
   - $S_k = R_k + \sum_{i=0}^{2n} W_i^{(c)} \left(\hat{\mathcal{Y}}_k^{(i)} - \mu_k\right)\left(\hat{\mathcal{Y}}_k^{(i)} - \mu_k\right)^T$
   - $C_k = \sum_{i=0}^{2n} W_i^{(c)} \left(\hat{\mathcal{X}}_k^{-(i)} - x_{k|k-1}\right)\left(\hat{\mathcal{Y}}_k^{(i)} - \mu_k\right)^T$

The probability of target existence is predicted assuming Markov chain one model

$$P(\mathcal{X}_k^\tau | Z^{k-1}) = \pi_{11} P(\mathcal{X}_{k-1}^\tau | Z^{k-1}) \tag{6.13}$$

π_{11} is a transition probability [48].

Update

Each of the confirmed tracks select a set of measurements according to (6.8) which will then go through the measurement partitioning step. After iterating though all target tracks and measurement cells, the modified clutter density is computed using (6.12). Now that the clutter density is modified to account for the presence of non-targets, we forgo the expensive computation of the joint data association events for the cheaper (but sub-optimal) single target data association events. For any of the measurement partitions of τ denoted by z_i, $\beta^\tau_{z_i} = p\left(z_i|\mathcal{X}^\tau_k, Z^k\right)$ is the event that target τ exists and that measurement cell z_i is a detection of target τ. Here, $Z_k = z_k \cup Z^{k-1}$. Likewise, the event that none of the measurement cells are detections of τ is denoted as β^τ_0.

$$\beta^\tau_{z_i} = \begin{cases} \frac{P^\tau_{D\xi_\tau}(P^\tau_G)^{\xi_\tau} p^\tau_{k,z_{\xi_\tau,n_\tau}}}{\Lambda^\tau_k \rho^\tau_{k,z_{\xi_\tau,n_\tau}}} \xi_\tau! & \text{if } z_i = z_{\xi_\tau,n_\tau} \\ \frac{1-\sum_{\xi_\tau=1}^{\xi_{\tau,max}} P^\tau_{D\xi_\tau}(P^\tau_G)^{\xi_\tau}}{\Lambda^\tau_k} & \text{if } z_i = 0 \end{cases} \tag{6.14}$$

where

$$\Lambda^\tau_k = 1 - \sum_{\xi_\tau=1}^{\xi_{\tau,max}} P^\tau_{D\xi_\tau}(P^\tau_G)^{\xi_\tau} + \sum_{j=1}^{\xi_{\tau,max}} \sum_{i=1}^{n_{\tau,max}} \frac{p^\tau_{k,z_{j,i}}}{\rho^\tau_{k,z_{j,i}}} P^\tau_{D\xi_\tau}(P^\tau_G)^{\xi_\tau}\xi_\tau! \tag{6.15}$$

where $n_{\tau,max}$ Now, the target existence probability update equation can be written as

$$P(\mathcal{X}^\tau_k|Z^k) = \frac{\Lambda^\tau_k P(\mathcal{X}^\tau_k|Z^{k-1})}{1-(1-\Lambda^\tau_k)\,P(\mathcal{X}^\tau_k|Z^{k-1})} \tag{6.16}$$

The updated state mean and covariance given the measurement partitions $p(x^\tau_k|\mathcal{X}^\tau_{k,\xi_\tau,n_\tau}, \mathcal{X}^\tau_k, Z^k)$ are computed as shown in (6.17). The state update equation is a Gaussian mixture weighted by the data association probabilities (6.14).

$$\begin{aligned} p(x^\tau_k|\mathcal{X}^\tau_k, Z^k) = \beta^\tau_0 p(x^\tau_k|\mathcal{X}^\tau_k, Z^{k-1}) + \\ \sum_{j=1}^{\xi_{\tau,max}} \sum_{i=1}^{n_{\tau,max}} \beta^\tau_{z_{j,i}} p(x^\tau_k|\mathcal{X}^\tau_{k,z_{j,i}}, \mathcal{X}^\tau_k, Z^k) \end{aligned} \tag{6.17}$$

Algorithm 2: Unscented Kalman Filter Update Equation (Modified)

Input : $x_{k|k-1}, P_{k|k-1}, \eta, R_k, W_i^{(m)}, W_i^{(c)}$
Output: $x_{k|k}, P_{k|k}$
1. Compute the filter gain, state and mean updates
   - $K_k = C_k S_k^{-1}$
   - $x_{k|k} = x_{k|k-1} + K_k[y_k - \mu_k]$
   - $P_{k|k} = P_{k|k-1} - K_k S_k K_k^T$

Track Management

A track management scheme handles track initiation, confirmation and termination procedures. Tentative tracks are initialized on each measurement not validated by any of the targets being tracked. We assume that our knowledge about the prior information on the tentative target velocity and acceleration vectors are limited to the maximum speed v_{max} and the maximum acceleration a_{max} [49],[50]. The initial state estimate and covariance matrix formulations follow a similar structure as presented in our previous works [51],[52], and [53].

The initial probability of object existence is given by:

$$P(\chi_k(\tau)|\mathbf{y}_k(i)) = P_0 \times \prod_{\tau} \big(1 - P(\chi_k(\tau)|Y^k)\beta_{k,i}(\tau)\big) \tag{6.18}$$

where P_0 is a tuning parameter for false track discrimination step.

Track-to-Track Fusion

The goal of track-to-track fusion is to fuse track outputs from independent multiple-detection trackers that run on separate sensors. This configuration offers a computationally attractive option that reduces the size of the measurement partition as compared to a single centralized tracker that operates on all detections from all sensors. With sensors that "inherently" generate target tracks, track-to-track fusion is the preferred option. However, if raw detections are available from sensors, one may also be inclined to consider clustering detections at sensor level and then track the processed multiple detections with reduced computational demand.

An illustration of track-to-track fusion is shown in Figure 6.3 where target vehicle detections are tracked by independent Trackers that run on three sensors' detections. Following a data association step, tracks are then fused together to get point estimate at the system level. It is important to

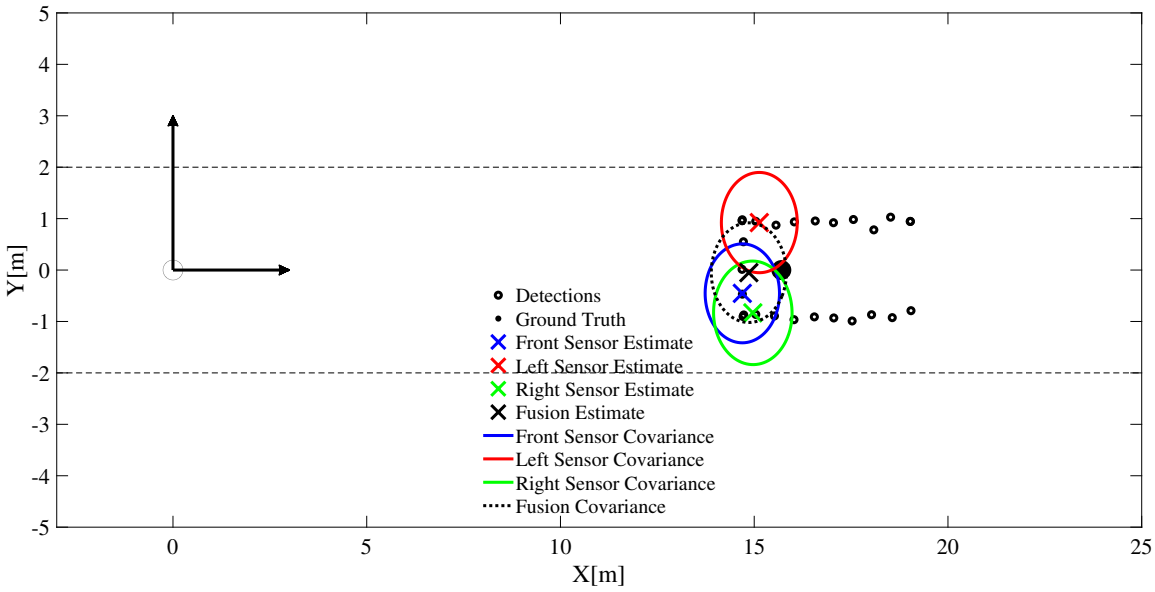

Figure 6.3: A multi-sensor multi-detection illustration.

mention that, in track-to-track fusion although local tracks are independently initiated and maintained on independent sensor detections, the tracks are still correlated due to the inherent nature of the time-correlated estimation schemes. In addition, tracks initiated on the same target, albeit based on detections from different sensors, cannot be treated as independent. This is partly due to the common priors and process noise terms utilized in the estimation process. There are several fusion techniques that address track de-correlation at the fusion level [11],[12],[13].

Another aspect that is critical to the performance of the fusion is the timing of events as seen from the fusion layer (system track). Local trackers receive detections at randomly spaced sampling instances dictated by the amount of information (the number of detections) processed at the sensor and its processing capacity. Here, we adopt the information de-correlation approach to track-to-track fusion as discussed in [13] and illustrated diagrammatically here in Figure 6.4. Equation (6.19) summerizes the same.

$$x_i = P\left[P_{i-1}^{-1}x_{i-1} + P_j^{-1}x_j - P_{j-1}^{-1}x_{j-1}\right] \tag{6.19}$$

where $P = \left(P_{i-1}^{-1} + P_j^{-1} - P_{j-1}^{-1}\right)^{-1}$ and $(x_j, P_j), (x_{j-1}, P_{j-1})$ are the local sensor estimate (and covariance) and its time-propagated previous estimate (and covariance), respectively. (x_{i-1}, P_{i-1})

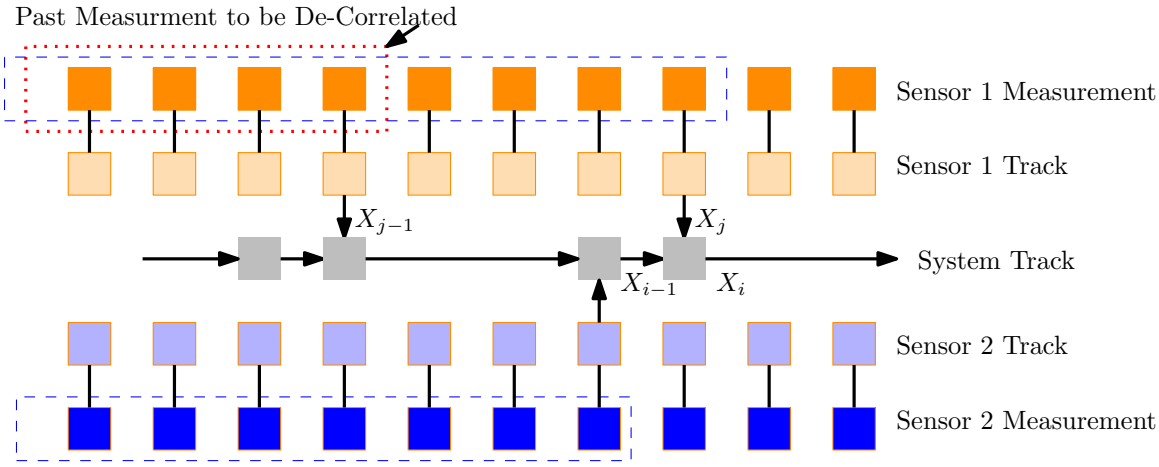

Figure 6.4: An illustration of a track-to-track fusion architecture where local tracks are fused to a system track. Past measurements are actively de-correlated to avoid "double-counting".

denote the system estimate and its covariance propagated to current time j.

6.4 Results and Discussions

In this section, we discuss and evaluate the performance of multi-detection algorithms on simulated and experimental target tracking scenarios. For the simulations, we use the driving scenario designer toolbox [54] to generate radar detections of a maneuvering target. We shall use the optimal sub-pattern assignment (OSPA) metric to evaluate the localization and cardinality error of various tracking algorithms and we also provide estimates of the computational times taken to complete a single iteration in each settings.

We briefly summarize the OSPA metric originally presented in [55] and [56] as follows. Let us represent the ground truth at time k by $\mathfrak{X}_k$ and a set of track estimates generated by the tracking algorithm as $\mathfrak{Y}_k$. Both $\mathfrak{X}_k$ and $\mathfrak{Y}_k$ are defined over a metric space $(\mathcal{X}, \mathcal{D})$, such that $\mathcal{D} : \mathcal{X}_k \times \mathcal{X}_k \rightarrow \mathbb{R}_+$ satisfies a distance metric in the usual sense. Furthermore, each element of the sets $\mathfrak{X}_k$ and $\mathfrak{Y}_k$ are of the form $(l_i, x_{k,i})$ and $(s_j, \tilde{x}_{k,j})$, respectively, where $l_i, i = (1, 2, \ldots, m)$ and $s_j, j = (1, 2, \ldots, n)$ are labels with cardinalities m, n such that $m \leq n$. For the sake of notational simplicity, we will write $x_{k,(.)}, \tilde{x}_{k,(.)}$ to refer to the labeled truth and estimated tracks of a target. The OSPA distance

between the sets $\mathfrak{X}_k$ and $\mathfrak{Y}_k$ is defined as:

$$\mathcal{D}_{p,c}(\mathfrak{X}_k, \mathfrak{Y}_k) = \left\{ \frac{1}{n} \left(\min_{\pi \in \Pi_n} \sum_{i=1}^{m} \left(d_c^{(x_{k,i}, \tilde{x}_{k,i})} \right)^p + C_e.c^p \right) \right\}^{\frac{1}{p}} \tag{6.20}$$

where Π_n is the set of permutations of length m with elements taken from $\{1, 2, \ldots, n\}$. p represents the order of the OSPA distance, where $1 \leq p < \infty$. $d_c^{(x_{k,i}, \tilde{x}_{k,i})} = \min\left(c, d^{(x_{k,i}, \tilde{x}_{k,i})}\right)$ is the distance between $x_{k,i}$ and $\tilde{x}_{k,i}$ cutoff at $c > 0$. Also, c determines the relative weight given to the cardinality error $C_e = (n - m)$ and localization error $d_c^{(x_{k,i}, \tilde{x}_{k,i})}$. The Normalized Estimation Error Squared (NEES), defined in (6.21), is used to measure the base distance, $d^{(x_{k,i}, \tilde{x}_{k,i})}$.

$$d^{(x_{k,i}, \tilde{x}_{k,i})} = (x_{k,i} - \tilde{x}_{k,i})^T P_{k/k}^{-1} (x_{k,i} - \tilde{x}_{k,i}) \tag{6.21}$$

6.4.1 Evaluations on Simulated Data

Single Target Tracking Performance

We consider two cases:- a single sensor and multi-sensor case. In the first case, the ego vehicle is fixed and the sensor is assumed to have a large enough FoV to cover detections from the maneuvering target. In the second case, the ego vehicle is equipped with multiple sensors and is moving in traffic. In this work, all simulations are done on a laptop with the specifications:- Intel Core i7 2.90 GHZ processor, installed Memory (RAM) of 16.0 GB and Windows 10 64-bit Operating system.

Stationary Ego Vehicle, Single Radar

The host vehicle is equipped with a radar sensor fitted into the front bumper. Assumptions about radar specifications are given in Table 6.1. In this scenario, the target vehicle ($length = 3.7m, width = 1.8m, height = 1.4m$) executes a "Figure-8" maneuver inside the radar's FoV as shown in Figure 6.5. The host vehicle is assumed to be stationary at the origin,$(0, 0)$ for the duration of the simulation. A sequence of detections as reported by the sensor are fed to the tracking algorithm at each scan time. The filtered target positions are plotted as a function of time in Figure 6.6. Figure 6.7 shows that the number of validated target detections varies between $2 - 10$; however, the possibility of missing target detections is low due to a high resolution sensor simulated here to generate a maximum of 10 detections per radar scan.

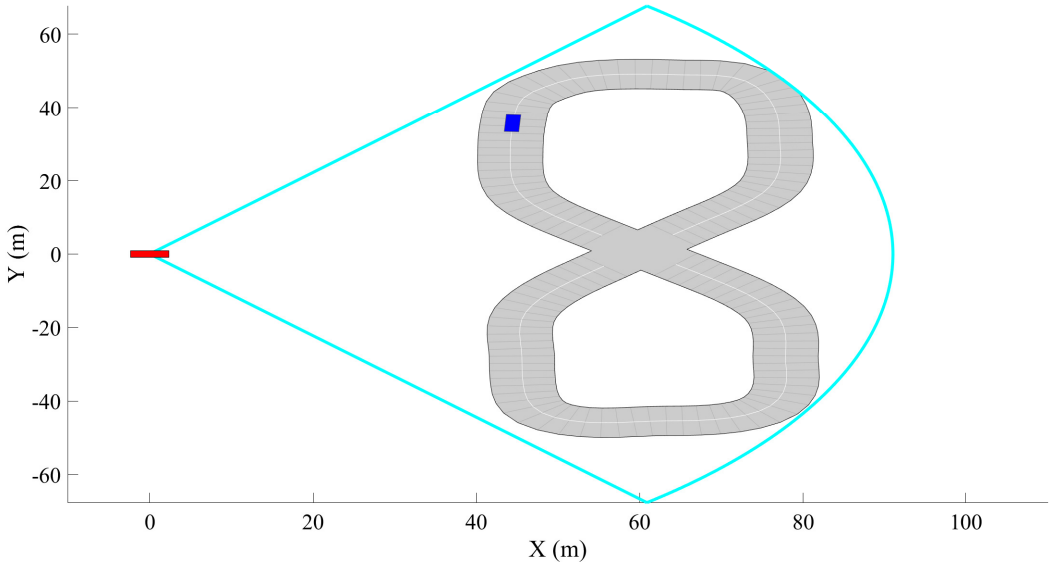

Figure 6.5: A stationary vehicle (red) equipped with a radar sensor observes as a target (blue) vehicle executes a "Figure-8" maneuver. The sensors FoV is represented by the sector (cyan). The ground truth trajectory is the center-line of the road which is 8m wide.

Stationary Ego Vehicle, Parameter Variation

The clutter density or False Alarm Rate, λ_o is varied from its default value given in Table 6.1 to further evaluate the tracking performance. The result of the simulation is shown in Figure 6.8. The variation of λ_o is seen to significantly affect the tracking error when the target is executing turns. For instance at the 2 second mark, the side of the target vehicle facing the radar changes gradually from the left side to the rear bumper, causing the centroid of the detections to shift in the process. As the clutter rate is increased to 10 fold of its nominal value, the mean OSPA error increases only slightly showing the robustness of the tracking algorithm to false alarm. As the target vehicle completes the

Table 6.1: Radar Specifications

Parameter	Value
Detection Probability	0.9
False Alarm Rate, λ_0	10^{-7}
Azimuthal Field of View (deg)	100
Range Field of View (m)	90
Azimuth Resolution (deg)	4
Range Resolution (m)	0.5
Update Interval (ms)	50
Maximum Number of Detections per Target	5

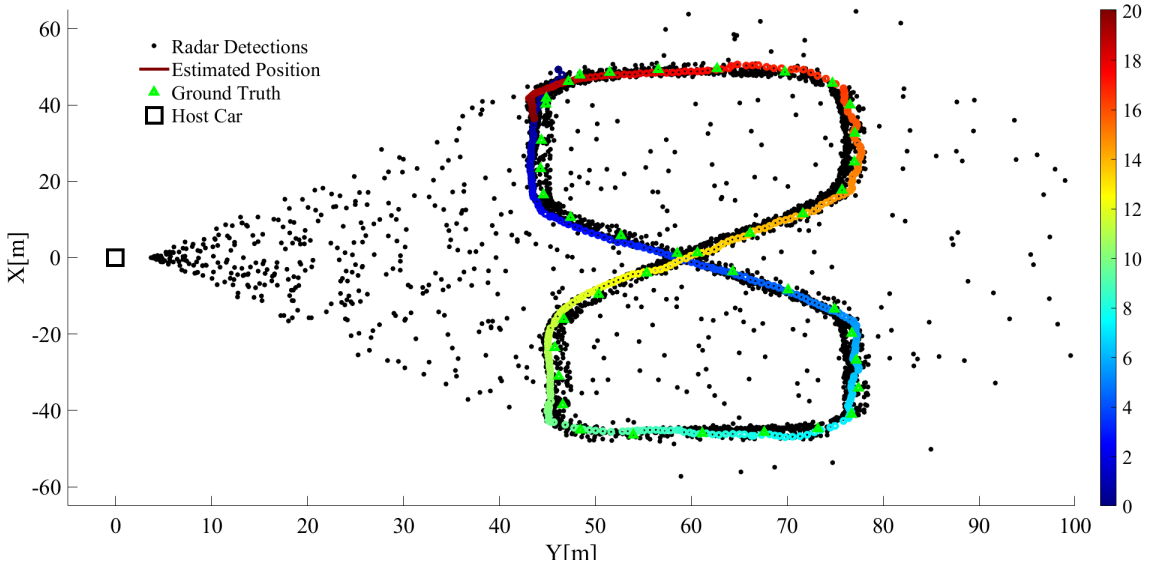

Figure 6.6: The filtered position of the target vehicle is shown along side the ground truth. The color varies steadily to reflect the progression of time as the vehicle starts at $(44, 37)$ and comes to a stop at approximately the same position.

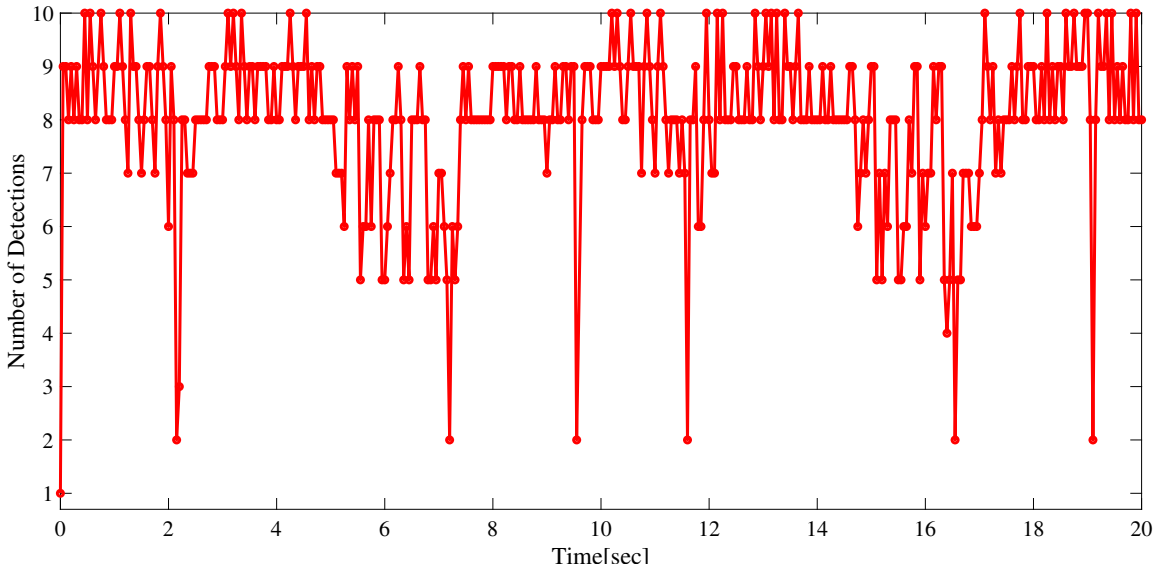

Figure 6.7: The number of validated radar detections for the single target as seen from a stationary vehicle (host). The radar is assumed to generate a maximum of 10 detections per target.

turn and moves along, the OSPA error decreases correspondingly, which agrees with the observation that detections in this segment of the trajectory mostly reflect off of the rear bumper of the vehicle. As shown in Figure 6.1, the ground truth positions of the target vehicle are essentially the trajectory of the center of the rear axle. Thus when the radar reports reflections from the other sides of the

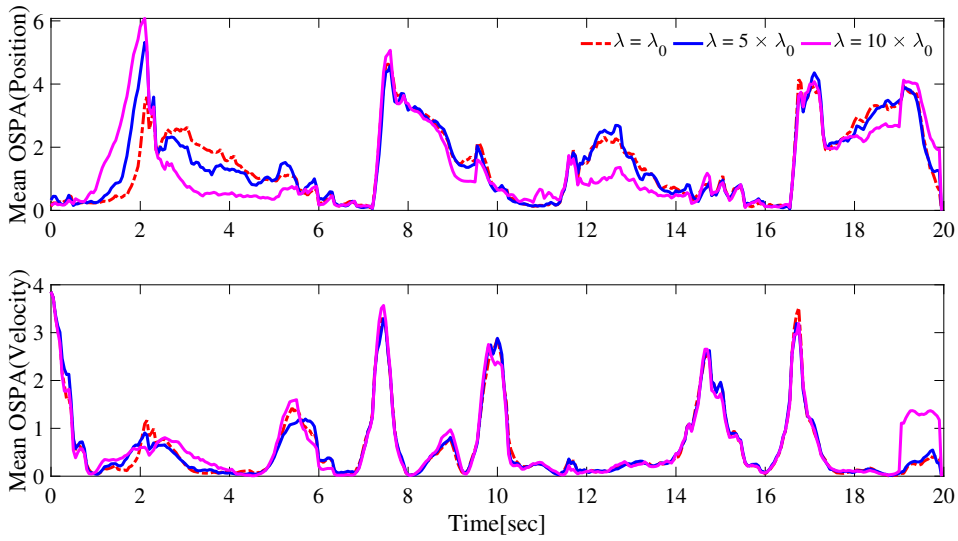

Figure 6.8: The mean position and velocity OSPA error of the tracking algorithm as the false alarm rate takes values $\lambda = \lambda_0$,$\lambda = 5 \times \lambda_0$ and $\lambda = 10 \times \lambda_0$.

vehicle, there is a deterministic error that depends on the dimensions of the vehicle.

Moving Ego Vehicle, Multiple Radar, Single Target Scenario

Three radar sensors, one long range (LRR) and two short range (SRR), are mounted on the ego vehicle as shown in Figure 6.9. Despite the azimuthal and range FoV differences, all sensors are assumed to process multiple detections from the target vehicle.

For the simulated radar settings, if 10 detections are validated per target, 1,024 measurement assignment hypothesis need to be evaluated! To cope with the increased computational complexity, we propose a hybrid tracking scheme that clusters detections at the sensor level while permitting multiple clusters per target vehicle. Unlike classical tracking algorithms that strive to cluster all detections of the target to get at most one cluster per target (hard decisions), we allow multiple clusters per target and feed the resulting clusters to the multi detection tracker which makes better decisions based on data association computations. In what follows, including the Hybrid MD-Tracker, we identify three multi-detection tracker configurations and evaluate them.

- **Single MD-Tracker**: All raw detections from the three sensors are fed to a single multi-detection tracker. This MD-Tracker has to deal with potentially multiple detections originating from a single reflection point, albeit being noisy, as independently reported from the three

sensors. The obvious drawback of this configuration is the computational complexity that increases with an increase in the number of detections.

- **Multiple MD-Trackers**: Three multi-detection trackers are run on each sensors' detections independently. A track-to-track fusion algorithm fuses confirmed tracks from the local trackers. Similar to the Single MD Tracker above, this configurations also suffers from computational complexity that increases with an increase in the number of detections per sensor. However, independent trackers that are based on separate sensors are amenable for parallel computation.

- **Hybrid MD-Tracker**: Radar detections are clustered at sensor level and the resulting detections are fed to a single multi-detection tracker. The clustering algorithm is based on DBSCAN [57], short for density-based spatial clustering of applications with noise. The selection of an "optimal" set of DBSCAN parameters that consistently work across multiple classes (truck, car, pedestrian, etc.) and over an arbitrary inter-vehicle distance (close or far) is not a straightforward decision.

The two DBSCAN parameters, i.e. the distance E and the minimum number of detections $minPts$ are tuned as follows. Choosing large values for E, results in the clustering of detections from nearby target and clutter together. Choosing a smaller value; however, results in multiple clusters per target vehicle which can be evaluated in the data association stage of the tracking algorithm. This is preferable as compared to a potentially erroneous hard decisions due to large E. Likewise, to discourage false alarms, large values for $minPts$ can be chosen owing to the high resolution sensors simulated here. In addition, for multiple tracks initiated on the same target, the track merging procedure undergoes a minimal overload compared to lower $minPts$ values.

A single target scenario is simulated as shown in Figure 6.9. The three high resolution sensors are configured to return at most 30 detections per sensor (including false alarms). The target vehicle progressively changes its lane exposing different sides to the radar sensors. E is varied in the range $[0, 1]$. Whereas, $minPts$ takes on discrete values from the set $\{1, 2, 3, 4, 5\}$. Choosing $E = [0.5, 0.6]$ and $minPts = \{2, 3, 4\}$, minimizes the number of clusters per target to at most 5 as shown in Figure 6.10. The ratio of clustered detections, i.e. (number of clustered detections)/(actual number of target detections), as shown in Figure 6.11 is also reasonably close to 1 for the chosen values of E and $minPts$.

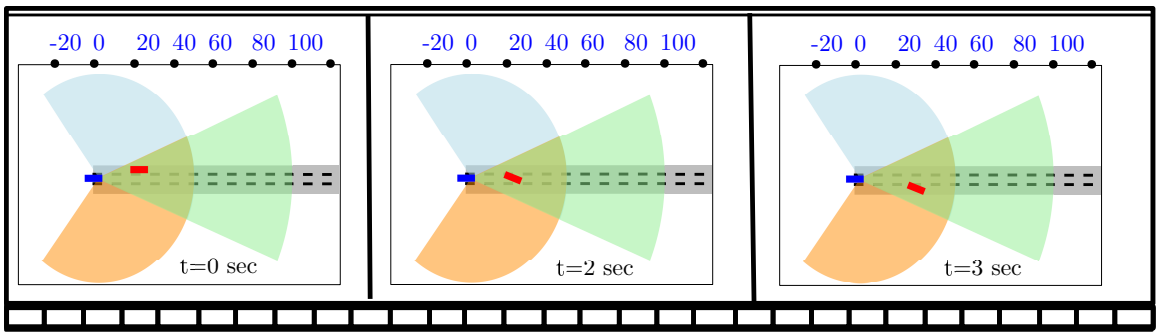

Figure 6.9: The relative position of a target vehicle (red) relative to the ego vehicle (blue) is shown at selected time instances. Both the ego and target vehicle travel at constant speed of $20m/s$.

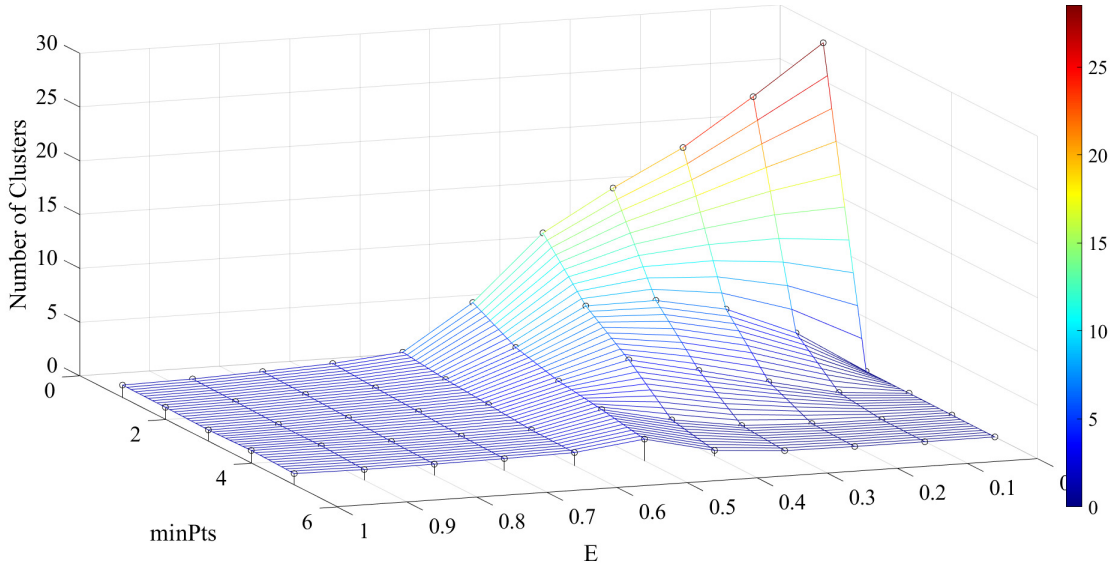

Figure 6.10: Average number of clusters for a single target. The number of clusters as E is varied in the range $[0, 1]$ and $minPts$ takes on values in the set $\{1, 2, 3, 4, 5\}$ is averaged for over a simulation run.

Although it is possible to track all the validated detections, for the sake of comparison, sensor detections are limited to utmost three as follows. After the measurement likelihood (Equation (6.9)) is computed for all the validated detections, the top three are selected for further processing and to ultimately update the target track. For the Single and Hybrid MD-Trackers this procedure is applied once. For the Multiple MD-Trackers, however, this step is applied at all the three trackers. The results are plotted in Figures 6.12 and 6.13.

The hybrid MD-Tracker option is seen to be computationally attractive and is also effective in estimating target track fairly well as shown in Figure 6.12 and 6.13. It takes less execution time

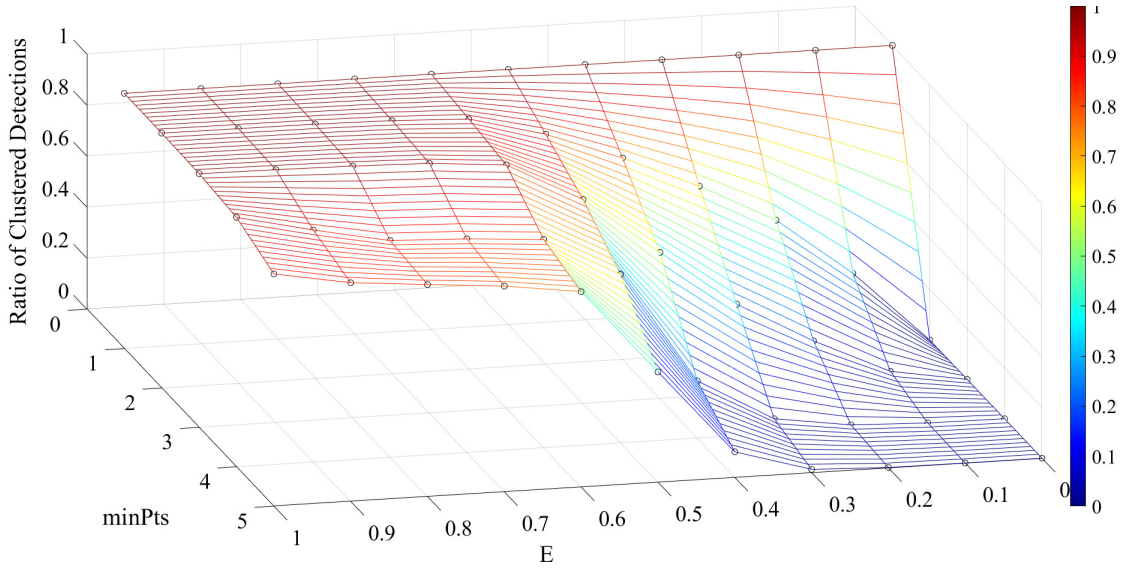

Figure 6.11: The ratio of clustered detections to the total target detections. The ratio is computed per target as (number of clustered detections)/(actual number of detections) and averaged over a simulation run.

than both the Single and Multiple MD-Trackers. The single MD-Tracker suffers from the exponential growth in the computational complexity as the number of sensors (and sensor detections) increases compared to the Hybrid MD-Tracker which only clusters detections at sensor level. As our comparison is under the assumption of utmost 3 detections per sensor (and 9 per target), the computational complexity increases as one attempts to optimally track all detections with the Single MD-Tracker. However, with the hybrid MD-Tracker, we expect to get a performance that scales well with increased detections as compared to the Single MD-Tracker. It is also seen that, the Multiple MD-Tracker exhibits less tracking error on average particularly for position estimates. The local trackers have the benefit of making better decisions by filtering out non-target detections, as compared to the hybrid approach which clusters detections based on proximity alone at the sensor level. Further improvements on hybrid MD-Tracker can be obtained by customizing the clustering technique used at the local sensor level. For instance, in [58], a faster and more reliable approach to the conventional DBSCAN technique is suggested that computes varying density grids offline for radar sensors.

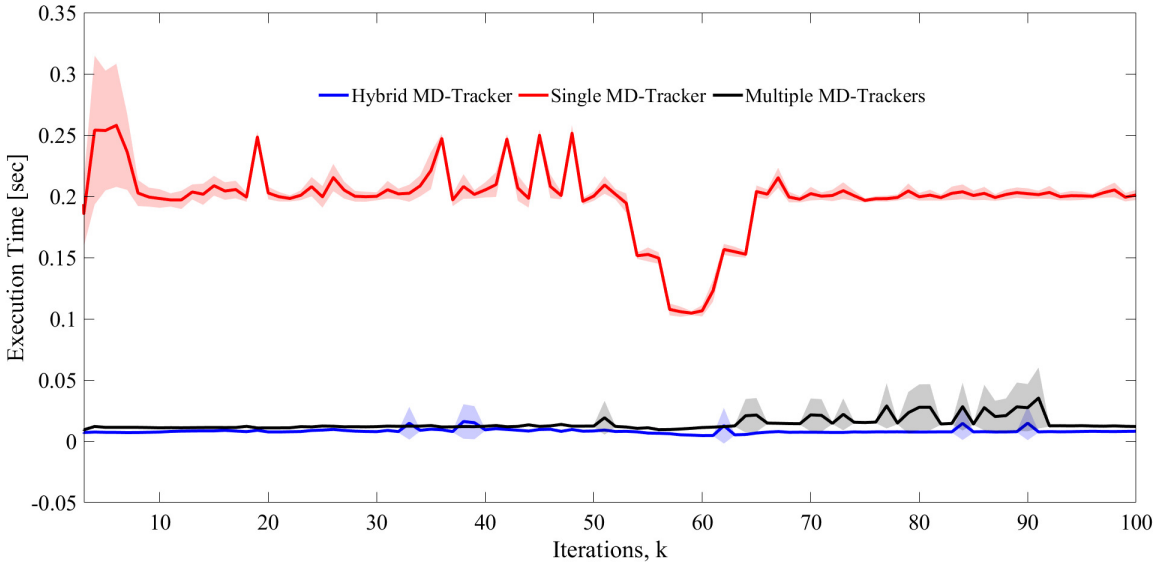

Figure 6.12: The time elapsed to execute detections from a single frame is plotted for the three MD-Tracker configurations. The shaded areas represent the 95 percentile confidence region.

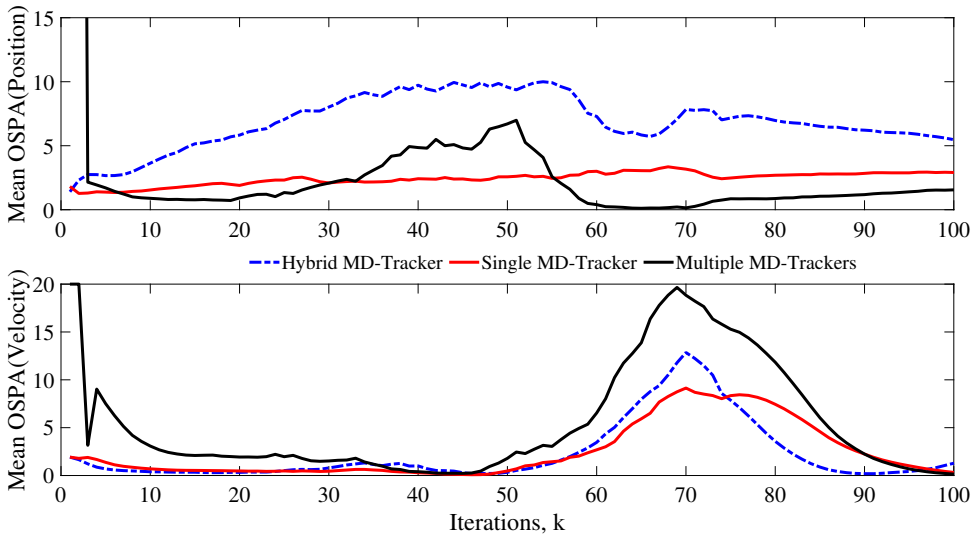

Figure 6.13: The position and velocity OSPA metric is shown for the three MD-Tracker configurations.

Moving Ego Vehicle, Multi-Sensor, Multi-Target

To evaluate the performance of the three trackers in multi-target scenarios, we simulate a 3 lane public road traffic with the time snapshots of main events as shown in Figure 6.14. Target vehicles T_1, T_2 and T_3 travel at $24m/s$, $20m/s$ and $19m/s$ respectively in front of the ego vehicle which has

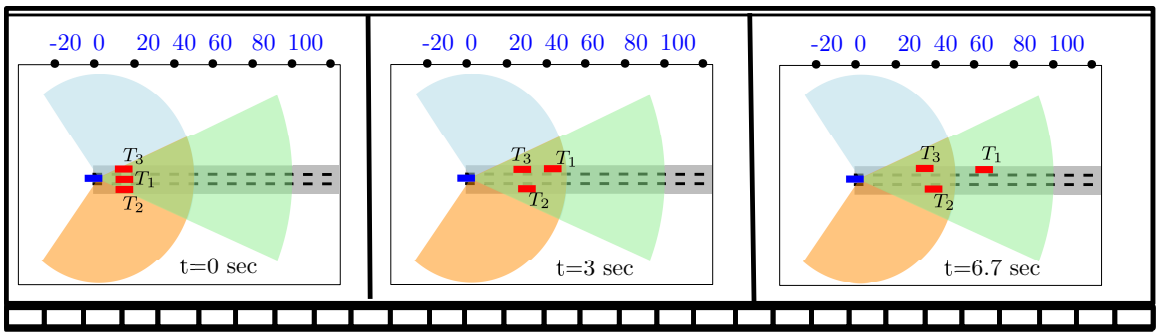

Figure 6.14: A multi-target traffic scenario. T_1 executes a lane change maneuver between $t = 0.85$ and $t = 2.75$ seconds from the ego lane $y = 0$ to the left lane $y = 4$.

a constant speed of $18m/s$. While T_1 is executing a lane change between $t = [0.85, 2.75]$seconds starting from the center lane $y = 0$ to left the lane $y = 4$, it encounters a considerable occlusion from target vehicle T_3 for a while. Apart from occlusion, sensor noise and clutter, the MD-Trackers have to deal with data association uncertainties under multi-target tracking scenarios. The data association worsens the execution time of the single MD-Tracker more as this tracker deals with all detections from all sensors centrally. Whereas, the Multiple MD-Tracker performs better as the three MD-Trackers consider the data association per sensor. Again, as seen in Figure 6.15, the Hybrid MD-Tracker performs better than the other two. Figure 6.16 shows the OSPA error for the position and velocity for the three trackers. Both the Single and Hybrid MD-Tracker perform better than the Multiple MD-Tracker under this setting.

6.4.2 Evaluations on Experimental Data

6.4.2.1 Single target tracking

In our experimental set up, the rover unit of the Real-time Kinematic (RTK) GPS is mounted on a maneuvering target vehicle, while the base station unit and the radar sensor are fixed to a stationary ego vehicle. The RTK GPS is capable of updating the position of the target vehicle at 10HZ within a centimeter level accuracy. In the meantime, the radar is streams point cloud detections at 20HZ over a serial channel to a tracking computer. While GPS positions are reported in East-North-Up (ENU) coordinates with respect to the base station unit, the radar detections are referred to the local (X_s, Y_s) coordinates shown in Figure 6.1. Ultimately, the GPS data is transformed to the local sensor frame coordinates and the GPS and radar timestamps are synchronized to use the RTK GPS

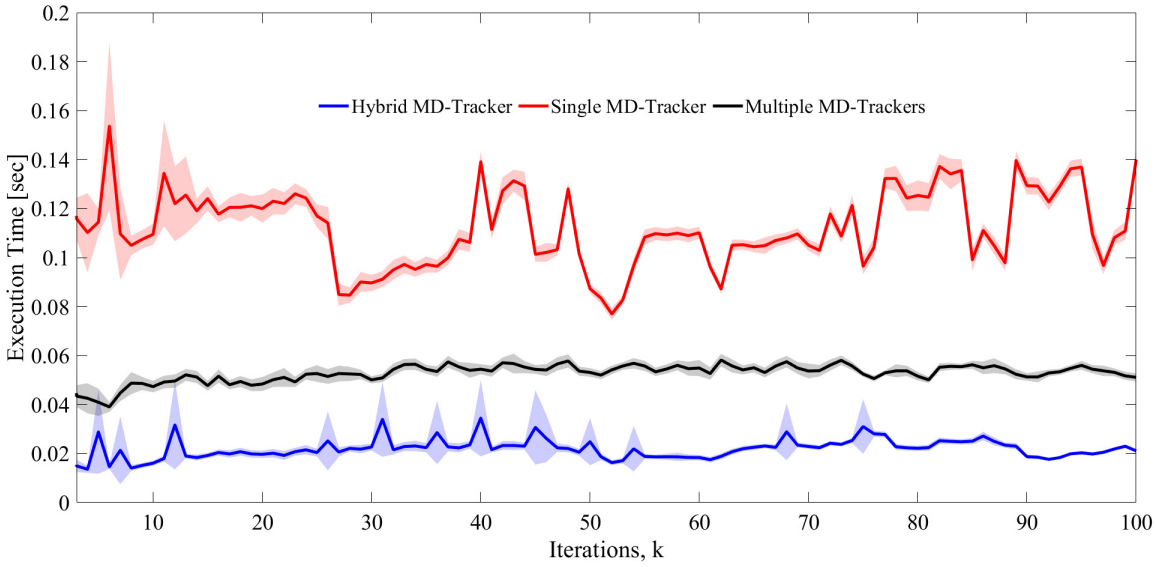

Figure 6.15: The time elapsed during iterations of the multi-sensor multi-target MD-Tracker configurations. The shaded areas represent the 95 percentile confidence region.

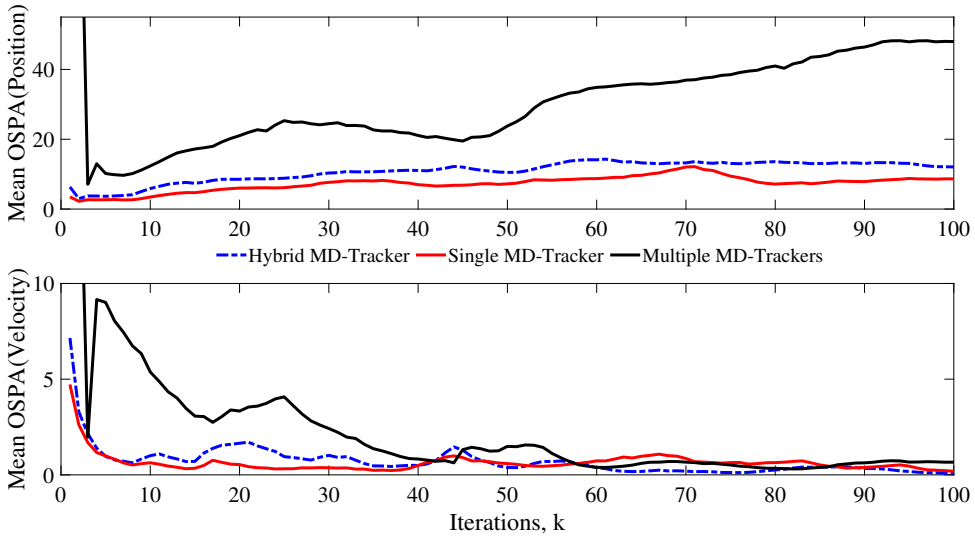

Figure 6.16: The position and velocity OSPA metric is shown for the three MD-Tracker configurations under multi-target scenarios.

location data as ground truth to validate the performance of tracking algorithms.

As shown in Figure 6.17, the target vehicle executes a lane-change maneuver as it moves away from the ego vehicle. The tracking result is shown to be within the 95 percentile confidence ellipse. In addition, the OSPA error given in the same subplot, further verifies the effectiveness of the algorithm

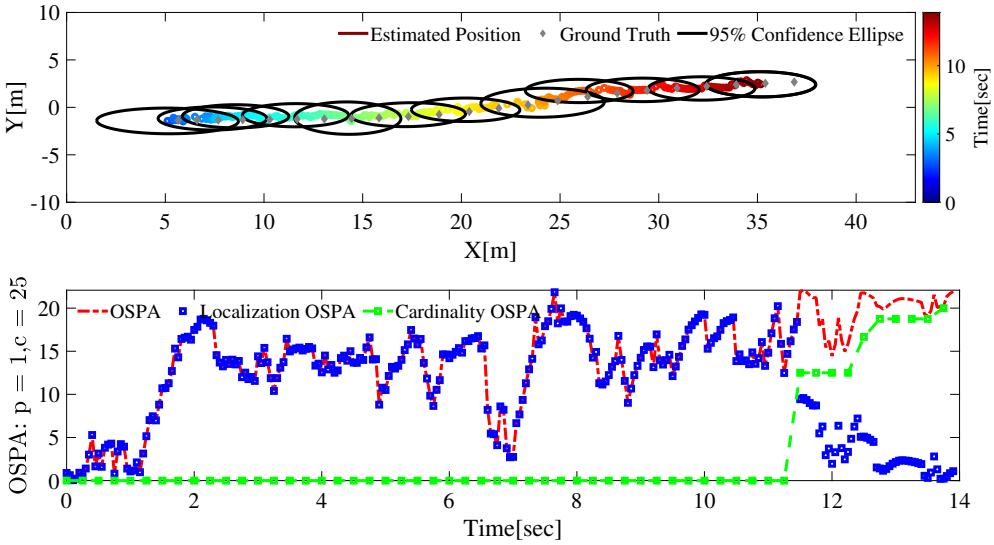

Figure 6.17: The position of the target vehicle is plotted with respect to the radar coordinate frame. The ground truth of the target vehicle obtained from RTK GPS is also shown superimposed on the tracker estimates. Radar detections are not shown in this figure.

in maintaining the cardinality error to zero. The large cardinality error close to the target destination is due to a confirmed false target not yet terminated as its existence probability is still above target termination threshold.

In Figure 6.18, the x, y states of the tracker estimates and the corresponding ground truth data are plotted. The corresponding number of validated measurements are plotted in Figure 6.19. The number of detections is seen to vary both with time and distance- higher close to the ego vehicle and lower at the far end. This result does not attest to the validity of "point-target" assumption, mainly because of the high density in which urban traffic usually operates. It is also noted that, occasionally detections are missing and thus the track managment part of the tracking algorithm is expected to main the target track.

6.4.2.2 Multi target tracking

To study the impact of measurement-to-target data association on the tracking performance, two target vehicles are driven in close proximity and in parallel as both drive away from the sensor station. The lateral inter-vehicle distance is intentionally kept approximately equal (and at times even less) than that exhibited in dense public traffic. Only one of the vehicles is equipped with

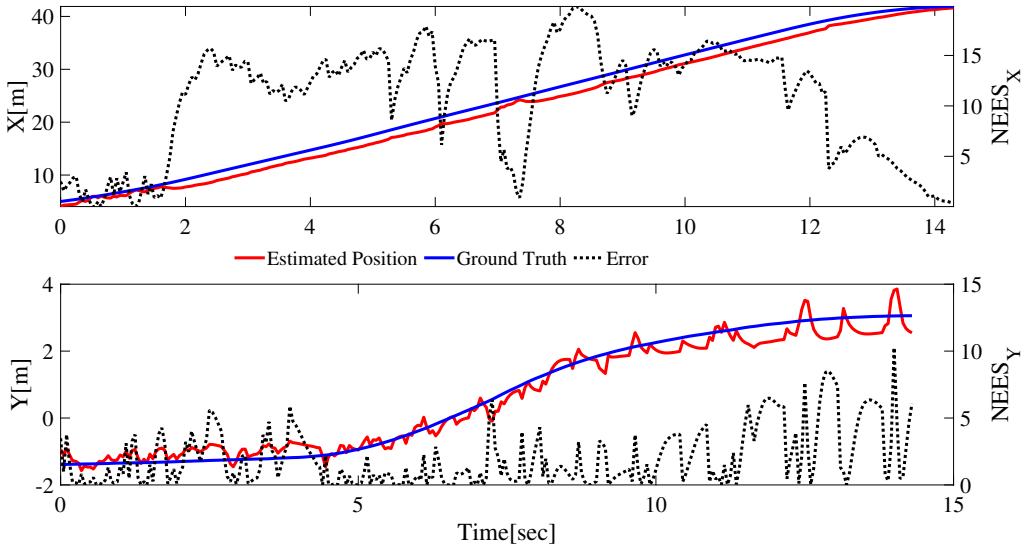

Figure 6.18: The position estimates and ground truth data of the target vehicle are independently plotted for the scenario in Figure 6.17. The corresponding NEES is also given independently for both Cartesian coordinates.

RTK GPS to record the ground truth data, the other vehicle is merely there to complicate the data association uncertainty. However, tracks are generated for both targets. The result of the investigation is presented in Figures 6.20 and 6.21. The MD-LMIPDA tracker does not deal with an optimal data association step which considers all targets and measurements jointly, but unlike single target trackers it deals with the presence of non-targets by modifying the clutter density. It is seen from the tracking results that the algorithm can be used to successfully generate multi-target state estimates in public traffic scenarios. In Figure 6.21, the OSPA metric penalizes the non-assignment of one of the target vehicle as there is only one ground truth available from the RTK GPS record.

6.5 Conclusions and Future Work

High resolution sensors, capable of generating multiple detections per target vehicles, pose a computational problem that challenge reliable real-time performance. In this paper, we have presented three tracker configurations suitable for multi-sensor multi-target tracking applications in public road traffic. All configurations address the multiplicity of target detections, but differ in the manner in which data is treated at local (sensor) and fusion (system) levels. The single MD-Tracker runs a single tracker on all detections from all sensors. Whereas, the multiple MD-Tracker configura-

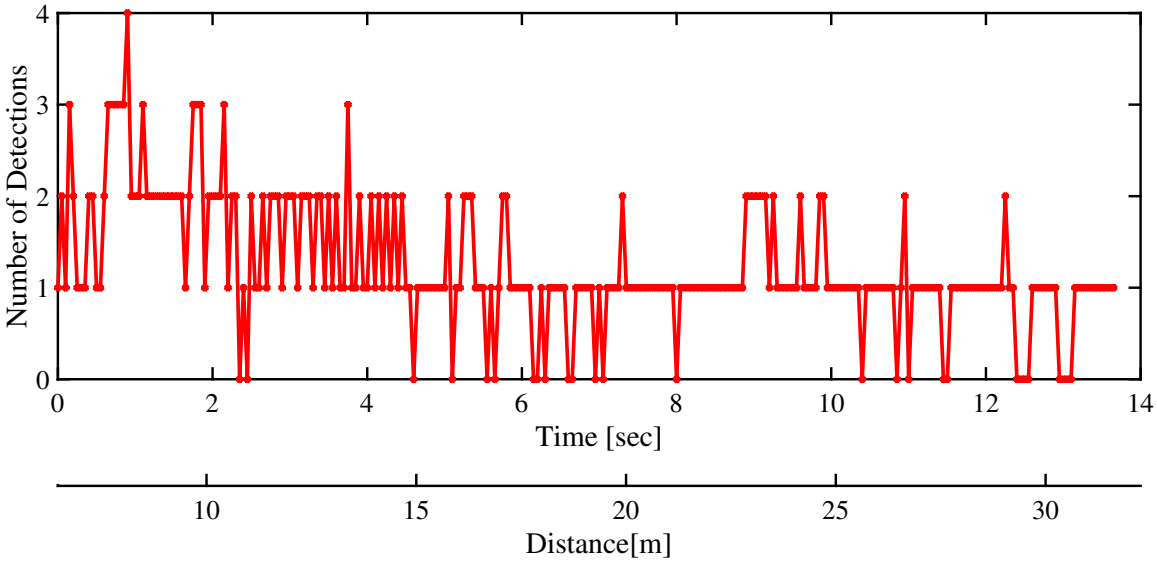

Figure 6.19: The number of validated detections as the target vehicle drives away from the radar is given as a function of time and distance. The maximum number of detections for this scenario is shown to be 4. Some missing detections (detections with cardinality of 0) are also noted.

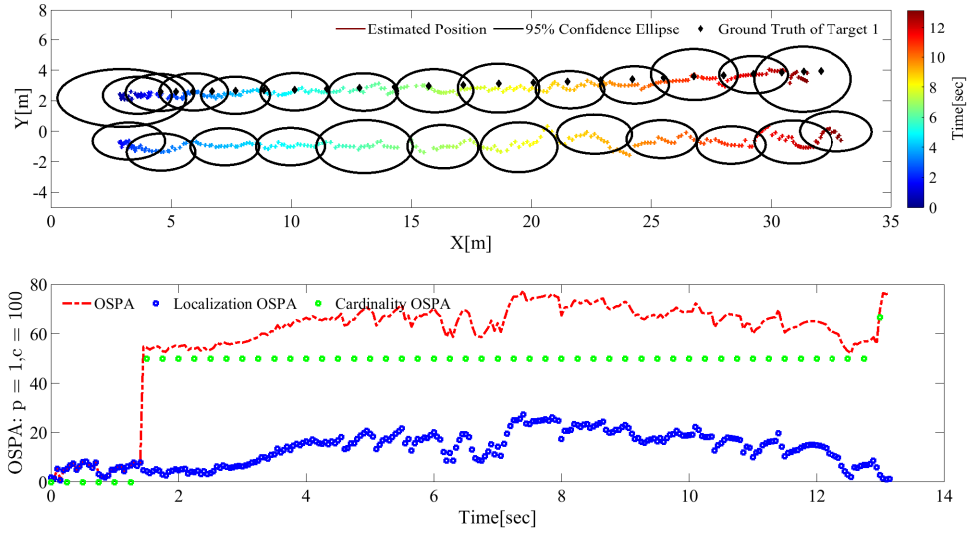

Figure 6.20: Two target vehicles are observed driving away from the ego vehicle. The radar detections are filtered to get state estimation for both vehicles. The position of both target vehicles are plotted with respect to the radar coordinate frame. The ground truth of the target vehicle is used for one of the vehicles only. Radar detections are not shown in this figure.

tion treats individual sensors independently and allocates trackers to each of the sensors that run in parallel. In addition, we have addressed a hybrid option that is computationally cheaper and, meanwhile, offers a relatively acceptable tracking accuracy.

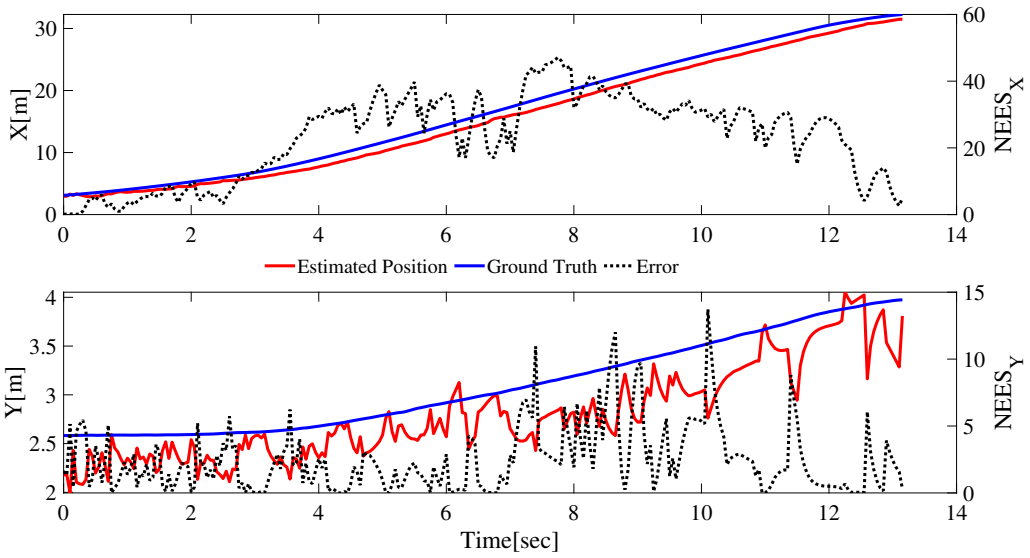

Figure 6.21: The position of the target vehicle is plotted with respect to the radar coordinate frame. The ground truth of the target vehicle obtained from RTK GPS is also shown.

The MD tracker is also put to test in practical radar-based single and multiple target tracking scenarios. Experiments were conducted to mimic public road traffic where multiple detectios from target vehicles driving closely with each other and with the ego vehicle are generated. The resulting tracker estimates are evaluated using OSPA metric. Data from RTK GPS is used as ground truth to estimate target vehicle trajectory. Both the cardinality and localization errors indicate a successful tracking performance.

Future extensions of the current work include incorporating feedback from track estimation of a group of targets into the tracking algorithm to improve individual target state estimation and evaluating the same for practical tracking applications.

References

[1] K. Granstrom, M. Baum, and S. Reuter, "Extended object tracking: Introduction, overview and applications," *arXiv preprint arXiv:1604.00970*, 2016.

[2] R. Mahler, "Phd filters for nonstandard targets, i: Extended targets," in *2009 12th International Conference on Information Fusion*, pp. 915–921, IEEE, 2009.

[3] A. Scheel, C. Knill, S. Reuter, and K. Dietmayer, "Multi-sensor multi-object tracking of vehicles

using high-resolution radars," in *2016 IEEE Intelligent Vehicles Symposium (IV)*, pp. 558–565, IEEE, 2016.

[4] G. Gennarelli, G. Vivone, P. Braca, F. Soldovieri, and M. G. Amin, "Multiple extended target tracking for through-wall radars," *IEEE Transactions on Geoscience and Remote Sensing*, vol. 53, no. 12, pp. 6482–6494, 2015.

[5] M. Baum, M. Feldmann, D. Fränken, U. D. Hanebeck, and W. Koch, "Extended object and group tracking: A comparison of random matrices and random hypersurface models," *INFORMATIK 2010. Service Science–Neue Perspektiven für die Informatik. Band 2*, 2010.

[6] B.-n. Vo, M. Mallick, Y. Bar-shalom, S. Coraluppi, R. Osborne III, R. Mahler, and B.-t. Vo, "Multitarget tracking," *Wiley Encyclopedia of Electrical and Electronics Engineering*, pp. 1–15, 1999.

[7] C. Qiu, Z. Zhang, H. Lu, and H. Luo, "A survey of motion-based multitarget tracking methods," *Progress In Electromagnetics Research*, vol. 62, pp. 195–223, 2015.

[8] Y. Huang, T. L. Song, and D. S. Kim, "Linear multitarget integrated probabilistic data association for multiple detection target tracking," *IET Radar, Sonar & Navigation*, vol. 12, no. 9, pp. 945–953, 2018.

[9] F. Castanedo, "A review of data fusion techniques," *The Scientific World Journal*, vol. 2013, 2013.

[10] Huang Xinhan and Wang Min, "Multi-sensor data fusion structures in autonomous systems: a review," in *Proceedings of the 2003 IEEE International Symposium on Intelligent Control*, pp. 817–821, Oct 2003.

[11] S. Matzka and R. Altendorfer, "A comparison of track-to-track fusion algorithms for automotive sensor fusion," in *2008 IEEE International Conference on Multisensor Fusion and Integration for Intelligent Systems*, pp. 189–194, Aug 2008.

[12] Y. Bar-Shalom, "On the track-to-track correlation problem," *IEEE Transactions on Automatic Control*, vol. 26, pp. 571–572, April 1981.

[13] Chee-Yee Chong, S. Mori, W. H. Barker, and Kuo-Chu Chang, "Architectures and algorithms for track association and fusion," *IEEE Aerospace and Electronic Systems Magazine*, vol. 15, pp. 5–13, Jan 2000.

[14] Y. Bar-Shalom, P. K. Willett, and X. Tian, *Tracking and data fusion.* YBS publishing Storrs, CT, USA:, 2011.

[15] S. Blackman and R. Popoli, "Design and analysis of modern tracking systems(book)," *Norwood, MA: Artech House, 1999.*, 1999.

[16] R. P. Mahler, *Statistical multisource-multitarget information fusion*, vol. 685. Artech House Norwood, MA, 2007.

[17] B.-T. Vo and B.-N. Vo, "Labeled random finite sets and multi-object conjugate priors," *IEEE Transactions on Signal Processing*, vol. 61, no. 13, pp. 3460–3475, 2013.

[18] S. Reuter, B.-T. Vo, B.-N. Vo, and K. Dietmayer, "The labeled multi-bernoulli filter," *IEEE Transactions on Signal Processing*, vol. 62, no. 12, pp. 3246–3260, 2014.

[19] D. Musicki and B. La Scala, "Multi-target tracking in clutter without measurement assignment," *IEEE Transactions on Aerospace and Electronic Systems*, vol. 44, no. 3, pp. 877–896, 2008.

[20] D. Musicki, "Limits of linear multitarget tracking," in *2005 7th International Conference on Information Fusion*, vol. 1, pp. 6–pp, IEEE, 2005.

[21] D. Musicki, R. Evans, and S. Stankovic, "Integrated probabilistic data association," *IEEE Transactions on automatic control*, vol. 39, no. 6, pp. 1237–1241, 1994.

[22] J. W. Koch, "Bayesian approach to extended object and cluster tracking using random matrices," *IEEE Transactions on Aerospace and Electronic Systems*, vol. 44, no. 3, pp. 1042–1059, 2008.

[23] M. Feldmann and D. Franken, "Advances on tracking of extended objects and group targets using random matrices," in *2009 12th International Conference on Information Fusion*, pp. 1029–1036, IEEE, 2009.

[24] M. Feldmann, D. Franken, and W. Koch, "Tracking of extended objects and group targets using random matrices," *IEEE Transactions on Signal Processing*, vol. 59, no. 4, pp. 1409–1420, 2010.

[25] J. Lan and X. R. Li, "Tracking of extended object or target group using random matrix" part i: New model and approach," in *2012 15th International Conference on Information Fusion*, pp. 2177–2184, July 2012.

[26] J. Lan and X. R. Li, "Tracking of extended object or target group using random matrix" part ii: Irregular object," in *2012 15th International Conference on Information Fusion*, pp. 2185–2192, July 2012.

[27] J. Lan and X. R. Li, "Tracking of maneuvering non-ellipsoidal extended object or target group using random matrix," *IEEE Transactions on Signal Processing*, vol. 62, no. 9, pp. 2450–2463, 2014.

[28] M. Baum and U. D. Hanebeck, "Random hypersurface models for extended object tracking," in *2009 IEEE International Symposium on Signal Processing and Information Technology (ISSPIT)*, pp. 178–183, IEEE, 2009.

[29] M. Baum and U. D. Hanebeck, "Extended object tracking with random hypersurface models," *IEEE Transactions on Aerospace and Electronic systems*, vol. 50, no. 1, pp. 149–159, 2014.

[30] M. Beard, S. Reuter, K. Granström, B.-T. Vo, B.-N. Vo, and A. Scheel, "Multiple extended target tracking with labeled random finite sets," *IEEE Transactions on Signal Processing*, vol. 64, no. 7, pp. 1638–1653, 2015.

[31] K. Granstrom, C. Lundquist, and O. Orguner, "Extended target tracking using a gaussian-mixture phd filter," *IEEE Transactions on Aerospace and Electronic Systems*, vol. 48, no. 4, pp. 3268–3286, 2012.

[32] K. Granström, M. Fatemi, and L. Svensson, "Gamma gaussian inverse-wishart poisson multi-bernoulli filter for extended target tracking," in *2016 19th International Conference on Information Fusion (FUSION)*, pp. 893–900, IEEE, 2016.

[33] N. WahlstrÃ¶m and E. Ã–zkan, "Extended target tracking using gaussian processes," *IEEE Transactions on Signal Processing*, vol. 63, pp. 4165–4178, Aug 2015.

[34] M. Wieneke and W. Koch, "A pmht approach for extended objects and object groups," *IEEE Transactions on Aerospace and Electronic Systems*, vol. 48, no. 3, pp. 2349–2370, 2012.

[35] B. K. Habtemariam, R. Tharmarasa, T. Kirubarajan, D. Grimmett, and C. Wakayama, "Multiple detection probabilistic data association filter for multistatic target tracking," in *14th International Conference on Information Fusion*, pp. 1–6, July 2011.

[36] B. Habtemariam, R. Tharmarasa, T. Thayaparan, M. Mallick, and T. Kirubarajan, "A multiple-detection joint probabilistic data association filter," *IEEE Journal of Selected Topics in Signal Processing*, vol. 7, pp. 461–471, June 2013.

[37] H. Cho, Y. Seo, B. V. K. V. Kumar, and R. R. Rajkumar, "A multi-sensor fusion system for moving object detection and tracking in urban driving environments," in *2014 IEEE International Conference on Robotics and Automation (ICRA)*, pp. 1836–1843, May 2014.

[38] M. Z. Ikram and M. Ali, "3-d object tracking in millimeter-wave radar for advanced driver assistance systems," in *2013 IEEE Global Conference on Signal and Information Processing*, pp. 723–726, IEEE, 2013.

[39] A. Metzner and T. Wickramarathne, "On multi-sensor radar configurations for vehicle tracking in autonomous driving environments," in *2018 21st International Conference on Information Fusion (FUSION)*, pp. 1–8, IEEE, 2018.

[40] M. Schuster, J. Reuter, and G. Wanielik, "Probabilistic data association for tracking extended targets under clutter using random matrices," in *2015 18th International Conference on Information Fusion (Fusion)*, pp. 961–968, July 2015.

[41] E. Hyun, Y.-S. Jin, and J.-H. Lee, "Moving and stationary target detection scheme using coherent integration and subtraction for automotive fmcw radar systems," in *2017 IEEE Radar Conference (RadarConf)*, pp. 0476–0481, IEEE, 2017.

[42] C. Will, P. Vaishnav, A. Chakraborty, and A. Santra, "Human target detection, tracking, and classification using 24 ghz fmcw radar," *IEEE Sensors Journal*, 2019.

[43] R. Mahler, "Phd filters for nonstandard targets, i: Extended targets," in *2009 12th International Conference on Information Fusion*, pp. 915–921, July 2009.

[44] Y. Huang, T. L. Song, and D. S. Kim, "Linear multitarget integrated probabilistic data association for multiple detection target tracking," *IET Radar, Sonar Navigation*, vol. 12, no. 9, pp. 945–953, 2018.

[45] D. Musicki, B. F. La Scala, and R. J. Evans, "Multi-target tracking in clutter without measurement assignment," in *2004 43rd IEEE Conference on Decision and Control (CDC) (IEEE Cat. No.04CH37601)*, vol. 1, pp. 716–721 Vol.1, Dec 2004.

[46] E. A. Wan and R. Van Der Merwe, "The unscented kalman filter for nonlinear estimation," in *Proceedings of the IEEE 2000 Adaptive Systems for Signal Processing, Communications, and Control Symposium (Cat. No.00EX373)*, pp. 153–158, Oct 2000.

[47] S. Srkk, *Bayesian Filtering and Smoothing*. New York, NY, USA: Cambridge University Press, 2013.

[48] D. Musicki, R. Evans, and S. Stankovic, "Integrated probabilistic data association," *IEEE Transactions on Automatic Control*, vol. 39, pp. 1237–1241, June 1994.

[49] D. Musicki and T. L. Song, "Track initialization: Prior target velocity and acceleration moments," *IEEE Transactions on Aerospace and Electronic Systems*, vol. 49, no. 1, pp. 665–670, 2013.

[50] S. Challa, M. R. Morelande, D. Mušicki, and R. J. Evans, *Fundamentals of object tracking*. Cambridge University Press, 2011.

[51] A. Hunde and B. Ayalew, "Automated multi-target tracking in public traffic in the presence of data association uncertainty," in *2018 Annual American Control Conference (ACC)*, pp. 300–306, June 2018.

[52] A. Hunde and B. Ayalew, "Linear Multi-Target Integrated Probabilistic Data Association Filter With Automatic Track Management for Autonomous Vehicles," vol. Volume 2: Control and Optimization of Connected and Automated Ground Vehicles of *Dynamic Systems and Control Conference*, 09 2018.

[53] A. Hunde, B. Ayalew, and Q. Wang, "Automated multi-object tracking for autonomous vehicle control in dynamically changing traffic," in *2019 American Control Conference (ACC)*, pp. 515–520, July 2019.

[54] "Matlab version 9.7.0.1247435 (r2019b)," 2019.

[55] D. Schuhmacher, B. Vo, and B. Vo, "A consistent metric for performance evaluation of multi-object filters," *IEEE Transactions on Signal Processing*, vol. 56, pp. 3447–3457, Aug 2008.

[56] B. Ristic, B. Vo, D. Clark, and B. Vo, "A metric for performance evaluation of multi-target tracking algorithms," *IEEE Transactions on Signal Processing*, vol. 59, pp. 3452–3457, July 2011.

[57] M. Ester, H.-P. Kriegel, J. Sander, X. Xu, *et al.*, "A density-based algorithm for discovering clusters in large spatial databases with noise.," in *Kdd*, vol. 96, pp. 226–231, 1996.

[58] D. Kellner, J. Klappstein, and K. Dietmayer, "Grid-based dbscan for clustering extended objects in radar data," in *2012 IEEE Intelligent Vehicles Symposium*, pp. 365–370, June 2012.

Chapter 7

Multi-Target State and Shape Estimation for High Resolution Automotive Sensor Detections

7.1 Introduction

Advances in automotive sensing technology and the ever-increasing demand for environmental perception have stimulated researchers and practioners alike in the development of tracking algorithms that address the accuracy and computational requirements of autonomous vehicles. While, sophisticated tracking algorithms as demonstrated in airborne/ground target tracking applications underwent profound treatment following world war II, the presence of clutter, false alarms, missed detections as well as maneuvering targets pose challenges in tracking. Perception and tracking in the automotive industry, is no different. In fact, owing to a significant leap in the development of automotive sensors, such sensors as RADAR and LIDAR can generate multiple detections/returns making measurement-to-track data associations even complicated. The improved sensor resolution has revitalized developments for tracking of extended and group targets. In this chapter, we discuss perception and tracking of individual as well as group targets as applied to multi-lane public traffic. We formulate the tracking problem as a two hierarchical layer: - at level 1, we distinguish

multi-target tracking based on multiple detections represented in the measurement space. A situation assessment layer at level 2 tracks group targets with birth and death as well as merging and splitting functionalities as they evolve. This arrangement enhances the multi-target tracking performance in situations including but not limited to target initialization (birth), target occlusion, missed detections, unresolved measurement, target maneuver, etc. In addition, group targets expose complex individual target interactions to help in a situation assessment study which are otherwise challenging to capture.

In short, we monitor both the group and individual extended object (EO) tracks from sensors' detections mounted on the moving ego vehicle. In addition to group behaviour, which is directly observable from sensor detections, the behaviour of individual EO is also equally important both in the short and long horizon control decisions. For instance, due to transient occlusions, detections from an EO might be missing for some duration at consecutive scan times. The study of the group dynamics that the target was known to be a part of can be used to complement missing detections, i.e. the group state essentially behaves as a virtual detection to update target state predictions of the EO. Also, before an EO (or groups of EO) splits away from a group that is being tracked, the tendency for such an event (splitting, in this case) together with the time history of the trajectory before and following the event, can be used to make informed decisions about the evolving traffic. Some of these decisions could be critical such as if the splitting EO (a group of EO) ultimately joins the lane of the ego vehicle. In general, group tracking can improve individual EO tracking performance under missing detections, merged detections and data association uncertainties.

Next, we shall highlight the objective of group tracking and comment on how it fits into the overall scheme of multi-target tracking discussed in the preceding chapters. In short, the relevance of group tracking, especially under EO (multiple detections) scenarios is evident in four main areas:

- **Data Association** The advent of high resolution automotive sensors resulted in multiple detections over the extent of a target vehicle. Which in turn necessitated the use algorithms capable of extended object tracking. This is a departure from conventional approaches to point target tracking that assumes at most one detection per object vehicle. The data association was simpler: the detection could be from a target or a close non-target or a clutter. Under multiple detections, the shear amount of data association that need to be resolved especially under groups of extended objects poses a computational challenge. With group tracking, we

can simplify the data association problem to mutually exclusive regions of clusters of detections which are treated as independent group detections. By way of contrast, the complexity of data association over a cluster of detections is less demanding than solving the same over all the measurement space.

- **Merged Measurement** Even under EO considerations, cases of unresolved measurement (also called merged measurement) can be a challenging problem in multi-target tracking problems. A Merged measurement occurs when the sensor returns a single detection for multiple objects in the scene. This is mainly due to sensor imperfections and poor resolution for sufficiently distant detections. Generally, modeling and integrating merged measurements into the tracking scheme, improves tracking by preventing premature track terminations. However, this comes with an added computational complexity. The literature under merged measurements tracking cases is very rare, often ignored under the *independent measurement assumption*. The earliest work that models merged measurements and integrates it into the Joint Probabilistic Data Association (JPDA) algorithm is presented in [1]. In [2], a resolution model is developed and implemented within the Multiple Hypothesis Tracker (MHT) method. The standard sensor measurement is generalized to the case of merged measurement and then implemented into the generalised labelled multi-Bernoulli(GLMB) filter [3]. Instead of explicitly modeling the case of merged measurements, we intend to track the group targets for which merged measurements are reported until enough resolutions are obtained to separate them into independent tracks.

- **Missing Detections** The rational for using the group state as a virtual measurement to update the target track (with missing detections) which is known to be a member of a group is discussed above.

- **Track Initialization** To start a new target track, we employ a one-point track initialization method. Also, any detections which are not associated with a confirmed track is used to initiate a tentative track. The target velocities and accelerations are assumed to be $0_{d,1}$, where $d \in \{2, 3\}$ is the dimension of the target track. Both state variables are estimated from filtering recursion which takes multiple scans to settle to a reasonably close estimation. Here, we intend to improve on the estimation by feeding the average velocities and accelerations of groups in the FoV of the ego vehicle to initialize the states. The suggestion to use group

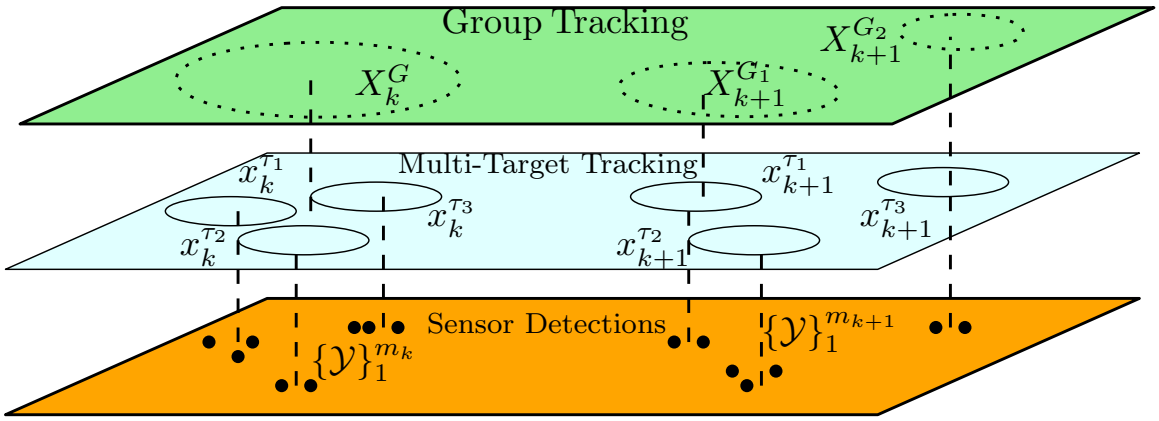

Figure 7.1: A double layer tracking scheme. The top layer tracks a set of target vehicles as a group, while the middle layer handles multi-target tracking as independent agents.

velocities and accelerations so as to initialize a new target track states is mentioned in [4].

Before closing this section, we shall clarify the use of the terms "extended" and "groups" targets which are often interchangeably used in literature without distinctions. From the viewpoint of sensor detections, an extended object tracking problem is closely related to group tracking, but there are multiple important differences. Groups have internal degree of freedom that affects the shape of the group whereas the extent of EO is relatively fixed in most circumstances and for most part of the its motion. Moreover, groups possess unique behaviours of splitting and merging which, generally, are not the characters tics of an EO. The objective here is not to model inter-group interactions, but rather focuses on the use of the group behavior in improving individual EO tracking performance. In that sense, we propose a hierarchical structure with feedback from the group to individual track layer arranged as shown in Figure 7.1.The hierarchical arrangement is first proposed in [5], but with a different objective and chiefly from the viewpoint of modeling abstraction.

7.2 Related Work

The self-organizing ability of vehicular traffic is the result of intelligent decisions by autonomous agents and/or human-driven vehicles driving in close proximity. These decisions are influenced by the desire to avoid collision while navigating structured multi-lane road network (repulsion) and by the intention to reach a common goal such as driving through an exit (cohesion) [6]. While individual behavioral responses can be modeled and predicated when taken in isolation; the aggregate dynamics

is remarkably complex and often unpredictable. To this end modeling approximations exist that range from a microscopic viewpoint captured by a system of ordinary differential equations to a kinetic theory description via mean-field limit and a macroscopic level via a suitable hydrodynamic approximation, for more detailed on this topic please see the discussions in [7]. In particular, the hydrodynamic model that presupposes the continuity assumption cannot be applied to traffic flow. This is due to the small number of participants even in the case of traffic jams to justify analogy with particle flows in fluid dynamics. Similarly, the kinetic theory is criticized for not taking into account the fact that a vehicle is not a particle, but rather an intelligent entity linking a driver and mechanics and hence the driver's reaction needs to be considered [8].

By far, a theoretically unified and rigorous framework for group detection, tracking and identification is presented by Mahler [5]. Using "finite-set statistics" (FISST), a theoretically optimal recursive Bayes filter for the multisensor-multigroup problem, which is cast as a three level statistical model, is constructed. Since the resulting filtering equations are computationally daunting even for the simplest of expected tracking problems, the author proposes computationally tractable approximation strategies by generalizing the concept of a probability hypothesis density (PHD) filter.

In [4], a dynamical model and Bayesian filtering algorithm are presented for detection and tracking of group and individual targets. The mathematical model is based on discrete stochastic differential equations that imitate behavioural properties of biological groups. Repulsive forces are introduced to model closely spaced targets and to prevent unintended collision. The resulting distribution for the dynamical and observation model is seen to be complex and highly nonlinear. As a result of which, a Markov chain Monte Carlo (MCMC) approach is implemented to perform sequential inference. Although the proposed model seeks to capture target interactions, there are some limitations that could prohibit its use in tracking of groups of EO. First, the observably of all of the individuals within the group is very questionable. Second, the high dimension of the joint target state that increases sN times as the number of targets (N) increases could be a challenge in real-time applications. Here, s is the dimension of the state variables. A group tracking scheme, similar in spirit to [4], that jointly estimates the group structure as well as the group states based on evolving networks and Monte Carlo methods is presented in [9]. The nodes in the graph correspond to targets within the group and connected components correspond to groups of targets. Further studies that incorporate group structure into the joint state estimation scheme include the works in [10],[11], and [12]. All

of them ([10] - [12]) [10],[11] and including the article in [12] fix the maximum number of groups anticipated.

The work in [13] presents a performance comparison of three cluster tracking techniques. These are the independent Sampling Importance Resampling (SIR) PFs, an extended object PHD filter, and a Gaussian mixture Markov chain Monte Carlo (MCMC). It is shown that the MCMC approach exhibits the best tracking accuracy, essentially yielding the least number of false detections. Further, efficient SMC implementations, both from algorithmic and hardware implementation directions, are discussed to make SMC methods suitable for high-dimensional problems and real time applications. In [14], a filtering algorithm based on a Markov chain Monte Carlo (MCMC) for tracking multiple clusters of coordinated objects is presented. A dynamic Gaussian mixture model is utilized for representing the time-varying clustering structure. This involves point process formulations of typical behavioral moves such as birth and death of clusters as well as merging and splitting.

The most common approach in EO and group target tracking considers an augmented state that jointly estimates the position of group center and its extent via either random hyper-surface or the random matrix approach. For the detailed treatment of the two approaches, see the references [15],[16],[17], [18],[19],[20], [21],[22]. In order not to repeat the discussion and for a brief summary of the theme of these articles, the reader is referred to the literature review section of Chapter 6. In general, for the approach based on the random matrices, the extent is considered as a random process and hence is normally assigned a respective prior (e.g., Wishart distribution [18],[19],[20]) and a transition kernel. In [23], in order to improve the estimation performance of interacting multiple model (IMM) tracking algorithm for group targets, two variable structure IMM algorithms are presented within the random matrices framework. A similar effort that uses the multiple model structure to improve the Gamma Gaussian inverse Wishart probability hypothesis density (GGIW-PHD) filter algorithm is also proposed in [24]. The multiple model structure is built into the estimation of kinematic state and extension state and is meant to improve the tracking performance during maneuvering stage.

7.3 Objectives and Contributions

Our objective is to improve the tracking performance of individual extended objects during common public traffic events involving occlusions, track initiation and merged measurements. To that end, we propose a hierarchical tracking structure where the lower layer takes care of multi-detection multi-target track estimation of individual extended objects and the upper layer executes group tracking to facilitate a feedback mechanism that provides group state to the lower tracking layer.

The specific objective at the upper layer is not to model inter-group interactions, but rather to emphasize the use of group behavior as a mechanism to enhance the performance of individual target tracks through feedback. This approach was first suggested in [25] and was identified to have the best potential for accurate tracking performance among the three methods compared in the article.

Contributions

In order to address the large data association uncertainty in the presence of high resolution detections, we use the linear multi-target (LM) IPDA approach for handling the data association problem. The joint kinematic and extent estimation is facilitated through the random matrix approach outlined in [20]. The work the combines the LMIPDA approach as applied to IPDA is not reported so far. In addition, the hierarchical scheme that combines the LMIDPA and random matrix as a joint extended target state at each of the two layers with an objective of improving the tracking performance is not presented elsewhere. The resulting method will be subject to challenging simulated scenarios and real radar obtained from experimental data to investigate its performance. The multi-detection Joint integrated track splitting (MD-JITS) filter is combined with the random matrix extent estimation technique in [26]. In [27], for the data association problem, a generalized probabilistic data association filter is applied. Although the data association uncertainties are handled by a closely related method, both [26] and [27] are confined to the discussion of individual extended target tracking problems.

7.4 Multiple Detection and Extended Object (Group) Tracking

For extended target tracking, the joint density of the kinematic state x_k and the objection extension X_k are iteratively computed. In Bayesian filtering recursion, the joint target density $p(x_k, X_k|Z^k)$ undergoes a prediction step followed by a measurement update.The prediction step is based on an assumed kinematic/dynamic evolution model that approximates the motion of the target.

$$p(x_{k-1}, X_{k-1}|Z^{k-1}) \rightarrow p(x_k, X_k|Z^{k-1}) \tag{7.1}$$

Which can be interpreted as a marginal density integrated as[18]:

$$p(x_k, X_k|Z^{k-1}) = \int dx_{k-1}dX_{k-1} \times p(x_k, X_k|x_{k-1}, X_{k-1}, Z^{k-1})p(x_{k-1}, X_{k-1}|Z^{k-1}) \tag{7.2}$$

The transition density $p(x_k, X_k|x_{k-1}, X_{k-1}, Z^{k-1})$ can be written as a product of kinematic and object evolution parts:

$$p(x_k, X_k|x_{k-1}, X_{k-1}, Z^{k-1}) = p(x_k|X_k, x_{k-1}, X_{k-1}, Z^{k-1})p(X_k|x_{k-1}, X_{k-1}, Z^{k-1}) \tag{7.3}$$

we make use of Markov-type assumptions for its kinematical part, i.e. $p(x_k|X_k, x_{k-1}, X_{k-1}, Z^{k-1}) = p(x_k|X_k, x_{k-1})$ and assume that the object's kinematical properties have no impact on the temporal evolution of the object extension and previous measurements if X_{k-1} is given, i.e.:

$$p(X_k|x_{k-1}, X_{k-1}, Z^{k-1} = p(X_k|X_{k-1}) \tag{7.4}$$

We thus have:

$$p(x_k, X_k|x_{k-1}, X_{k-1}, Z^{k-1}) = p(x_k|X_k, x_{k-1})p(X_k|X_{k-1}) \tag{7.5}$$

We now obtain the prediction formula:

$$p(x_k, X_k|Z^{k-1}) = \int dx_{k-1}dX_{k-1} \times p(x_k, X_k, x_{k-1})p(X_k|X_{k-1})p(x_{k-1}|X_{k-1}, Z^{k-1})p(X_{k-1}|Z^{k-1}) \tag{7.6}$$

Further discussion is much simplified if we additionally assume that the temporal If the temporal evolution of the object extension is assumed to have no effect on the prediction of the kinematic object properties, the derivation can be simplified. That is, we can make the assertion $p(x_{k-1}|X_{k-1}, Z^{k-1}) \approx p(x_{k-1}|X_k, Z^{k-1})$ or, in simple terms, we intend to replace X_{k-1} by X_k. We can write, from Bayes theorem, the joint predicted density as given in Equation (7.7).

$$p(x_k, X_k|Z^{k-1}) = p(x_k|X_k, Z^{k-1})p(X_k|Z^{k-1}) \tag{7.7}$$

The two densities can then be independently integrated out from Equations (7.8) and (7.9).

$$p(x_k|X_k, Z^{k-1}) = \int p(x_k|X_k, x_{k-1})p(x_{k-1}|X_k, Z^{k-1})dx_{k-1} \tag{7.8}$$

$$p(X_k|Z^{k-1}) = \int p(X_k|X_{k-1})p(X_{k-1}|Z^{k-1})dX_{k-1} \tag{7.9}$$

The update step incorporates new data (Z_k) and propagates the sensor prediction to time t_k as follows.

$$p(x_k, X_k|Z^{k-1}) \rightarrow p(x_k, X_k|Z^k) \tag{7.10}$$

Given the measurement likelihood defined as $p(Z_k, m_k|x_k, X_k)$ and the predicted density of Equation (7.7), we can write the update step as shown in Equation (7.11).

$$p(x_k, X_k|Z^k) = \frac{p(Z_k, m_k|x_k, X_k)p(x_k, X_k|Z^{k-1})}{\int p(Z_k, m_k|x_k, X_k)p(x_k, X_k|Z^{k-1})dx_k dX_k} \tag{7.11}$$

7.4.1 Bayesian Extended Object Tracking

We assume that the sensor detections include a set of position measurements in two dimensions ($x - y$ plane). However, the kinematic state variable corresponds to velocity and acceleration in addition the position states.

Measurement Model

At each measurement scan k, a random number of measurements n_k is y_k^i is collected from the sensor[20].

$$y_k^i = Hx_k + w_k^i \tag{7.12}$$

where $Y_k = \{y_k^i\}_{i=1}^{n_k}$ and $\mathcal{Y}_k := \{Y_t, n_t\}_{t=0}^{k}$. The noise w_k^i takes the form of a Gaussian density with zero mean and variance X_k. For the measurement set Y_k, the likelihood is computed as in Equation (7.13).

$$p(Y_k|n_k, x_k, X_k) = \prod_{i=1}^{n_k} \mathcal{N}(y_k^i; Hx_k, X_k) \tag{7.13}$$

For the set of measurements Y_k, define the mean and the measurement spread as in Equations (7.14) and (7.15).

$$\bar{y}_k = \frac{1}{n_k} \sum_{i=1}^{n_k} y_k^i \tag{7.14}$$

$$\bar{Y}_k = \sum_{i=1}^{n_k} \{y_k^i - \bar{y}_k\}\{y_k^i - \bar{y}_k\}^T \tag{7.15}$$

(7.13), can be written as:

$$p(Y_k|n_k, x_k, X_k) \propto \mathcal{N}\left(\overline{y}_k; Hx_k, X_k/n_k\right) \times \mathcal{W}\left(\overline{Y}_k; n_k - 1, X_k\right) \tag{7.16}$$

where

$$\mathcal{W}(X; m, C) = \frac{|X|^{\frac{m-d-1}{2}}}{2^{\frac{md}{2}} \Gamma_d(\frac{m}{2}) |C|^{\frac{m}{2}}} exp\left(tr\left[-\frac{1}{2} XC^{-1}\right]\right) \tag{7.17}$$

with $m \geq d$, $\mathcal{W}(X; m, C)$ is the Wishart density of a d-dimentional SPD random matrix X with an expected SPD matrix mC.

Tracking Algorithm

Applying the Chapman-Kolmogorov theorem and the concept of conjugate priors, a recursive joint state estimation scheme is derived in [18]. The joint probability density is factored as follows.

$$p(x_k, X_k|Y^k) = p(x_k|X_k, Y^k) p(X_k|Y^k) \tag{7.18}$$

Under the assumed probability density functions, further results in

$$p(x_k, X_k|Y^k) = \mathcal{N}(x_k; x_{k/k}, P_{k/k} \oplus X_k)\mathcal{IW}(X_k; \nu_{k/k}, X_{k/k}) \tag{7.19}$$

where $\oplus$ represents the Kronecker product. The inverse Wishart density is parameterized as follows:

$$\mathcal{W}(X; m, C) = \frac{|C|^{\frac{m}{2}}}{2^{\frac{md}{2}}\Gamma_d(\frac{m}{2})|X|^{\frac{m+d+1}{2}}} exp\left(tr\left[-\frac{1}{2}CX^{-1}\right]\right) \tag{7.20}$$

The authors in [20], proposed the measurement likelihood (7.13) to take the form of a Gaussian density as shown in Equation (7.21).

$$p(Y_k|n_k, x_k, X_k) = \prod_{i=1}^{n_k} \mathcal{N}(y_k^i; Hx_k, zX_k + R) \tag{7.21}$$

where, the overall covariance matrix is composed of the sensor error covariance matrix R and an additional term that includes the spread contribution of the object extension scaled by a factor of z. Further, from Equation (7.18), we approximate that:

$$p(x_k|X_k, Y_k) \approx p(x_k|Y_k) \approx \mathcal{N}(x_k; Hx_k, zX_k + R) \tag{7.22}$$

where

$$x_{k|k} = x_{k|k-1} + K_{k|k-1}(\bar{y}_k - Hx_{k|k-1}) \tag{7.23}$$

$$P_{k|k} = P_{k|k-1} - K_{k|k-1}S_{k|k-1}K_{k|k-1}^T \tag{7.24}$$

where

$$S_{k|k-1} = HP_{k|k-1}H^T + \frac{Y_{k|k-1}}{n_k} \tag{7.25}$$

$$K_{k|k-1} = P_{k|k-1}S_{k|k-1}^{-1} \tag{7.26}$$

$$Y_{k|k-1} = zX_{k|k-1} + R \tag{7.27}$$

The extension update $p(X_k|Y_k)$ is approximated as

$$p(X_k|Y_k) \approx \mathcal{IW}(X_k; v_{k/k}, \alpha_{k|k} X_{k|k}) \tag{7.28}$$

where

$$X_{k|k} = \frac{1}{\alpha_{k|k}}(\alpha_{k|k-1} X_{k|k-1} + \hat{N}_{k|k-1} + \hat{Y}_{k|k-1}) \tag{7.29}$$

$$\alpha_{k|k} = \alpha_{k|k-1} + n_k \tag{7.30}$$

The authors in [20] assume independence between the kinematics and extent estimates. In addition, if the dynamic models for the kinematics and extent prediction are independent, we can use standard Kalman filter prediction equations as follows.

$$x_{x|k-1} = F x_{k-1|k-1} \tag{7.31}$$

$$P_{x|k-1} = F P_{k-1|k-1} F^T + Q \tag{7.32}$$

$$X_{x|k-1} = X_{k-1|k-1} \tag{7.33}$$

$$\alpha_{k|k-1} = 2 + exp(\frac{-T}{\tau})(\alpha_{k-1|k-1} - 2) \tag{7.34}$$

7.4.2 Group Tracking Algorithm

In the hierarchical tracking scheme, the group tracks and the EO tracks share a similar structure in the manner they handle tracks. This is illustrated in Figure 7.2.

To improve the tracking performance of individual extended objects a hierarchical tracking structure is shown in Figure 7.2. The lower layer takes care of a multi-detection multi-target track estimation of individual extended objects and the upper layer executes group tracking to facilitate a feedback

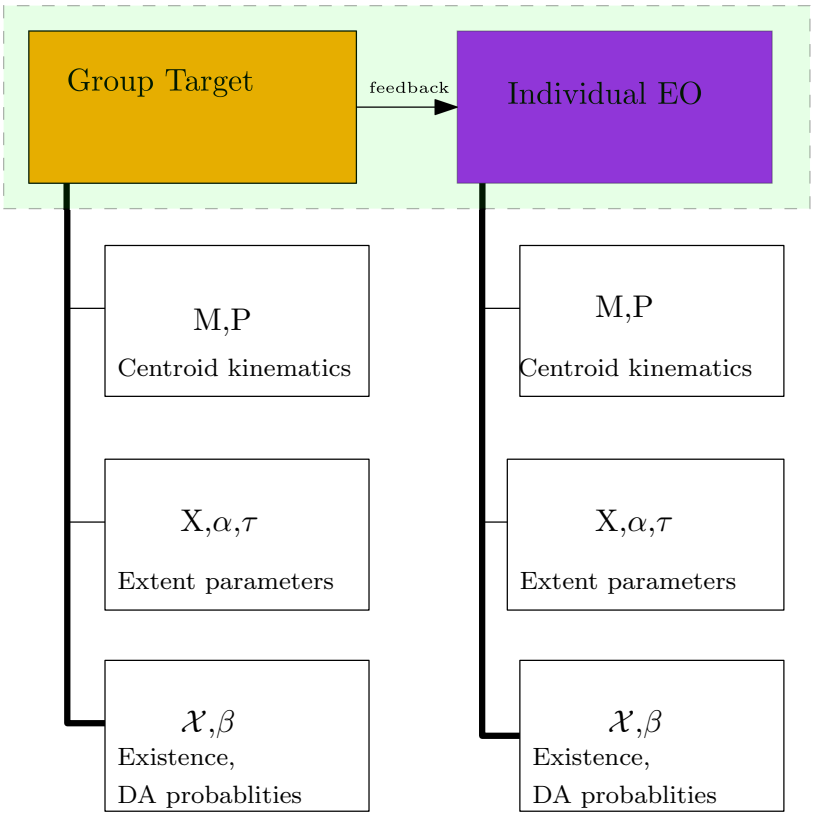

Figure 7.2: Groups of targets like individual EO target tracks go through birth/death process i.e. can be initialized/terminated and maintained when updates are available.

mechanism that provides group state to the lower tracking layer. At both layers, track management schemes handle track initiation, confirmation and termination procedures. Tentative tracks are initialized on measurements not validated by any of the tracked targets. Also, the prevalent assumption about track initiation is that our knowledge of the prior information about the tentative target velocity and acceleration vectors are limited to the maximum speed v_{max} and the maximum acceleration a_{max} [28],[29]. In this approach, the initial state estimate and covariance matrix formulations follow a similar structure as presented in our previous works [30],[31], and [32]. However, the presence of other groups in the FoV of the ego vehicle can be used to improve our prior information on the velocity and acceleration of a tentative track.

In addition to the track initiation, maintenance and termination attributes that a group track shares with individual EO tracks, track splitting and merging events that are specific to group tracks need to also be handled, see Figure 7.3. Conceptually, the merging process terminates either of the sub-groups while initiating a new group track with unique identity. The same logic, applies to the

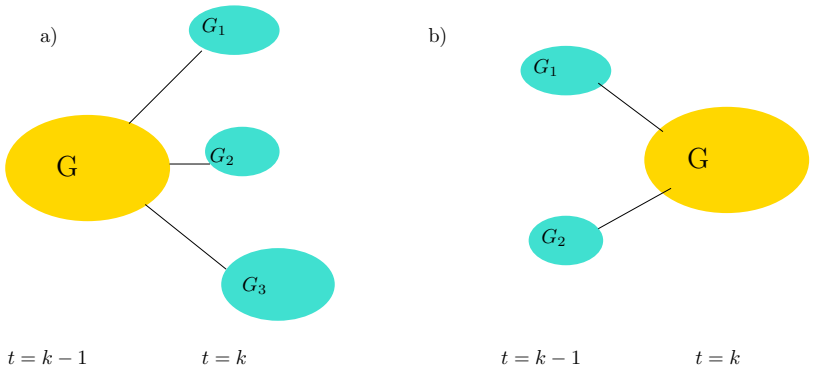

Figure 7.3: Unlike individual EO target tracks, group tracks a) can be split into smaller subgroups or b) merge to form an even larger group

splitting event. The parent group might survive into one of the splitting sub-groups or an a new track may be initiated for all the split up sub-groups. Both, merging and splitting events are handled by the tracking algorithm which is based on LMIPDA.

7.5 Results and Discussions

In this section, we discuss and evaluate the performance of multi-detection algorithms on simulated and experimental target tracking scenarios. Since EO tracking considers the simultaneous estimation of the kinematic state and the shape parameters of a moving object, a performance metric that can measure both is required. For EO tracking, a distance measure should incorporate geometric shape[33],[34]. We evaluate the location and extent errors simultaneously with a single score by means of the Gaussian Wasserstein distance as follows:

$$d(\mu_1, \Sigma_1, \mu_2, \Sigma_2) = ||\mu_1 - \mu_2|| + tr\left\{\Sigma_1 + \Sigma_2 - 2\sqrt{\sqrt{\Sigma_1}\Sigma_2\sqrt{\Sigma_1}}\right\} \tag{7.35}$$

where $\mu_1, \mu_2 \in \mathcal{R}^2$, $\Sigma_1, \Sigma_1 \in \mathcal{R}^{2\times 2}$

7.5.1 Evaluations on Simulated Data

A single target in front of the ego vehicle executes a lane change manoeuvre from the left to the right lane. Both the target and the ego vehicle are traveling at a constant speed of $20m/s$. Initially, the target vehicle is $20m$ ahead of the ego vehicle in the middle of the left lane ($y = 4m$). The approximate trajectory both vehicles traverse is shown in Figure 7.4. The measurement is assumed

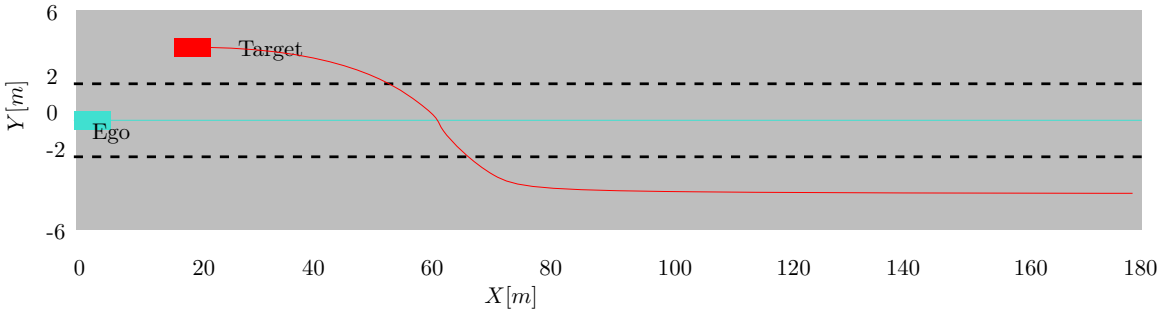

Figure 7.4: A maneuvering vehicle executes a lane change in front of the ego vehicle which is equipped with a high resolution sensor.

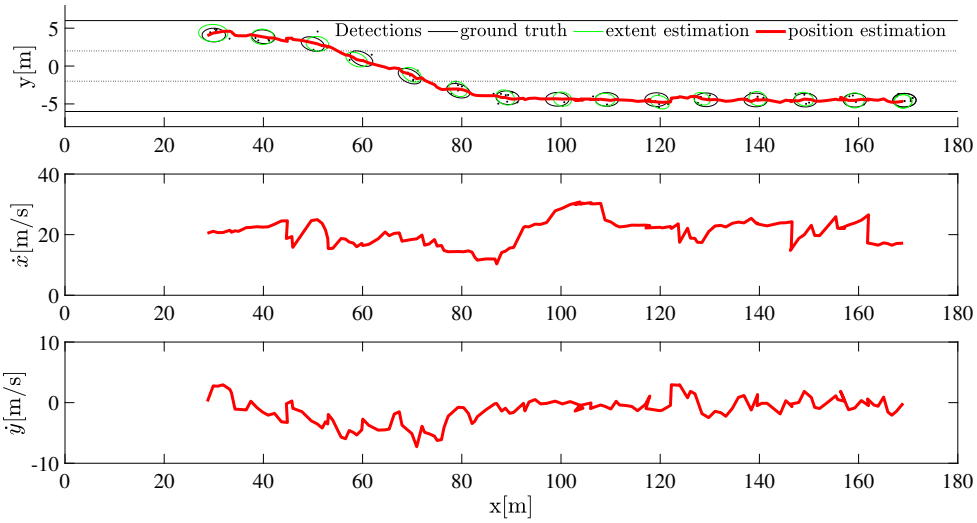

Figure 7.5: The tracking result of a maneuvering target with a measurement distribution assumed to be Poisson with parameter $\lambda = 5$.

to have a Poisson distribution with a known rate.

The case of Low Measurement Density, $\lambda = 5$

First, we fix Poisson distribution with parameter $\lambda = 5$. The tracking result is given in Figure 7.5 and 7.6. Comparing to the ground truth, the extent estimation as well as the filtered velocities show more deviation compared to the case when λ is higher.

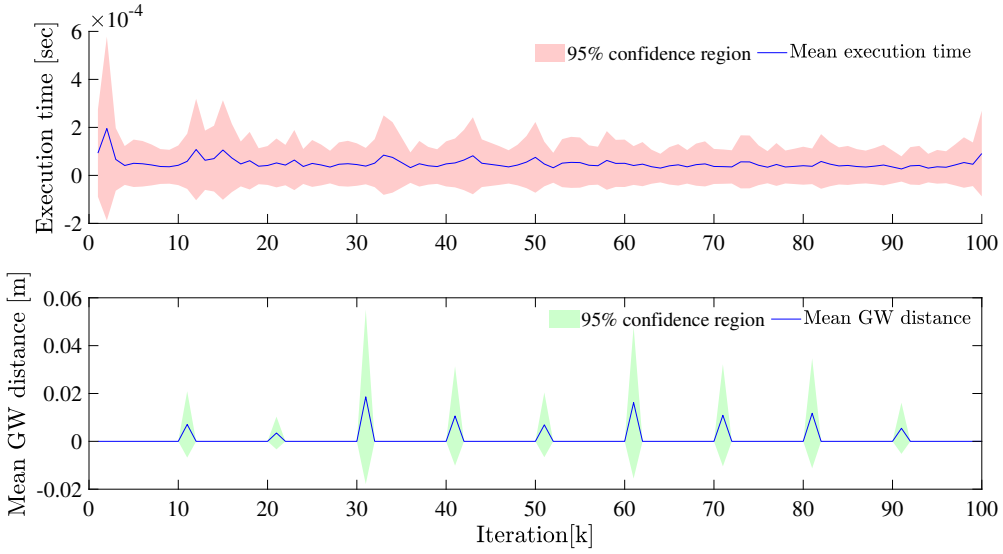

Figure 7.6: The mean GW distance and execution time at each iteration is plotted, $\lambda = 5$.

The case of High Measurement Density, $\lambda = 50$

Here, we fix the Poisson rate at $\lambda = 50$. As seen in Figures 7.7 and 7.8, the extent estimation is better than the case with $\lambda = 5$. Because of the coupling of the kinematic state and extent, the filtered velocities are seen to be reasonably close to the ground truth values and show less deviation compared to the case when the $\lambda = 5$.

The case of Missing Detections, Without Group Information

Figure 7.9 shows, a scenario where five extended objects are depicted deriving in close proximity and thus creating two groups of vehicles, three of them to the left and the remaining two to right of the ego vehicle. The initial configuration in terms of the relative position with respect to the ego vehicle and the absolute velocities of the EO is as shown given. We also simulate a scenario where due to an assumed occlusion, the detections from the leftmost EO are missing for 70 consecutive scans, i.e. from $t = [1.55]$ seconds into the simulation. Without feedback from group tracking module, the tracks of the EO whose detections are missing is terminated. The track ID and only its attributes will be deleted as shown in Figure 7.10. When the occlusion is over and detections are available from the target, a new track is initiated. Even though the target vehicle is the same, two tracks are initiated with separate IDs because of the occlusion.

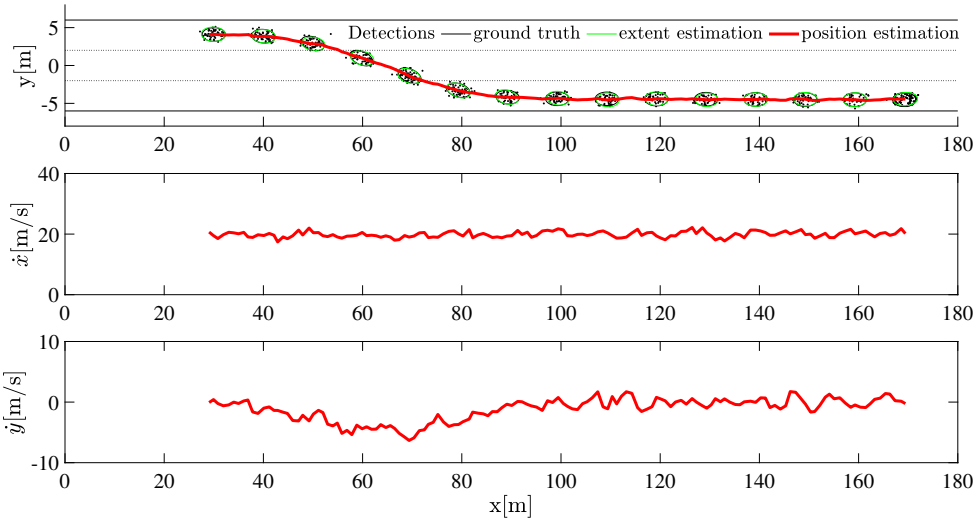

Figure 7.7: The tracking result of a maneuvering target with a measurement distribution assumed to be Poisson with parameter $\lambda = 50$.

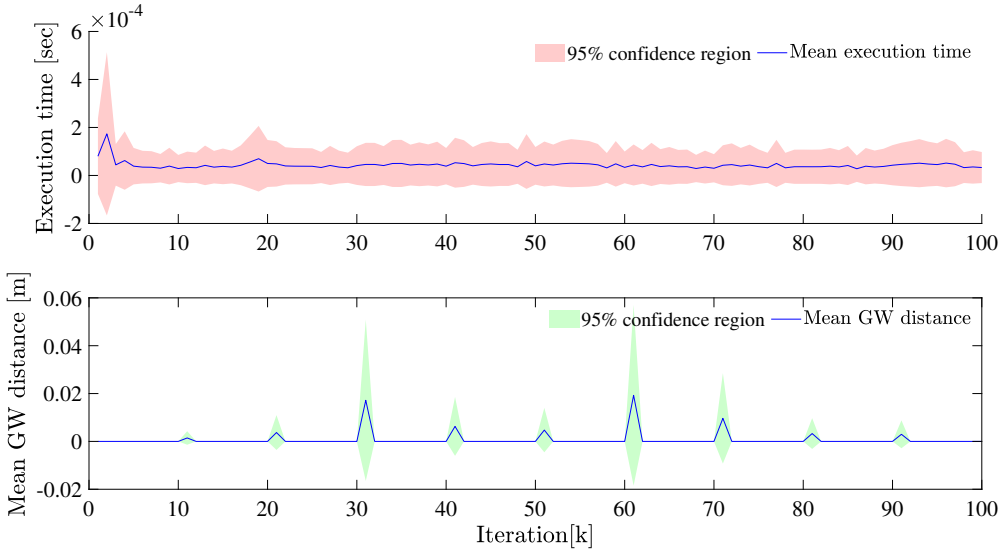

Figure 7.8: The mean GW distance and execution time at each iteration is plotted, $\lambda = 50$.

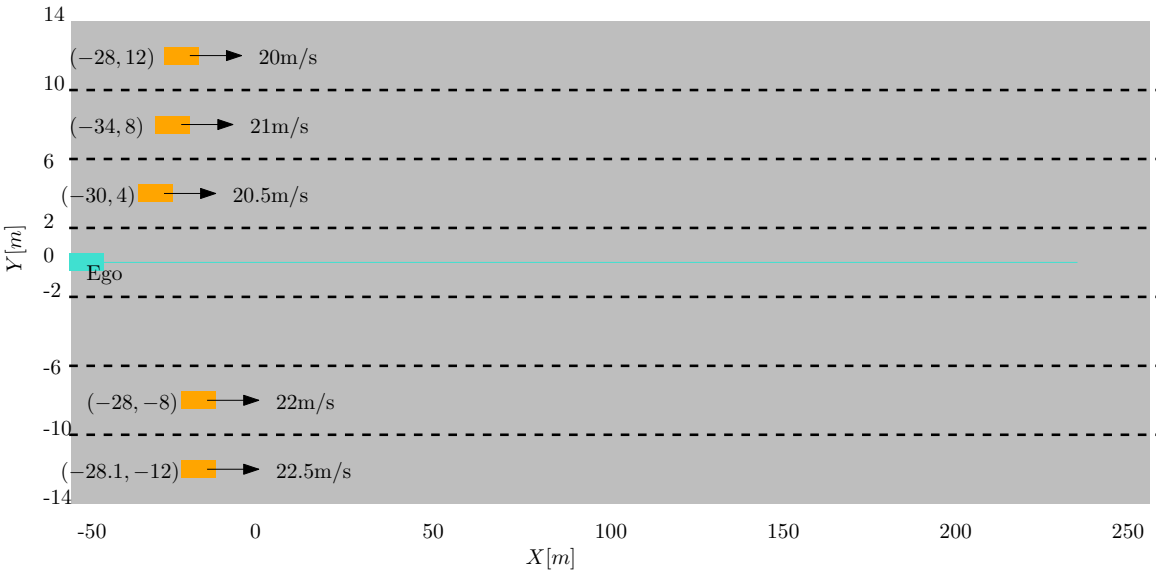

Figure 7.9: Scenario to demonstrate the use of group state information in the presence of occlusions.

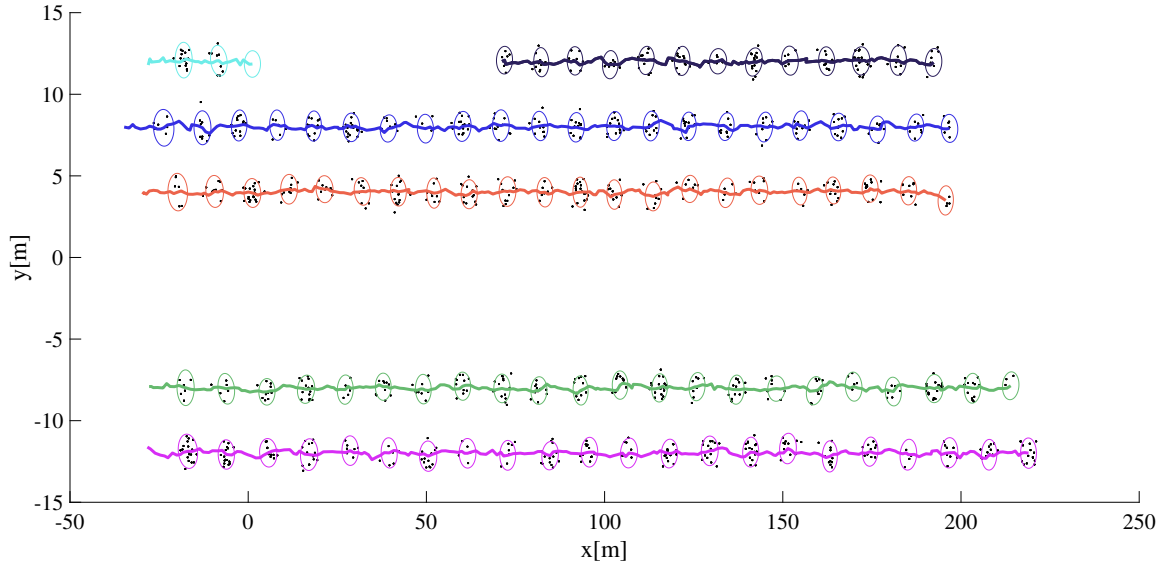

Figure 7.10: One of the EO has missing detections for a duration of 70 measurement scans. Its track is terminated and a new track is initiated when the target detections are available.

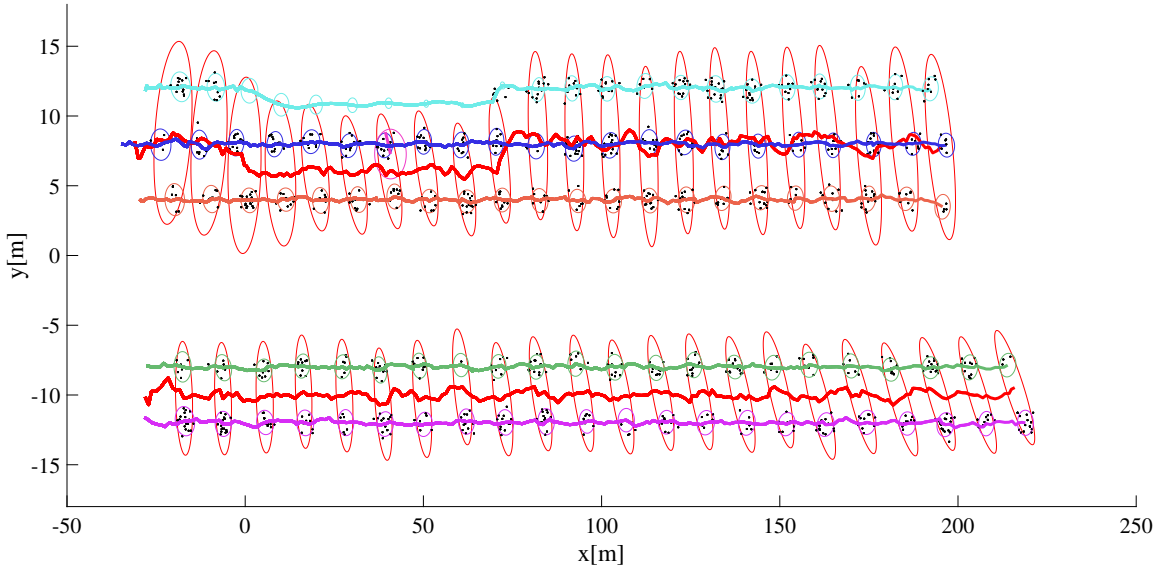

Figure 7.11: One of the EO has missing detections for a duration of 70 measurement scans. The group state information the EO is known to be a member of is used to update its track.

The case of Missing Detections, With Group Information

For the same scenario given in Figure 7.9, feedback from the group track layer of the proposed hierarchical layer is made available to the individual EO multi-target tracking layer to illustrate its effectiveness. First, the group consisting of the left three extended objects is tracked for a while until the occlusion deemed the detections from the leftmost EO is unavailable. Since, the EO is known to be a member of this group, a virtual measurement is fed back to update the target track. Here, we use as a virtual measurement

$$y_k^\tau = H_{pos} x_k^\tau + H_{vel} x_k^G dt \tag{7.36}$$

where, H_{pos} and H_{vel} select the position and velocity entries of the state variable, respectively.

$$H_{pos} = \begin{bmatrix} 1 & 0 & 0 & 0 & 0 & 0 \\ 0 & 0 & 0 & 1 & 0 & 0 \end{bmatrix} \tag{7.37}$$

$$H_{vel} = \begin{bmatrix} 0 & 1 & 0 & 0 & 0 & 0 \\ 0 & 0 & 0 & 0 & 1 & 0 \end{bmatrix} \tag{7.38}$$

7.5.1.1 Single target tracking

The positive directions of the x-y coordinate axes of the radar sensor are shown in the experimental set up depicted in Figure 7.12. On the other hand, the coordinate axes of the Real-time Kinematic (RTK) GPS is given in East-North-Up system. While the base station unit of the RTK GPS is fixed close to the radar coordinate frame, a suitable transformation is needed to align the East-North-Up readings to the local coordinate axes.

The rover unit of the RTK GPS is mounted on the target vehicle; logging positional data at a rate of 10Hz,will serves as the ground truth. Radar point cloud detections are sampled and recorded on a tracking computer at a rate of 20Hz. Ultimately, the GPS data is transformed to the local sensor frame coordinates and the GPS and radar timestamps are synchronized to use the RTK GPS location data to validate the performance of the tracking algorithms.

As shown from the pose of the target at t_0 and t_f in Figure 7.13, the target vehicle executes a lane-change maneuver as it moves away from the ego vehicle. The kinematic and state estimation result is shown in Figure 7.13.

In Figure 7.14, the number of radar returns from the target is seen to decrease as the target moves away from the ego vehicle. For the extent estimation, a large enough value for the maneuvering time constant is chosen. This is particularly important considering the fact that the extent of the target remains approximately fixed. In addition, the extent estimation is improved because of a larger value of $\theta = 100\Delta t$ chosen to compensate for less number of target detections at the far end. It is also noted that, occasionally detections are missing and thus the track management part of the tracking algorithm is expected to maintain the target track.

In Figure 7.15, the time taken to execute a single iteration is plotted against time. Generally, the execution time depends on a number of factors, but most importantly on the number of radar detections and the number of targets (including false tracks which are based on ghost targets). We note that the mean and worst execution time per iteration are respectively 2.5 and 10.4 milliseconds.

7.5.1.2 Multi target tracking

Next, group target tracking is demonstrated in a multi-target scenario that involves two target vehicles. The availability of resources limit the number of targets to two, we expect the result

Figure 7.12: Pictured here is the experimental setup for a single target tracking scenario. a) The target vehicle is shown at its starting pose at t_0. The rover station of the RTK GPS is also shown positioned at approximately the center of the real axle. b) The target vehicle is shown positioned at $t = t_f$. The positive x-y coordinate axes of the radar are also depicted.

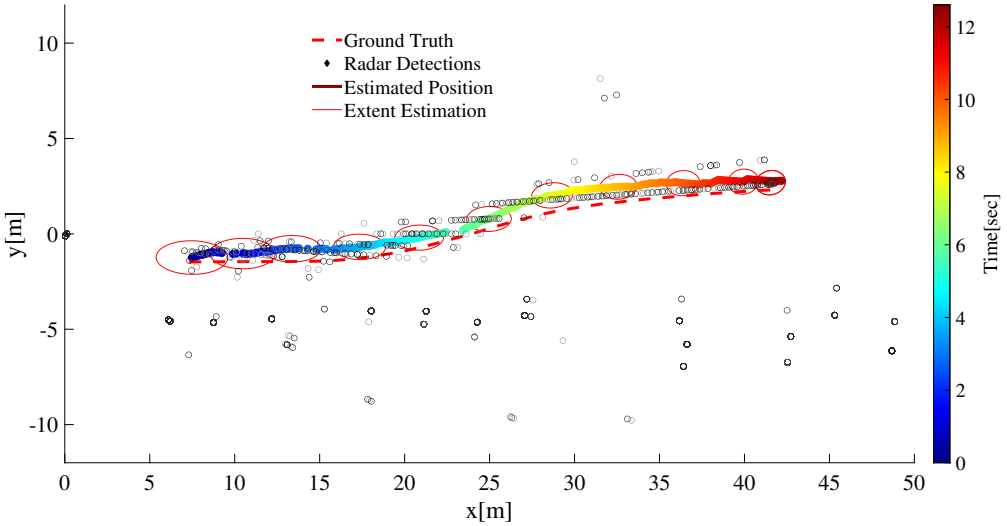

Figure 7.13: An extended target tracking result. The extent estimation is better with a high enough maneuver time constant $\theta = 100\Delta t$ to compensate for less target detections at the far end.

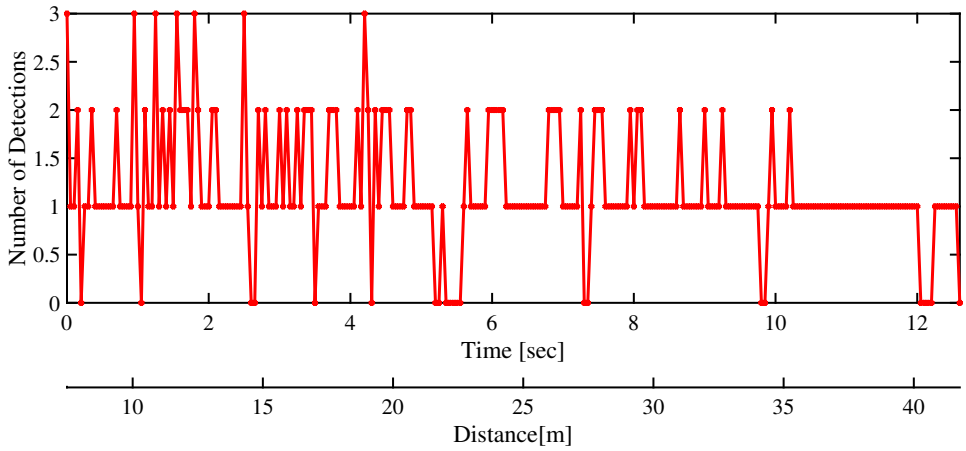

Figure 7.14: The number of radar target detections confirmed for the target are shown plotted as a function of the target distance from the ego vehicle. As the distance increases the number of detections is seen to correspondingly decrease.

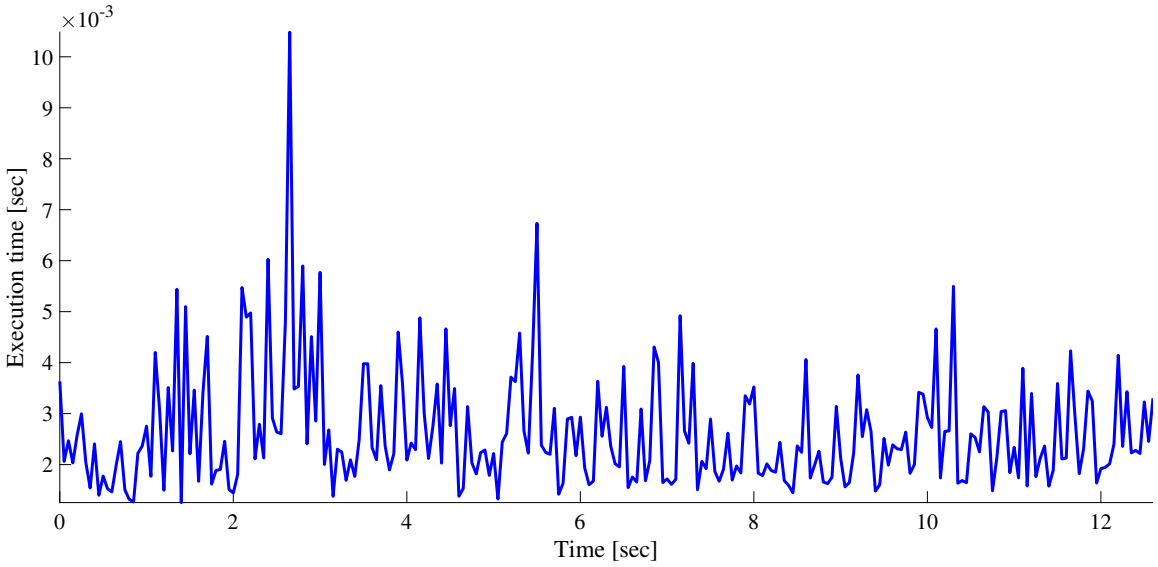

Figure 7.15: Execution time required to complete a single iteration for the case of a single ET.

to extend easily to scenarios involving more than two target vehicles. One of the target vehicles is equipped with RTK GPS to record the ground truth data, the other vehicle is merely there to facilitate the group target discussion (and to complicate the data association uncertainty). As seen from the time-snapshots at $t = t_0$ and $t = t_f$ of Figure 7.16, the two vehicles are driven in close proximity and in parallel as both drive away from the sensor station. The lateral inter-vehicle distance and the relative speed is intentionally kept reasonably close to simulate group target dynamics. The extent estimation for the individual ET as well as the group target is presented in Figure 7.17. In addition, the kinematic state estimate (for the position) is shown for both group and ET cases. Similar to the single ET case above, the maneuver time constant $\theta = 100\Delta t$ is kept large enough to counter the extent estimation with fewer target detections.

The MD-LMIPDA tracker is able to resolve measurement-to-target data association without the need to compute the data association jointly for all the measurements and targets simultaneously. In addition, it is shown in Figure 7.17 that even under non-uniform and sparse target detections, extent estimations for both individual ET as well as group targets is possible. It is seen from the tracking discussions both under Section 7.5.1.1 and 7.5.1.2 that the algorithm can be used to successfully generate extended and group multi-target state estimates in public traffic scenarios.

The applicability of the tracking algorithm under real-time requirement is further justified in the

a)

b)

Figure 7.16: Experimental setup for the case of multiple ET target tracking scenario. a) The target vehicles (ET_1(Sedan Car), ET_2(SUV Car)) are pictured at the starting pose $t = t_0$. The rover station of the RTK GPS is placed at the center of the real axle of ET_1(Sedan Car). b) The time-snapshot of both target vehicles is shown at $t = t_f$. The positive x-y coordinate axes of the radar sensor are also depicted.

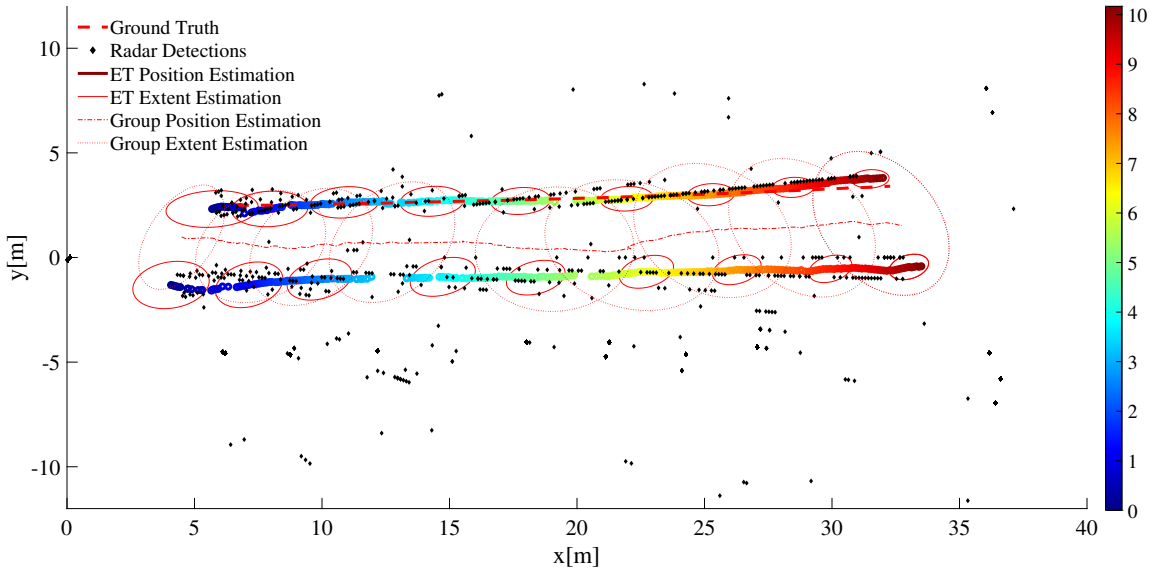

Figure 7.17: Tracking result of two extended targets. Both the position and extent estimation result for single ET and group target is shown.

results plotted under Figure 7.18. As shown in the figure, the mean and maximum total execution time per iteration are respectively 8.5 and 19.8 milli seconds. The total time is computed by simply adding the execution time for both group and ET tracking at a given radar scan time. In this work, all simulations are done on a laptop with the specifications:- Intel Core i7 2.90 GHZ processor, installed Memory (RAM) of 16.0 GB and Windows 10 64-bit Operating system.

The notion of group objects is interpreted under stricter constraints of inter-target distances, relatives speeds and orientations. Targets in formation are required to have "similar" velocities and tight inter-object distances [12] to maximize the chances of being in a group. In Figure 7.19, the relative distance and speed between the group target and constituent extended targets is plotted against time. In addition, the inter-target distance and speed differences are shown on the same figure. Under the simulated scenario, a relative speed of $-0.4 \leq \Delta\dot{y} \leq 0.2, -0.6 \leq \Delta\dot{x} \leq 0.3$ and a relative distance of $|\Delta y| \leq 4, |\Delta x| \leq 2$ is observed.

7.6 Conclusions

Application of high-resolution automotive radar to public traffic presents a multi-detection tracking problem. In chapter 6, we proposed a hybrid tracking scheme that exploits the measurement parti-

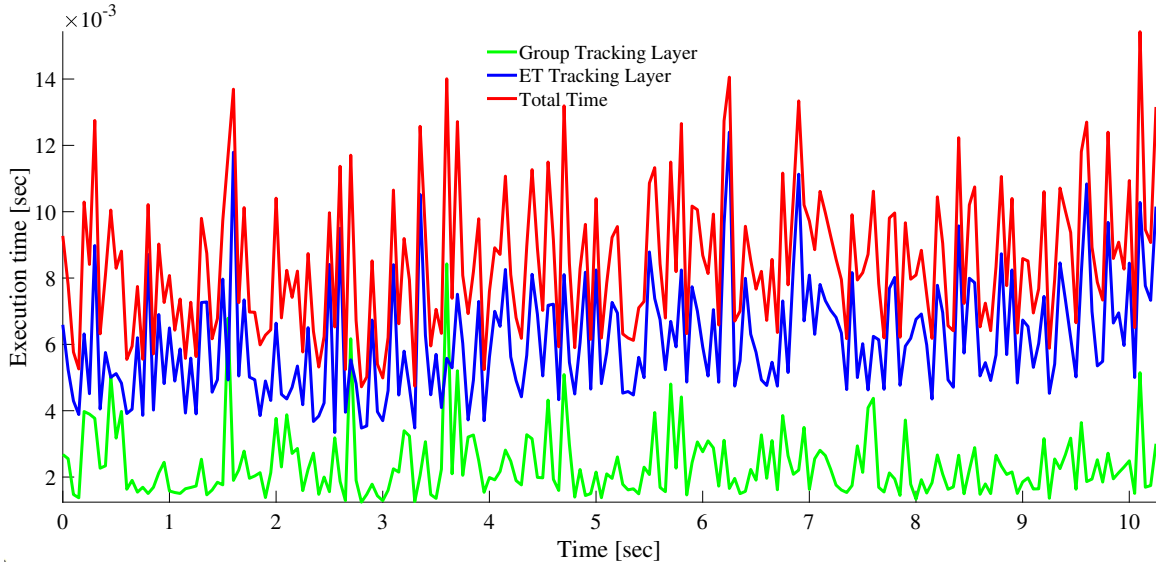

Figure 7.18: The execution time for per iteration for both group as well as ET tracking.

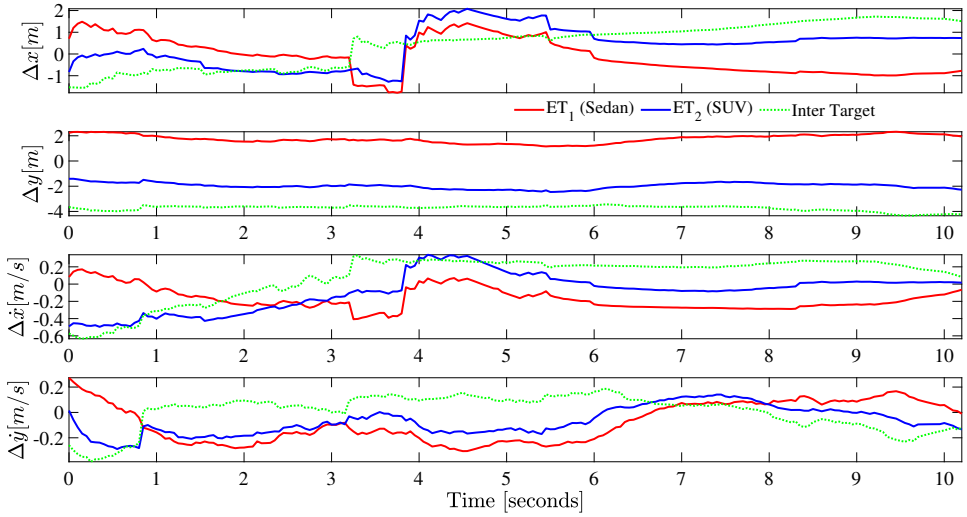

Figure 7.19: Relative distance and speed between the group and individual extended targets is plotted against time. The plots ET_1 and ET_2, measure the distance of individual target states from the group target. Whereas,the inter-target plots show the distance and speed differences between the two extended targets.

tioning approach to address the tracking problem under multi-sensor multi-target scenarios. In the present chapter, we proposed and demonstrated the use of group tracks to complement and improve individual extended object tracks under circumstances of missing detections, occlusions, target initialization and merged measurements. We used the Gaussian Wasserstein distance that incorporates both the shape and kinematic state in a single metric to evaluate the estimation performance of the tracking algorithm for various simulated examples.

The evaluation of the tracking algorithm for real radar detections is conducted for a single ET and promising results are obtained for real-time application. In particular, we noted the mean and maximum execution time per iteration in the order of 2.5 and 10.4 milli seconds respectively. A further experiment exploiting two extended targets was setup to emulate a dynamic group target. Radar detectios from both target vehicles as well as RTK GPS data on one of the target vehicles is collected from two vehicles driving closely with each other and infront of the ego vehicle. The tracking problem is formulated as a two hierarchical layer:- at the bottom layer, extended multi-target tracking algorithm is presented; at the top layer a group target tracking algorithm captures group evolution including merging and splitting of groups targets. The observed mean and maximum execution time per iteration are respectively 8.5 and 19.8 milli seconds respectively, justifying the use of the proposed tracking scheme for real-time applications.

More reliable extent estimation for both individual ET and group targets could be obtained under more dense sensor detections that also preferably take a uniform distribution across the extent of the ET and/or the group target. In this study, we employed an assumption on the extent evolution that tends to constrain the extent to vary only gradually. Practical traffic scenarios support this assumption: owing to the presence of structured lanes, tight traffic regulations and the inherent desire to avoid collisions, the extent varies rather slowly. This assumption also favors radar detections which tend to resemble a line segment or an "L-shape" even for high resolution options. Adding miss-detections and the possibility of relatively larger ego-to-target distances that reduce target detections, the extent estimation under the above assumption is clearly justified. However, for highly maneuvering targets and if the sole objective is to get reliable extent estimation, other sensors such as lidar and camera could be explored.

References

[1] Kuo-Chu Chang and Y. Bar-Shalom, "Joint probabilistic data association for multitarget tracking with possibly unresolved measurements and maneuvers," *IEEE Transactions on Automatic Control*, vol. 29, no. 7, pp. 585–594, 1984.

[2] W. Koch and G. Van Keuk, "Multiple hypothesis track maintenance with possibly unresolved measurements," *IEEE Transactions on Aerospace and Electronic Systems*, vol. 33, no. 3, pp. 883–892, 1997.

[3] M. Beard, B.-T. Vo, and B.-N. Vo, "Bayesian multi-target tracking with merged measurements using labelled random finite sets," *IEEE Transactions on Signal Processing*, vol. 63, no. 6, pp. 1433–1447, 2015.

[4] S. K. Pang, J. Li, and S. J. Godsill, "Detection and tracking of coordinated groups," *IEEE Transactions on Aerospace and Electronic Systems*, vol. 47, no. 1, pp. 472–502, 2011.

[5] R. P. S. Mahler, "Detecting, tracking, and classifying group targets: a unified approach," in *Signal Processing, Sensor Fusion, and Target Recognition X* (I. Kadar, ed.), vol. 4380, pp. 217 – 228, International Society for Optics and Photonics, SPIE, 2001.

[6] J. A. Carrillo, M. Fornasier, G. Toscani, and F. Vecil, "Particle, kinetic, and hydrodynamic models of swarming," in *Mathematical modeling of collective behavior in socio-economic and life sciences*, pp. 297–336, Springer, 2010.

[7] G. Albi and L. Pareschi, "Modeling of self-organized systems interacting with a few individuals: from microscopic to macroscopic dynamics," *Applied Mathematics Letters*, vol. 26, no. 4, pp. 397–401, 2013.

[8] N. Bellomo and A. Bellouquid, "On the modelling of vehicular traffic and crowds by kinetic theory of active particles," in *Mathematical modeling of collective behavior in socio-economic and life sciences*, pp. 273–296, Springer, 2010.

[9] A. Gning, L. Mihaylova, S. Maskell, S. K. Pang, and S. Godsill, "Group object structure and state estimation with evolving networks and monte carlo methods," *IEEE Transactions on Signal Processing*, vol. 59, no. 4, pp. 1383–1396, 2011.

[10] S. K. Pang, J. Li, and S. J. Godsill, "Models and algorithms for detection and tracking of coordinated groups," in *2008 IEEE Aerospace Conference*, pp. 1–17, IEEE, 2008.

[11] F. Septier, S. K. Pang, S. Godsill, and A. Carmi, "Tracking of coordinated groups using marginalised mcmc-based particle algorithm," in *2009 IEEE Aerospace conference*, pp. 1–11, IEEE, 2009.

[12] S. K. Pang, J. Li, and S. J. Godsill, "Detection and tracking of coordinated groups," *IEEE Transactions on Aerospace and Electronic Systems*, vol. 47, no. 1, pp. 472–502, 2011.

[13] L. Mihaylova, A. Y. Carmi, F. Septier, A. Gning, S. K. Pang, and S. Godsill, "Overview of bayesian sequential monte carlo methods for group and extended object tracking," *Digital Signal Processing*, vol. 25, pp. 1–16, 2014.

[14] A. Carmi, F. Septier, and S. J. Godsill, "The gaussian mixture mcmc particle algorithm for dynamic cluster tracking," *Automatica*, vol. 48, no. 10, pp. 2454–2467, 2012.

[15] M. Baum and U. D. Hanebeck, "Random hypersurface models for extended object tracking," in *2009 IEEE International Symposium on Signal Processing and Information Technology (ISSPIT)*, pp. 178–183, IEEE, 2009.

[16] M. Baum, M. Feldmann, D. Fränken, U. D. Hanebeck, and W. Koch, "Extended object and group tracking: A comparison of random matrices and random hypersurface models," *INFORMATIK 2010. Service Science–Neue Perspektiven für die Informatik. Band 2*, 2010.

[17] M. Baum and U. D. Hanebeck, "Extended object tracking with random hypersurface models," *IEEE Transactions on Aerospace and Electronic systems*, vol. 50, no. 1, pp. 149–159, 2014.

[18] J. W. Koch, "Bayesian approach to extended object and cluster tracking using random matrices," *IEEE Transactions on Aerospace and Electronic Systems*, vol. 44, no. 3, pp. 1042–1059, 2008.

[19] M. Feldmann and D. Franken, "Advances on tracking of extended objects and group targets using random matrices," in *2009 12th International Conference on Information Fusion*, pp. 1029–1036, IEEE, 2009.

[20] M. Feldmann, D. Franken, and W. Koch, "Tracking of extended objects and group targets using random matrices," *IEEE Transactions on Signal Processing*, vol. 59, no. 4, pp. 1409–1420, 2010.

[21] W. Koch and R. Saul, "A bayesian approach to extended object tracking and tracking of loosely structured target groups," in *2005 7th International Conference on Information Fusion*, vol. 1, pp. 8–pp, Ieee, 2005.

[22] W. Koch and M. Feldmann, "Cluster tracking under kinematical constraints using random matrices," 2008.

[23] Z.-X. Li, Y. Wang, J.-M. Liu, N. Peng, and L.-H. Gan, "Variable-structure interacting multiple-model estimation for group targets tracking with random matrices," *Proceedings of the Institution of Mechanical Engineers, Part G: Journal of Aerospace Engineering*, vol. 232, no. 7, pp. 1201–1211, 2018.

[24] Y. Wang, G.-P. Hu, and Z.-X. Li, "Tracking of group targets using multiple models ggiw-phd algorithm based on best-fitting gaussian approximation and strong tracking filter," *Proceedings of the Institution of Mechanical Engineers, Part G: Journal of Aerospace Engineering*, vol. 232, no. 2, pp. 331–343, 2018.

[25] S. Blackman and R. Popoli, "Design and analysis of modern tracking systems(book)," *Norwood, MA: Artech House, 1999.*, 1999.

[26] Y. Huang, T. L. Song, W. J. Lee, and T. Kirubarajan, "Multiple detection joint integrated track splitting for multiple extended target tracking," *Signal Processing*, vol. 162, pp. 126–140, 2019.

[27] M. Schuster, J. Reuter, and G. Wanielik, "Probabilistic data association for tracking extended targets under clutter using random matrices," in *2015 18th International Conference on Information Fusion (Fusion)*, pp. 961–968, IEEE, 2015.

[28] D. Musicki and T. L. Song, "Track initialization: Prior target velocity and acceleration moments," *IEEE Transactions on Aerospace and Electronic Systems*, vol. 49, no. 1, pp. 665–670, 2013.

[29] S. Challa, M. R. Morelande, D. Mušicki, and R. J. Evans, *Fundamentals of object tracking.* Cambridge University Press, 2011.

[30] A. Hunde and B. Ayalew, "Automated multi-target tracking in public traffic in the presence of data association uncertainty," in *2018 Annual American Control Conference (ACC)*, pp. 300–306, June 2018.

[31] A. Hunde and B. Ayalew, "Linear Multi-Target Integrated Probabilistic Data Association Filter With Automatic Track Management for Autonomous Vehicles," vol. Volume 2: Control and Optimization of Connected and Automated Ground Vehicles of *Dynamic Systems and Control Conference*, 09 2018.

[32] A. Hunde, B. Ayalew, and Q. Wang, "Automated multi-object tracking for autonomous vehicle control in dynamically changing traffic," in *2019 American Control Conference (ACC)*, pp. 515–520, July 2019.

[33] K. Thormann and M. Baum, "Optimal fusion of elliptic extended target estimates based on the wasserstein distance," *arXiv preprint arXiv:1904.00708*, 2019.

[34] S. Yang and M. Baum, "Extended kalman filter for extended object tracking," in *2017 IEEE International Conference on Acoustics, Speech and Signal Processing (ICASSP)*, pp. 4386–4390, IEEE, 2017.

This page is intentionally left blank.

Appendices

Appendix A Time Complexity

The efficiency of various algorithms were given as compared on the basis of the cpu time it takes for a single iteration to execute. The same laptop is used for all comparisons; besides the results were averaged over several simulation runs. In the following, the Big-O time complexity of these algorithms are addressed.

Background

An important observation is that the time-complexity may vary from scan to scan, based mainly on the number of measurements shared among tracks and the number of (confirmed or tentative) tracks available. This can be explained by a representative example. The following function computes the measurement (cell) prior for all the measurements (measurement cells) validated for a given track.

```
% Probablistic weight of targets on meas partition
% 11/1/2018
% Author: Andinet Hunde
function [P_k] = probablistic_weight(target,tracks)
meas_i    = tracks{target}.T_j;
rho       = tracks{target}.rho_k;
for i=1:length(meas_i)
    z_phi_i = meas_i(i);
    for t=1:size(tracks,2)
        if t==target
            continue;
        end
        meas_t      = tracks{t}.T_j;
        [mem,index] = ismember(z_phi_i,meas_t);
        if mem
            rho(i)  = rho(i) + tracks{t}.p_k(index)*tracks{t}.P_D*tracks{t}.P_G*
    tracks{t}.Existance(end);
        end
    end
end
if ~isempty(meas_i)
    normalize = tracks{target}.p_k./rho;
    P_k = tracks{target}.P_D*tracks{target}.P_G*tracks{target}.Existance(end)*
    normalize;
```

```
23      normalize = sum(normalize);
24      P_k = P_k/normalize;
25  else
26      P_k = 0;
27  end
```

The arguments passed to the function are:- the current target ID and a structure of target tracks. Lines $5, 6$ and $[21-24]$ or 26 all involve simple variable assignments and/or arithmetic operations whose time-complexity is given as $\mathcal{O}(1)$. The inner loop iterates over $T-1$ tracks, where T is the number of (confirmed or tentative) tracks. Line 16 executes if a non-target track shares a measurement with the current track as returned from the *ismember* function in the logical variable *mem*. If **all** of the measurements *meas_i* are shared with **all** the non-targets (worst-case scenario), this will have a time-complexity of $\mathcal{O}((T-1) \times Z_i)$, where Z_i is the cardinality of *meas_i*. However, such a scenario where all the measurements validated by a given track are also shared by another non-target will lead to a track merging procedure at the next iteration. The *ismember(A,B)* function is an inbuilt Matlab routine that returns an array containing logical 1 (true) where the data in A is found in B. The function first verifies if B is sorted, via *issorted(B)*. The complexity of sorting array B is $log_2|B|$, where $|B|$ is the number of elements in array B. Thus, the overall time-complexity for the *ismember* function will be: $\mathcal{O}(|z\_phi\_i| \times log_2|Z_t|) = \mathcal{O}(log_2|Z_t|)$, where Z_t is the cardinality of *meas_t*. Line 14 will have a complexity of $O(|T-1| \times log_2|Z_t|)$, while the worst complexity occurs at lines $13, 16$ with $O(|Z_i| \times |T-1|)$.

Tracking Architectures

We have noted that the time-complexity for one of the functions is given as $O(|Z_i| \times |T-1|)$ which also happens to be the worst-case time-complexity for the overall tracking algorithm. We can further argue that due to the nature of traffic on structured highways (such as the tendency to avoid collision), the number of measurements shared between tracks is less than the worst-case assumed above. Besides, particularly for high resolution sensors, a clustering step is implemented to reduce the number of detections which cuts down the time-complexity even further. Furthermore, as noted above, the track merging procedure tends to prohibit the possibility of multiple measurements shared among different tracks.

A hybrid tracking architecture that clusters detections at local sensor level and tracks the resulting

multiple cluster centers is proposed to cope with the data association complexity. The proposed architecture is also compared to two popular approaches from the literature. These approaches employ centralized and distributed fusion schemes to deal with multiple sensors. In Figure A.1, the three tracking architectures are schematically shown highlighting the main differences. For all the three architectures, time-complexity increases linearly with the number of detections (measurements). The hybrid multiple detection tracker has the advantage of working on a reduced set of detections owing to the clustering step implemented on the local senor detections. The following text is repeated from section 6.4.1 to summarize the main differences among the three architectures.

- **Single MD-Tracker**: All raw detections from the three sensors are fed to a single multi-detection tracker. This MD-Tracker has to deal with potentially multiple detections originating from a single reflection point, albeit being noisy, as independently reported from the three sensors. The obvious drawback of this configuration is the computational complexity that increases with an increase in the number of detections.

- **Multiple MD-Trackers**: Three multi-detection trackers are run on local sensor detections independently. A track-to-track fusion algorithm fuses confirmed tracks from the local trackers. Similar to the Single MD Tracker above, this configuration also suffers from computational complexity that increases with an increase in the number of detections per sensor. However, independent trackers that are based on separate sensors are amenable for parallel computation.

- **Hybrid MD-Tracker**: Radar detections are clustered at sensor level and the resulting detections are fed to a single multi-detection tracker. The clustering algorithm is based on DBSCAN.

The selection of an "optimal" set of DBSCAN parameters that consistently work across multiple classes of vehicles (truck, car, pedestrian, etc.) and over an arbitrary inter-vehicle distance (close or far) is decided on the following observation. The two DBSCAN parameters, i.e. the distance E and the minimum number of detections $minPts$ are tuned as follows. Choosing large values for E, results in the clustering of detections from nearby target and clutter together. Choosing a smaller value; however, results in multiple clusters per target vehicle which can be evaluated in the data association stage of the tracking algorithm. This is preferable as compared to potentially erroneous hard decisions due to large E. Likewise, to discourage false alarms, large values for $minPts$ can be chosen owing to the high resolution sensors simulated here. In addition, for multiple tracks initiated

on the same target, the track merging procedure undergoes a minimal overload compared to lower $minPts$ values.

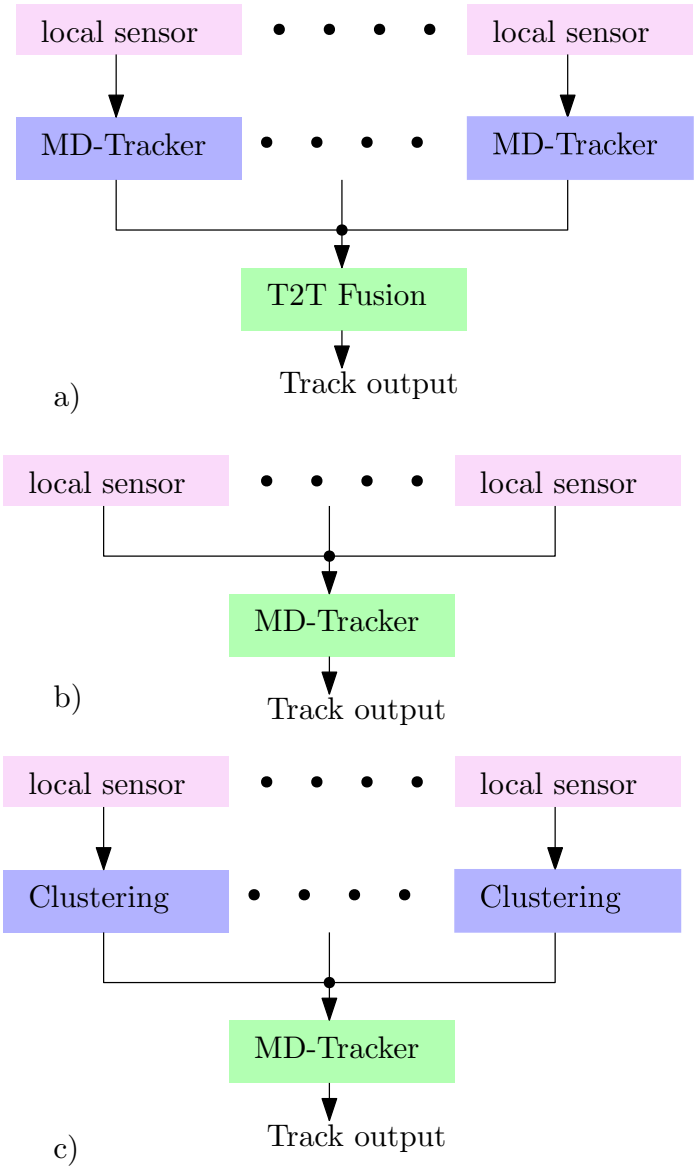

Figure A.1: Three multi-detection(MD) tracker architectures are shown schematically. a) Multiple MD-Trackers b) Single MD-Tracker c) Hybrid MD-Tracker

Concluding Remark

The main problem in tracking targets is the data association problem. Here, for linear multi-target (LM) approach, it starts with the computation of the prior data association probability and

modification of clutter density followed by the computation of posterior data association probability. For LM approach, the computation time increases linearly with the number of measurements and targets. For comparison, the CPHD filter has complexity cubic in the number of targets $\mathcal{O}(|Z_i|^3)$ and linear in the number of targets. Although the LM approach has a computational advantage, it comes to a challenge in scenarios of close or crossing targets where the data association is quite difficult.

Appendix B Crossing Targets

LM Tracking Assumptions

The tracking algorithm implemented in this thesis is based on Linear Multi-target Integrated Probabilistic Data Association Filter (LMIPDAF). In addition to the kinematic state, the extent estimation is also integrated into the filtering recursion. For the LM approach, the data association assumption is that a measurement is either originating from:

- A single target, or
- Clutter

The presence of other non-target vehicles which might have also generated the measurement are considered by modifying the clutter density at the measurement shared among the targets and the non-targets. Optimal data association methods compute the measurement-to-target assignment jointly by taking all targets and all detections at the same time. However, these methods are hit by increased complexity especially under high resolution applications. A structured road environment with clearly demarcated lanes, rules on speed limits, presence traffic signs and signals all tend to regulate the traffic flow. In addition, the intrinsic desire of traffic participants to avoid potential collisions and dangerously close encounters seems to justify the use of LM approach from the outset. However, to investigate how the LM data association assumptions hold in targets with crossing trajectories, we simulate the following hypothetical example.

Simulation Settings

Two vehicles are traveling at 20 m/s and at an angle with intersecting trajectories. The measurement has a Poisson distribution with a clutter rate of 10. Target detections (x, y positions) are sampled at a rate of 20Hz. Both target vehicles have a physical dimension of 4.7 X 1.8 m^2. As seen in Figure A.2, both the state and extent (approximated by ellipsoids) estimations are correctly retrieved from multiple sensor detections, especially when the target trajectories are crossing each other at $(0, 0)$. More importantly, track identities are not switched at the intersection. Track identities are represented with a randomly assigned color during the track initiation phase.

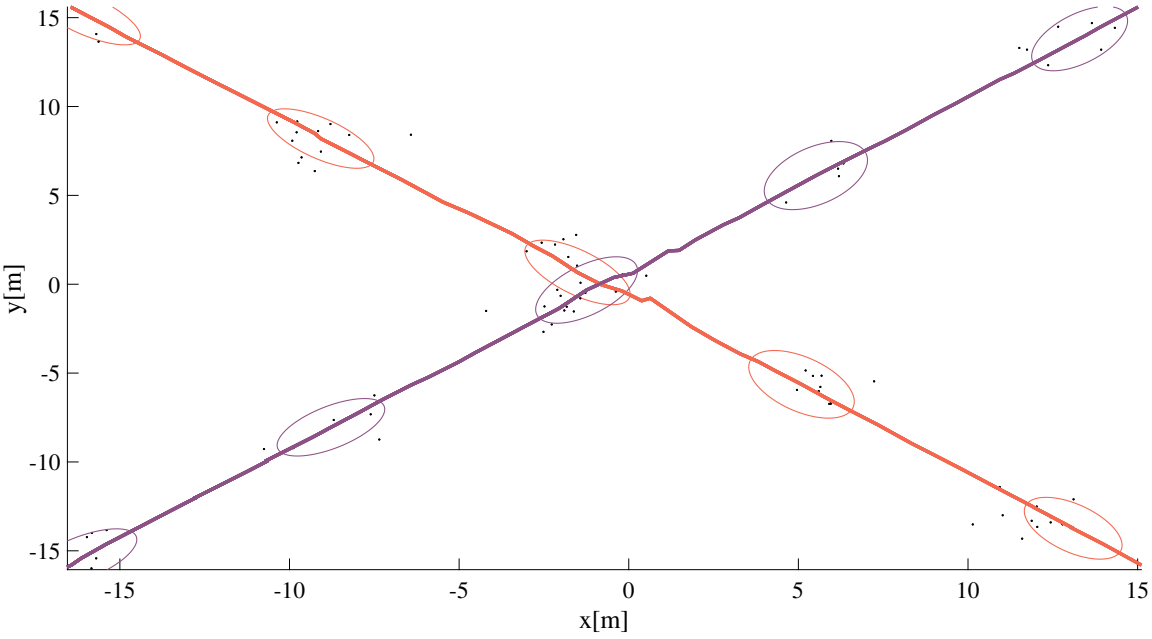

Figure A.2: State and extent estimation for two crossing targets. Colors represent different tracks.

Appendix C Mixed Traffic

So far, we confined our study to the tracking problem of target vehicles in both simulated and practical scenarios. However, realistic traffic scenes exhibit multiple classes of targets including vehicles, cyclists, pedestrians, etc. Here, the same filtering parameters are used for both vehicles and pedestrians alike. More refined results can be obtained if we make distinction among different classes and choosing appropriately tuned parameters (process and measurement noise, extent dimension, clustering parameters, maximum speed/acceleration limits, etc.). The required target classes can be

obtained during an object detection step by using a camera image and an object detection algorithm.

Simulation Settings

The ego and target vehicles are simulated traveling at 5m/s. Both have dimensions 4.7 m X 1.8 m. Two pedestrians with physical dimensions 0.24 m X 0.45 m, one jogging at 2.7 m/s on the sidewalk and the other walking on the crosswalk at 1.5m/s are included in the simulation.

The tracking algorithm is based on LMIPDA with kinematic and extent estimations. As shown in Figure A.3, the estimated positions and extent estimations for all the 4 traffic participants is plotted every other 50^{th} iteration. Prior knowledge of the class of each target detections enables the selection of simulation model as well as tuning parameters relevant for the target under consideration.

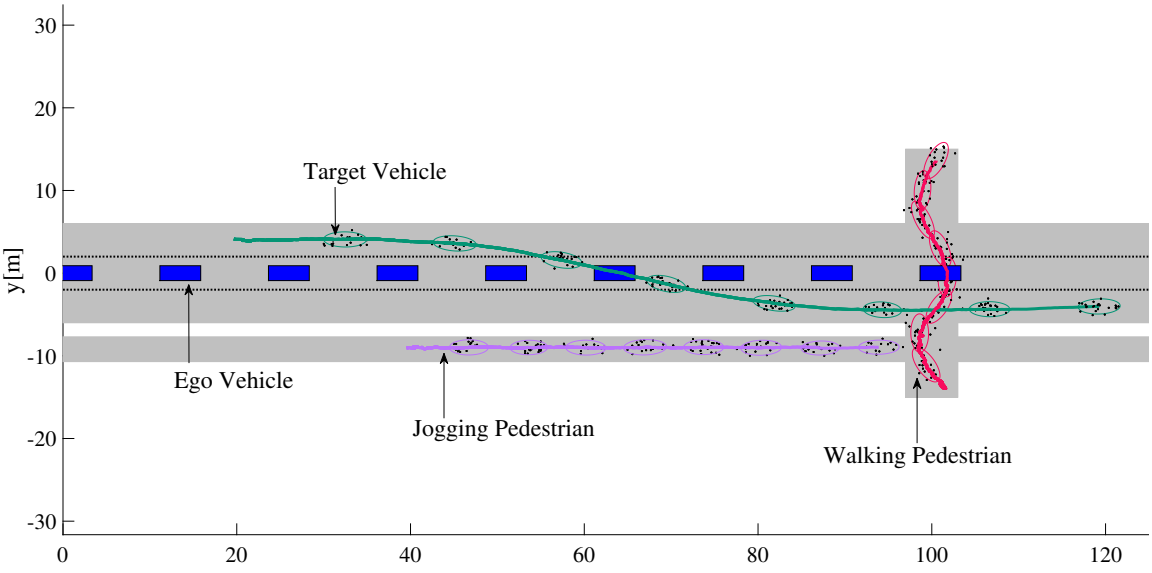

Figure A.3: State and extent estimation for mixed traffic simulation with two vehicles and two pedestrians.

Appendix D Faulty Sensor

In general, faulty detections result in unreliable tracking which in turn leads to wrong control action and potential crash. If the sensor fault is such that the sensor is just inactive, the missed detections can be compensated temporarily by kinematic state and extent predictions. Long term predictions tend to deviate from true trajectories. This is largely due to target vehicles are driven by humans or some artificial intelligence that are characterized by reactions ('aggressiveness', 'promptness') which

are not captured with the Newtonian motion models. Changes in road curvatures, presence of exit and entrance ramps, obstacles such as traffic signs, etc. give rise to dynamic traffic that render the predictions based on kinematic models less effective. This is more pronounced for predictions over extended range of time. Another known solution is the use of sensor redundancy often with overlapping FoV. This is the topic of discussion of Chapter 6.

If the fault is such that the sensor is behaving rather randomly, generating detections inconsistent with the implemented motion model predictions, then the sensor's detections are most likely treated like a clutter. Again, sensor redundancy is one possible solution; where with sensor fusion and a tracking algorithm target states could be retrieved from noisy detections. In our implementations, the track management module uses two more layers of verifications:

- The detections must fall within a region determined by the predictions based on the motion and sensor model. This region is called a validation gate and effectively clips out most clutter and non-target detections.
- Consecutive detections should obey some rules, for instance the maximum allowable speed is such that the position difference $\Delta x < V_{max}\Delta t$. Where Δx, V_{max}, and Δt are respectively the incremental position change, maximum anticipated speed and sampling interval.

In general, fault tolerance requires a systematic treatment that goes beyond the scope of this work.